PREPARATION AND CHARACTERIZATION OF ELECTROSPUN POLY (D,L-LACTIDE-CO-GLYCOLIDE) SCAFFOLDS FOR VASCULAR TISSUE ENGINEERING AND THE ADVANCEMENT OF AN IN VITRO BLOOD BRAIN BARRIER MODEL

A Thesis Presented to the Faculty of

California Polytechnic State University, San Luis Obispo

In Partial Fulfillment of the Requirements for the Degree

Master of Science in Biomedical Engineering

By

Deven Chandrakant Patel

June 2012

COMMITTEE MEMBERSHIP

TITLE:	Preparation and Characterization of Electrospun Poly(D,L-lactide-co-glycolide) Scaffolds for Vascular Tissue Engineering and the Advancement of an In Vitro Blood Brain Barrier Model
AUTHOR:	Deven Chandrakant Patel
DATE SUBMITTED:	June 2012
COMMITTEE CHAIR:	Kristen O'Halloran Cardinal, PhD
COMMITTEE MEMBER:	Trevor Cardinal, PhD
COMMITTEE MEMBER:	Daniel Walsh, PhD

Abstract

PREPARATION AND CHARACTERIZATION OF ELECTROSPUN POLY (D,L-LACTIDE-CO-GLYCOLIDE) SCAFFOLDS FOR VASCULAR TISSUE ENGINEERING AND THE ADVANCEMENT OF AN IN VITRO BLOOD BRAIN BARRIER MODEL

Deven Chandrakant Patel

Developing an *in vitro* Blood Brain Barrier model that will replicate the physiological, anatomical, and functional characteristics of the native BBB has gained significant attention. Such a model would enable prediction of the penetration of CNS targeting drug candidates across the BBB, allow pre-screening and optimization strategies to be developed for new drugs and gene delivery formulations, and permit research groups to further understand how a dysfunctional BBB is involved in the pathogenesis of several neurological diseases.

The Tissue Engineering laboratory at the California Polytechnic State University, San Luis Obispo is currently in the process of developing a dynamic *in vitro* blood brain barrier model that will implement an in-house fabricated electrospun PLGA scaffold pressure sodded with C6 glial cells and BAECs (Bovie Aortic Endothelial Cells). The aims of this thesis were to upgrade and refine the existing electrospinner system, develop a BBB scaffold electrospinning protocol, and characterize and evaluate the consistency of the scaffolds fabricated using the protocol.

Ultimately, the electrospinner system was optimized in the following areas: the high voltage power supply, electrical layout and safety, as well as the syringe pump and stand. The modifications to the system will now permit new electrospinning strategies and ensure operator safety. The protocol developed for electrospinning scaffolds for the DIV-BBB system utilized 15 wt% PLGA in $CHCl_3$ with a 4.5 ml/hr flow rate, an applied voltage of 18,000V with a negative polarity, and a gap distance of 25.4 cm.

Characterization and consistency studies revealed that scaffolds electrospun were statistically inconsistent with one another with regards to fiber diameter ($P < 0.0001$), porosity ($P < 0.0001$), and wall thickness ($P < 0.0001$). However, the scaffolds were mechanically consistent (P-value of 0.6134) according to the calculated Young's modulii. The average fiber diameter for the electrospun scaffolds was 2.556 µm, and had an average porosity of 70.06 μm^2. Additionally, the wall thickness between the electrospun scaffolds ranged between 0.31 and 0.54 mm. The average Young's modulus of the electrospun scaffolds was determined to be 86.141 MPa. While the results associated with fiber diameter, porosity, and wall thickness were statistically inconsistent, it will be important to evaluate whether the variation between each scaffold will translate to a difference when conducting cellular studies after the DIV-BBB system is complete.

Acknowledgements

Words cannot express how grateful I am to have met Dr. Kristen O'Halloran Cardinal. Since meeting her, I have developed a set of invaluable qualities that will greatly assist me in my future endeavors. It has been a great honor to work with her, and receive her complete support throughout my time at Cal Poly.

I would also like to thank my thesis committee, Dr. Trevor Cardinal and Dr. Daniel Walsh. I have had the privilege to take classes and get to know both of them and will never forget the dedication and commitment they had to all of their students. Additionally, I thank Ms. Becky Powell, whose devotion to graduating bright Cal Poly students annually truly is remarkable.

In merely a year, I have created bonds with my fellow lab members in the Tissue Engineering lab that I will never forget. It is rare to find a group that meshes so well, so I truly consider myself blessed to have had the opportunity to work with all of them. I will always cherish the times we had inside and outside of the lab.

I would also like to thank Mr. Dave Laiho and Mr. Ralph Nicovich, both of whom were instrumental in upgrading and refining the electrospinner system. I also thank Dr. Eugene Boland, whose expertise in the field of electrospinning was key to the work presented in this Thesis.

I would like to thank my parents, Chandrakant and Meera Patel. Everything I have done worth achieving has been for the both of them. They are the most selfless people that I have ever met, and have always made their children their first priority. I consider myself blessed to have parents like them. I am also very grateful to have a caring brother and sister, Suraj and Anisha, as they have always supported me through thick and thin. And, my heartfelt thanks to my grandfather, Durlabhbhai Patel, whose courage to leave a small farming village in India to pursue Civil Engineering continues to inspire a family of engineers. Lastly, it is the strength of my grandmother, Godavariben Patel, that is the foundation of the entire family.

TABLE OF CONTENTS

LIST OF TABLES ix
LIST OF FIGURES x
CHAPTER 1 - INTRODUCTION 1
1.1 MOTIVATION 1
1.2 THE BLOOD BRAIN BARRIER STRUCTURE 3
1.3 PROMINENT CENTRAL NERVOUS SYSTEM DISORDERS INVOLVING BBB DYSFUNCTION 6
1.4 CURRENT *IN VITRO* BBB MODELS 7
1.5 ELECTROSPINNING 10
1.5.1 History of Electrospinning 12
1.5.2 Electrospinning Theory and Process 13
1.5.3 Effects of Various Parameters on Electrospinning 15
1.5.3.1 *Solution Parameters* 16
1.5.3.2 *Applied Voltage* 18
1.5.3.3 *Flow Rate* 19
1.5.3.4 *Gap Distance* 20
1.5.3.5 *Ambient Parameters* 20
1.6 CELL INTERACTIONS WITH AN ELECTROSPUN SCAFFOLD 21
1.7 OVERALL OBJECTIVE AND AIMS OF THE THESIS 23
CHAPTER 2 - OPTIMIZATION OF THE ORIGINAL ELECTROSPINNER SYSTEM 25
2.1 INTRODUCTION 25
2.2 ORIGINAL ELECTROSPINNER SYSTEM 26
2.3 HIGH VOLTAGE POWER SUPPLY 28
2.3.1 Original Power Supply 28
2.3.2 Criteria Used to Select New Power Supply 30
2.3.3 New High Voltage Power Supply 34
2.4 ELECTRICAL LAYOUT AND SAFETY 35
2.5 SYRINGE PUMP SETUP 37

2.6 COMPARISON OF THE ORIGINAL AND OPTIMIZED ELECTROSPINNER SYSTEMS 39
2.7 PROOF OF CONCEPT STUDY 41
2.7.1 Materials and Methods 41
2.7.2 Results and Discussion 42
2.8 CONCLUSION 44
CHAPTER 3 - BLOOD BRAIN BARRIER SCAFFOLD PROTOCOL DEVELOPMENT 45
3.1 INTRODUCTION 45
3.2 MATERIALS AND METHODS 46
3.2.1 Polymer Mixing and Electrospinning 46
3.2.2 SEM and Image Analysis 47
3.3 RESULTS 47
Electrospin #1 48
Electrospin # 2 50
Electrospin # 3 52
Electrospin # 4 54
Electrospin # 5 57
Electrospin # 6 59
Electrospin # 7 61
Electrospin # 8 63
Electrospin # 9 66
Electrospin # 10 68
3. 4 DISCUSSION AND CONCLUSION 70
CHAPTER 4 - CHARACTERIZATION AND CONSISTENCY STUDY OF THE BBB SCAFFOLD 73
4.1 INTRODUCTION 73
4.2 MATERIALS AND METHODS 73
4.2.1 Electrospinning Parameters for the Characterization and Consistency Study 73
4.2.2 Sampling Method 74
4.2.3 Fiber Diameter Measurement 75
4.2.4 Porosity Measurement 76

4.2.5 Thickness Measurement 77
4.2.6 Uniaxial Tensile Testing 79
4.2.7 Statistical Analysis 80
4.3 RESULTS 81
4.3.1 Results and Statistical Analysis of Fiber Diameter 81
4.3.2 Results and Statistical Analysis of Scaffold Porosity 83
4.3.3 Results and Statistical Analysis of Wall Diameter 85
4.3.4 Results and Statistical Analysis of Tensile Testing 87
4.4 DISCUSSION AND CONCLUSIONS 89
CHAPTER 5 - DISCUSSION AND CONCLUSION 94
5.1 OVERVIEW 94
5.2 LIMITATIONS AND FUTURE WORK 97
5.2.1 Sample Size and Biological Cellular Assessment 97
5.2.2 Improving Wall Thickness Assessment 98
5.2.3 Tensile Testing Assessment 99
5.2.4 Reassessment of the Solution Parameters 100
5.2.5 Modifying the Ambient Parameters 101
5.2.6 Improving Scalability of Electrospun Scaffold Fabrication 101
5.2.7 New Electrospinning Strategies 102
5.3 CONCLUSION 103
LIST OF REFERENCES: 104
APPENDIX A: MIXING PLGA SOLUTIONS FOR ELECTROSPINNING 114
APPENDIX B: ORIGINAL ELECTROSPINNING PROTOCOL 117
APPENDIX C: BBB ELECTROSPINNING PROTOCOL 123
APPENDIX D: IMAGE J SOFTWARE ANALYSIS PROTOCOL 128
APPENDIX E: POROSITY MEASUREMENT PROTOCOL 131
APPENDIX F: CHARACTERIZATION AND CONSISTENCY STUDIES SEM IMAGES 134
APPENDIX G: TENSILE TESTING FIGURES 139

LIST OF TABLES

Table 1: *Summary of options considered for the new high voltage power supply*.....33

Table 2: *Summary of Syringe pumps considered for replacement*.....39

Table 3: *Intrascaffold ANOVA fiber diameter results*.....83

Table 4: *Intrascaffold ANOVA porosity results*.....85

Table 5: *Intrascaffold ANOVA Wall Diameter results*.....86

Table 6: *Young's Modulus (MPa) per section of each scaffold*.....88

LIST OF FIGURES

Figure 1: *Locations of the Blood Brain Barrier in the CNS*.....4
Figure 2: *Molecular composition of endothelial tight junctions of the BBB*.....5
Figure 3: *Dynamic in vitro BBB model (DIV-BBB*).....9
Figure 4: *Schematic of an electrospinning apparatus employing a horizontal setup*..... 14
Figure 5: *Image of the formation of a Taylor cone* 15
Figure 6: *"Beads on a string" formation*.....16
Figure 7: *Metal Mandrel translation and rotation capabilities*.....27
Figure 8: *Original High Voltage Power Supply setup*.....29
Figure 9: *New high voltage power supply*.....35
Figure 10: *Isolation chamber fitted with electrical bulkhead fittings*.....37
Figure 11: *(**A**) Original Syringe Pump Stand (**B**) New Syringe Pump Stand*.....38
Figure 12: *Original Electrospinner System employed at Cal Poly*.....40
Figure 13: *Optimized Electrospinner System setup*.....40
Figure 14: *SEM images at 180x of the inner lumen of a BBB scaffold electrospun using the optimized **(A)** and original **(B)** electrospinner systems*.....43
Figure 15 - *500x SEM image of the inner lumen of the tubular scaffold fabricated from Electrospin #1*.....49
Figure 16 - *1000x SEM image of the inner lumen of scaffold from Electrospin #1*.....49
Figure 17:*1000x SEM image of the interior surface of the electrospun scaffold # 2*.....51
Figure 18: *SEM image of the interior surface of a Electrospun #3 scaffold (1000x)*.....53
Figure 19: *1000x SEM image of the interior surface of Electrospun scaffold #4*.....55
Figure 20: *SEM image of interior surface at 500x*.....56
Figure 21: *SEM image (1000x) of the interior surface of Electrospun scaffold #5*.....58
Figure 22: *SEM image of the interior surface of Electrospun scaffold #5 at 2500x*.....58
Figure 23: *SEM image of the interior surface of Electrospun scaffold # 6*.....60
Figure 24: *2500x SEM image of the interior scaffold of Electrospin #6*.....61
Figure 25: *SEM image of the interior surface of scaffold fabricated from Electrospin # 7*.....62
Figure 26: *SEM image (1500x) of the interior surface of scaffold fabricated from Electrospin # 8*.....64
Figure 27: *SEM image of the interior surface at 250x*.....65
Figure 28: *SEM image (500x) of the interior surface of scaffold fabricated in Electrospin #9*.....67
Figure 29: *SEM image (150x) of the interior surface of the scaffold fabricated in Electrospin #10*.....69
Figure 30: *1500x SEM image of the interior surface of Electrospun scaffold #10*.....69
Figure 31: *Methodology used to section each scaffold for characterization and consistency studies*.....75
Figure 32: *Example image of fiber diameter measurement image with a fixed selection mask..* 76

Figure 33: *Example image of porosity measurement*.....77
Figure 34: *Example image of SEM image used to measure wall thickness*.....78
Figure 35: *Mean Fiber Diameter (µm) by Scaffold*.....81
Figure 36: *Boxplots of the fiber diameters data illustrates how the fiber diameter varied between each scaffold and respective intrascaffold section*.....82
Figure 37: *Mean Porosity (μm^2) versus Scaffold*.....84
Figure 38: *Boxplots of the porosity data illustrates how the porosity varied between each scaffold and respective intrascaffold section*.....84
Figure 39: *Mean Wall Diameter (mm) versus Scaffold*.....86
Figure 40: *Mean Young's modulus (MPa) versus Scaffold*.....87
Figure 41: *Mean Young's modulus (MPa) by Section*.....89
Figure 42: *Electrospun PLGA scaffold installed in the Cal Poly DIV-BBB model bioreactor*.....94

CHAPTER 1 - INTRODUCTION

1.1 MOTIVATION

Over a century ago evidence was found that the central nervous system (CNS) is shielded by a functional barrier preventing the passage of polar compounds from the blood to the brain [1]. It was clear that the complex and delicate neural function within the brain requires a level of homeostasis and protection from the human circulatory system more so than other tissues in the body [2]. Moreover, an understanding of the anatomy and physiology of the Blood Brain Barrier (BBB) has been and continues to be instrumental when addressing the intricate applications of drug delivery and the pathogenesis of chronic neurological diseases.

Developing an *in vitro* BBB model has garnered a tremendous amount of interest for several reasons: to enable prediction of the penetration of drug candidates across the BBB[1], to provide an understanding of how dysfunctional BBB is involved in the pathogenesis of various neurological diseases [3], and to allow pre-screening and optimization strategies for new drug and gene delivery formulations prior to performing experimentation and clinical trials on animals and humans [4]. Ideally, an *in vitro* BBB model will reproduce the physiological, anatomical, and functional characteristics of the native BBB.

Over the past several decades, research has rapidly progressed to provide information regarding the anatomy and several molecular pathways across the BBB [5,6,7,8]. This information has proven useful in developing drug delivery strategies to target sites

in the CNS in order to treat neural disorders. The use of an *in vitro* system enables research groups several major advantages, including; the ability to perform multiple tests for the same substance or to test the effects of different substances at the same time, the lack of limitation to any particular cell type, cost effectiveness compared to in vivo testing, and the lack of limitation to any specific pharmacology (i.e. modulation of phenotypic characteristics of capillary ECs) [1,5] .

Several pathologies of the CNS involve disturbance of blood brain barrier function, typically characterized with abnormal astrocyte-endotheilial cell cooperation. Specific pathological states include Alzheimer's disease, Multiple Sclerosis, Parkinson's disease, and Epilepsy [7,9,10]. Given the evidence for involvement of BBB damage as a precursor to many neurological conditions, there is a growing interest in the BBB as a therapeutic target. Rationally, if BBB dysfunction could be reduced, halted, or reversed there could be a valuable therapy to neural conditions that are altered by the aforementioned pathological states. The *in vitro* BBB model system presents the opportunity to investigate at a biochemical level the mechanisms responsible for regulating the permeability of the BBB and better understand the grounds for BBB dysfunction.

Furthermore, researchers could better predict and develop strategies for the penetration of their respective drugs across the BBB using an *in vitro* model. Cucullo et al. discussed that some of the most promising CNS drugs "failed in clinical trials due to misleading predictive permeability data extrapolated from models that were not capable of fully reproducing the functional properties of the BBB *in vivo*," [1]. As a result many groups have turned to animal models in the drug discovery process as the most reliable

means for evaluating drug permeation across the BBB [11]. However, studies performed using animal models are labor intensive, low throughput, pose an enormous burden financially, and cannot be directly extrapolated to human physiology. Accordingly, the development of a successful *in vitro* BBB system stands to potentially address these issues.

The subsequent sections of this Introduction will provide the background for which this thesis is based upon. A brief summary of the BBB structure and physiology will be provided. This will be followed by a review of several CNS disorders that are suggested to be instigated by BBB dysfunction, and the currently available *in vitro* BBB models. In order to understand the aims and goals of this thesis, a review of the methodology and theory of electrospinning will be elaborated upon, as well as current literature on cellular interactions with an electrospun scaffold. The Introduction will close with the overall goals and specific aims for this thesis.

1.2 THE BLOOD BRAIN BARRIER STRUCTURE

The Blood Brain Barrier represents the principal route of entry for most substances into the CNS. The BBB is formed by a complex cellular system of endothelial cells neighbored by astroglia, pericytes, perivascular microglia, and neurons [3]. The BBB is present at three major areas; the arachnoid epithelium, the middle layer of the meninges, and the choroid plexus epithelium as seen in Figure 1. Unlike peripheral endothelium, brain microvessel endothelial cells are characterized by the presence of a high transendothelial electrical resistance (TEER), intercellular tight junctions, minimal pinocytotic activity, and the virtual absence of fenestrations [12].

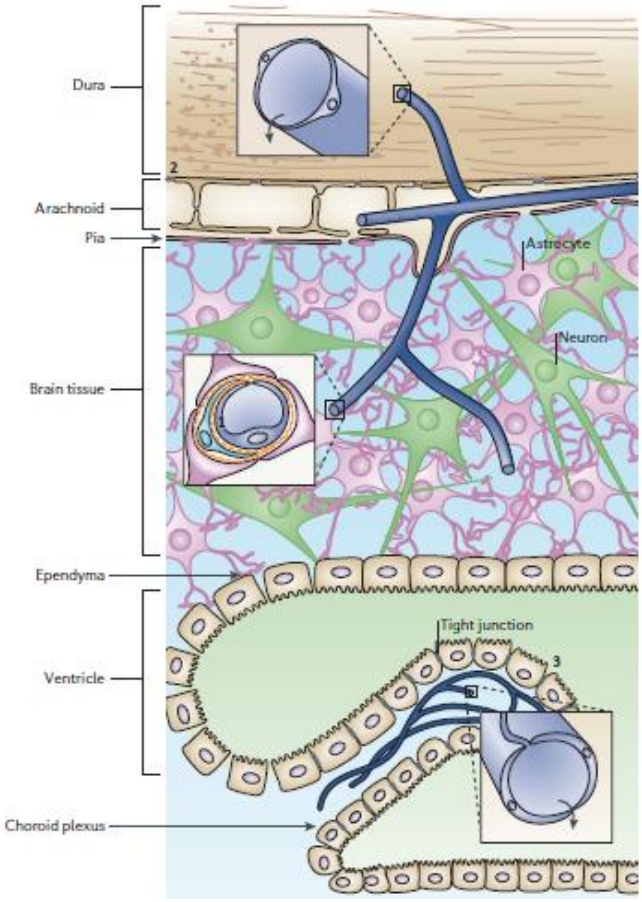

Figure 1: *Locations of the Blood Brain Barrier in the CNS*: the arachnoid epithelium, middle layer of meninges, and the choroid plexus epithelium [7].

The specialized tight junctions between the endothelial cells prevent leakage of blood-borne substances from the systemic circulation into the brain parenchyma. These tight junctions not only restrict paracellular flux, but also maintain polarity of enzymes and receptors on both luminal and abluminal sides. Signature membrane tight junction proteins includes; occludin, claudin-1, and -5, and junction adhesion molecules (JAMS) [5]. These tight junction proteins distinguish cerebral capillaries from the capillaries of other organs in the body, as illustrated in Figure 2. The brain microvasculature also includes a variety of enzymes that can activate or inactivate compounds that travel across the BBB

[8]. Additionally, the BBB is comprised of a very high level of ATP dependent transporters like nutrient carrier systems and P glycoprotein which regulate the influx and efflux of a range of compounds [8].

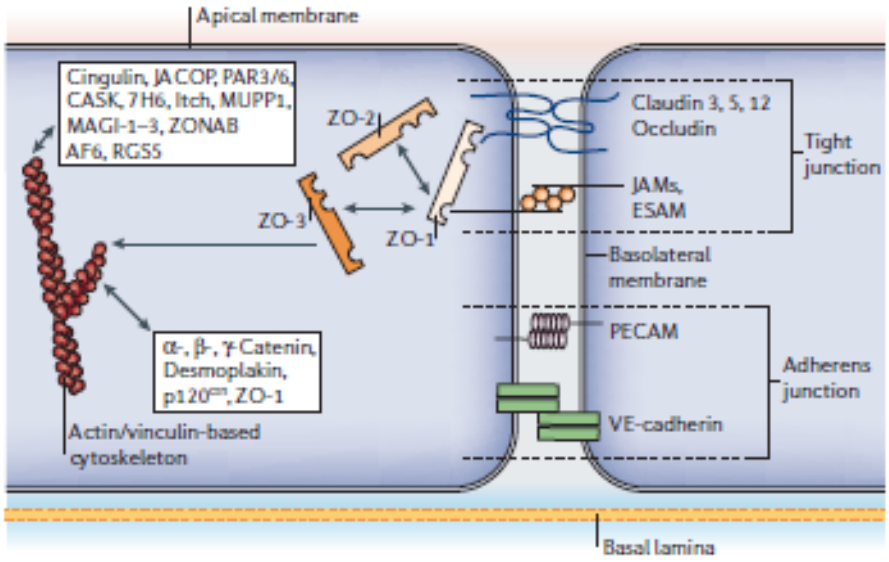

Figure 2: *Molecular composition of endothelial tight junctions of the BBB*[7]. Hallmark tight junction proteins that distinguish cerebral capillaries from capillaries elsewhere in the body include occludin, JAMS, and claudin 3 & 5.

Besides standing as a formidable obstacle for compounds that could be detrimental to the CNS, the BBB has several homeostatic functions. It restricts ionic and fluid movements, allows ion transporters and channels to regulate ionic traffic, and produces a brain interstitial fluid (ISF) that is conducive to neuronal function [6]. The BBB, with the largest surface area and shortest diffusion distances to neurons, is the most critical structure in regulating inward and outward molecular traffic, maintaining a homeostatic environment for the brain, and protecting the CNS system from harmful

toxins in the circulatory system[13]. The following section will review several pathologies that are instigated by a dysfunctional BBB.

1.3 PROMINENT CENTRAL NERVOUS SYSTEM DISORDERS INVOLVING BBB DYSFUNCTION

In several pathologies, the function of the BBB is altered, typically caused by a disturbance of the endothelial and glial cell interaction. One form of BBB disruption includes a loss of Agrin from the abluminal side of the brain endothelial cells adjacent to the astrocytic endfeet, which has been identified as an early indicator for Alzheimer's disease [14]. In addition, other characteristics of BBB dysfunction that lead to Alzheimer's disease include: increased glucose transport, up-regulation of glucose transporter GLUT 1, up-regulation of AQP4 expression, and an accumulation of amyloid β by the endothelial cells [7]. Berzin et al. demonstrated that an accumulation of amyloid-β was toxic to endothelial cells and astrocytes of the BBB before any significant neuronal loss was found in animal models exhibiting preliminary stages of Alzheimer's disease [14].

Brain tumors have been found to commonly occur with a down regulation of the tight junction proteins claudin-1 and -3 [6]. The reduction of tight junction proteins are a hallmark indicator of a dysfunctional BBB that has become significantly more permeable. As capillary endothelium of tumor vessels is highly abnormal and expresses a varied degree of fenestrated regions, vesicles, open junctions, and fragmented basal lamina to a high degree, there will be a considerable increase in permeability of the tumor vascular bed [15]. Since the capillaries of the tumor vasculature lack a complete BBB, there is

limited regulation from the systemic circulation, and additional disorders can be imminent [12].

Parkinson's Disease is another pathology that has been suggested to be influenced by BBB dysfunction. Kortekaas et al. noticed an elevated uptake of the Pgp (P glycoprotein) substrate [^{11}C]verapamil using positron emission tomography (PET) in the midbrain of patients with Parkinson's Disease [9]. This high level of Pgp substrate that is found in the midbrain is consistent with a disturbed Pgp function in the BBB [7]. Consequently, the vulnerability of a patient to Parkinson's disease has been connected to BBB dysfunction of the P glycoprotein. The stimulation of Pgp using prescription drugs or progesterone in the BBB has accordingly been considered as a novel neuroprotective strategy in preventing Parkinson's disease [9,16,17]. The next section will briefly outline currently available *in vitro* BBB models.

1.4 CURRENT *IN VITRO* BBB MODELS

In vitro BBB models have emerged as a potential investigational tool complementary to *in vivo* and human studies in basic, translational, clinical, and pharmaceutical research [13,18,19]. When compared to animal experimentation, *in vitro* models are relatively inexpensive and enable a high throughput testing (a major advantage for pharmaceutical companies studying drug permeability) [4]. In addition, the environment of an *in vitro* model allows for ease in studying and manipulating the BBB without the complex number of additional variables present when working with an entire organism.

To this point no single *in vitro* BBB model has been adopted as an industry standard. Nevertheless, the field currently consists of computational models (*in silico*), mono- and bi-dimensional cell culture models, and dynamic *in vitro* blood brain barrier (DIV-BBB) models. The DIV-BBB models have shown the most promise as a possible solution in the drug discovery process and as a resource for studying CNS pathologies [1,4,18]. This type of *in vitro* model classically consists of co-culturing endothelial cells and glial cells in hollow microporous fiber tubes that are exposed to luminal flow [4]. The shear stress derived from the luminal flow in this model has been suggested to assist in differentiation of a BBB phenotype [11]. The DIV-BBB enables reproduction of multiple functional properties and physiological responses that would be observed at the BBB *in situ* [19]. As demonstrated in Figure 3, the functional core of a typical DIV-BBB model is represented by the bundle of miroporous fibronectin-coated polyproplyene hollow fibers which permit co-culturing of endothelial cells from various origins with glial cells.

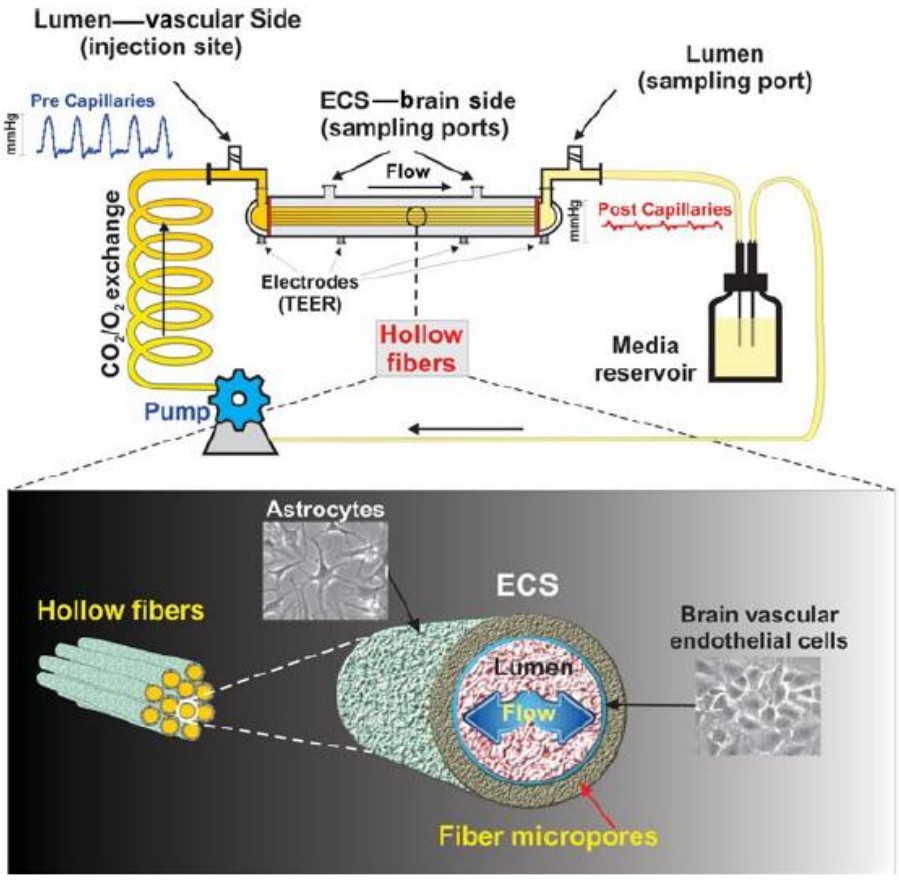

Figure 3: *Dynamic in vitro BBB model (DIV-BBB*). The top half illustrates a schematic representation of the setup. In this specific system, cerebral endothelial cells are cultured in the lumen of a several microporous pronectin coated polyproylene hollow fibers. Astrocytes were cultured on the outer surface of the hollow fibers which were coated with poly-D-lysine. The luminal side of the fiber tube is exposed to pulsatile flow and an intraluminal pressure that is physiologically comparable to that of a native capillary - typically between 5 and 23 dynes/cm^2 [19].

The hollow fiber tubes that are implemented as a scaffold in the DIV-BBB model are typically thermoplastic polymers, such as polysulfone [19] and polypropylene [4]. Other scaffolds that have been used include: polytetrafuoroethylene, polycarbonate, and polyethylene terephthalate. However, these materials have normally been used for non-dynamic bidimensional models - basically a co-culture of glial and endothelial cells in a Transwell system [18]. Moreover, the overwhelming choice of research groups

implementing the DIV-BBB has been polypropylene hollow tubes that are coated with fibronectin [1,4,13,19,20,21,22,23]. A major disadvantage to the current use of polypropylene tubes as a scaffold for culturing cells is that it is a poor substrate for cellular attachment and thus requires the application of a matrix molecule such as fibronectin or ProNectin F [4,24]. Cell attachment coatings can be fairly costly and still does not guarantee effective cell attachment [4]. Generally, the microporous polypropylene hollow fibers are fabricated using the dry-wet phase inversion method [25,26,27,28]. This method poses a major limitation on the type of polymer that can be used, as it must be soluble in a sufficiently volatile solvent [29].

Another scaffold fabrication method includes electrospinning. Electrospinning is a relatively robust and simple technique used to produce fine fibers from a wide variety of polymers [30]. Although this process has not been used for BBB scaffold production, it has long been a successful scaffold fabrication approach in the field of tissue engineering [30,31,32,33,34,35]. Accordingly, the aim of this thesis is to develop and characterize an electrospun scaffold that can be effectively utilized in the dynamic *in vitro* BBB model that is currently being developed by the Tissue Engineering group at the California Polytechnic State University, San Luis Obispo.

1.5 ELECTROSPINNING

Electrospinning is a broadly used technology for electrostatic fiber formation that utilizes a high voltage electric field to produce electrically charged jets from polymer solutions or melts, which upon drying of the solvent produce fibers with diameters ranging from 2 nm to several micrometers [30,36,37]. The process of using electrospinning

has garnered a tremendous amount of interest in the past few decades due to its versatility in spinning a wide variety of polymeric fibers and the ability to consistently produce fibers in the submicron range that is otherwise difficult to achieve using standard mechanical fiber spinning technologies [38]. Electrospun fibers have been successful in a range of applications and a variety of fields including; nanocatalysis, tissue engineering, protective clothing, filtration, biomedical, pharmaceutical, optical electronics, healthcare, biotechnology, defense and security, and environmental engineering [39].

The relatively simple and robust technique of producing electrospun fibers offers several advantages such as: an extremely high surface to volume ratio, wide variety of polymers able to be spun, tunable porosity, malleability to conform to a wide variety of sizes and shapes, and the ability to control fiber composition to achieve the desired properties and functionality [30]. Besides the success achieved from electrospinning, several obstacles still need to be addressed. In particular, scalability of electrospun fibers poses a huge challenge. The scale up of fibers through a single jet is not very feasible, and the success of several applications are contingent on a large quantity of fibers [40]. To address this, multiple research groups have used a hollow tube with several pores instead of a single syringe tip. The porous hollow tube enables several jets rather than the traditional single jet, which can increase the production rate of electrospun fibers [41]. Nevertheless, electrospinning is a unique fiber fabrication method that is constantly being studied and refined as there are many variables that influence the actual mechanics of the process.

1.5.1 History of Electrospinning

Electrospinning is a century old technique that began with the production of synthetic filaments using electrostatic forces. In 1934, Anton Formhals patented his first invention regarding the electrospinning process and the apparatus for producing artificial filaments using electric charges [31]. Formhals's spinning process consisted of a movable collector device to gather the threads or fibers. Formhals was reported to have initially spun cellulose acetate fibers using acetone as the solvent. In subsequent patents, Formhals refined his electrospinning work [36]. In the 1960s, studies were conducted by Sir Geoffrey Ingram Taylor to mathematically understand the theory of electrospinning. In particular, he modeled the shape of the cone that would form by the liquid droplet under the influence of an electric field. Hence, the field's current reference to the polymer droplet's shape out of the spinneret as the Taylor cone. In a detailed report, Taylor determined that an angle of 49.3 degrees is required to balance the surface tension of the polymer with the electrostatic forces [42]. The conical shape of the jet is an integral aspect of electrospinning as it defines the extensional velocity gradients in the fiber forming process [43].

In later years, the research shifted to studying the structural morphology of the spun fibers. Electrospun fibers were characterized using wide-angle x-ray diffraction (WXAD), scanning electron microscopy (SEM), transmission electron microscopy (TEM), and differential scanning calorimetry (DSC). In 1971, Peter Baumgarten reported the electrospinning of acrylic fibers whose diameters ranged from 0.05 to 1.1 μm [44]. His work demonstrated that the diameter of the jet reached a minimum value after an initial

increase in the applied field, and after a critical voltage point the diameter became larger with increasing electric fields. In the early 1990s, with the surge of nanotechnology and nanoscience, electrospinning gathered a great amount of interest for applications using the fibers for a variety of fields; such as high efficiency filter for media, protective clothing, catalyst substrates, and absorbent materials [45]. In the subsequent years, a variety of different polymers and melts were used for the electrospinning process. In particular, within the last decade, there has been a growing interest to exploit the electrospinning technology for tissue engineering [46]. Specifically, electrospinning has been used for the fabrication of fibrous scaffolds using a variety of natural and synthetic polymers, such as; polylactic acid [47], silk fibroin [32], collagen [48], hyaluronic acid [49], polyurethanes [50], cellulose [51], and chitosan/collagen [52].

1.5.2 Electrospinning Theory and Process

Electrospinning is a unique technique that uses electrostatic forces to create fine fibers from polymer solutions or melts. In order to produce these fibers with diameters ranging from nanometers to micrometers, a DC voltage supply with a capacity of tens of kilovolts is required. Although there is no standard setup for electrospinning, the field is primarily dominated by a setup that consists of three major components: a high voltage power supply, a spinneret (syringe tip), and a grounded collector. The collector can be a variety of materials and shapes, where some of the more common collectors include metal screens, plates, or rotating mandrels. Currently in the field, there are two electrospinning setups used, vertical and horizontal [41]. The latter has a set up in which the syringe containing the polymer solution will be located level or parallel to the collector, as seen in Figure 4.

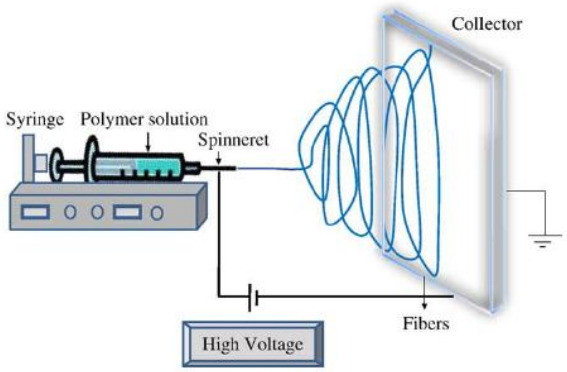

Figure 4: *Schematic of an electrospinning apparatus employing a horizontal setup* [30]. Primary components include the syringe containing polymer solution, the high voltage supply, and the grounded collector.

Prior to electrospinning, most polymers are dissolved in some type of solvent. Once the polymer is dissolved, it is loaded into a syringe, and placed onto a syringe pump. Typically, a spinneret or a needle is attached to the syringe [45]. The syringe pump is responsible for ejecting the polymer solution through the capillary tube of the spinneret. Once the polymer solution reaches the end of the spinneret, it will form a drop that is held by its surface tension. This polymer solution drop will then be subjected to an electric field. The electric field will accordingly create an electric charge onto the liquid polymer solution drop. When the electric field reaches a critical value, the repulsive electrical forces within the polymer solution drop will overcome the surface tension forces [53]. This will result in causing the drop to stretch into what is known as a Taylor cone off of the tip of the spinneret as seen in Figure 5 [54]. From the tip of the Taylor cone a charged jet is ejected. The charged jet will maintain a uniform shape and is stable for only a few millimeters beyond the spinneret [55]. After a few millimeters, the jet demonstrates an

unstable and rapid whipping until it reaches the collector. As the jet is unstable and making its way to the collector, the solvent of the polymer solution is evaporating, hence, leaving a polymer behind that aggregates on the collector [30].

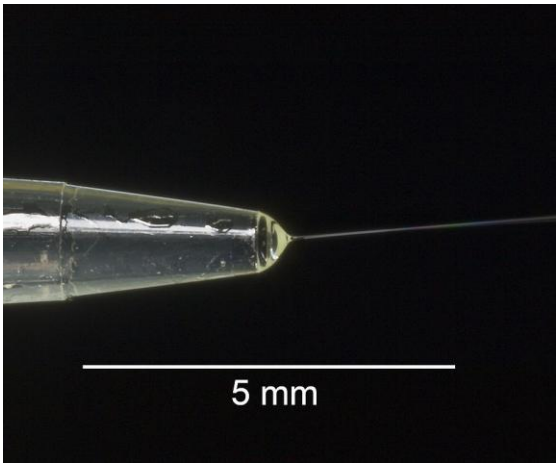

Figure 5: *Image of the formation of a Taylor cone* [54]

1.5.3 Effects of Various Parameters on Electrospinning

The electrospinning process is controlled by many parameters that are broadly categorized into solution parameters, process parameters, and ambient parameters. Solution parameters consist of viscosity, conductivity, molecular weight, and surface tension. The processing parameters encompass the applied electric field, tip to collector distance, and flow rate or ejection rate of the polymer solution. The ambient parameters include the humidity and ambient temperature. By properly manipulating any of the parameters listed above, the morphology and fiber diameter of the electrospun fibers can be controlled.

1.5.3.1 Solution Parameters

Depending on the polymer and solvent that is used to create the polymer solution for the electrospinning process, an optimal solution concentration is required. With a low solution concentration, a common trend is to see "beads on a string" form along the fibers as shown in figure 6 [30,45,56]. Sukigara et al. demonstrated that too low of a solution concentration resulted in no fiber formation, and that an 8% solution concentration of fibroin silk in formic acid produced fibers with beads or drops of polymer within the fibers [56]. The formation of these droplets or beads is due to the capillary breakup of the jet by the surface tension of the polymer solution. The filaments between the droplets are stabilized and the characteristic "bead on a string" structure is formed [57]. Whereas with a high solution concentration, the formation of continuous fibers is impeded because of the inability to maintain the flow of the solution through the needle or spinneret [56].

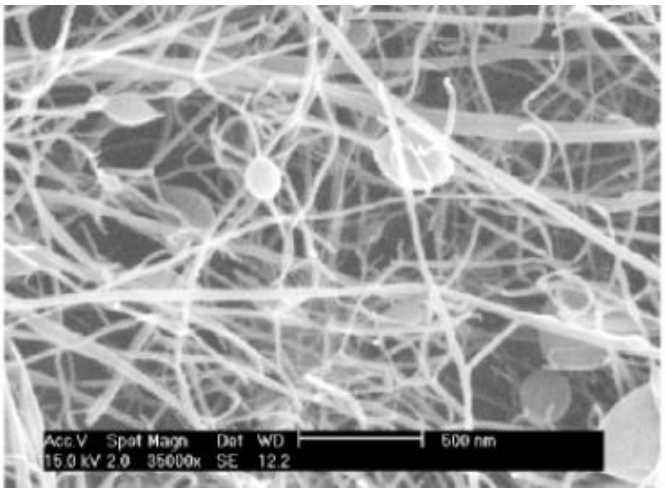

Figure 6: *"Beads on a string" formation.* Gold sputtered SEM image of electrospun fibers at 35000x. A fibroin silk was dissolved in formic acid to produce a solution concentration of 8% [56].

The molecular weight of the polymer influences properties like the viscosity, surface tension, conductivity, and dielectric strength. Molecular weight of the polymer suggests the number of entanglements of the polymer chains, which can influence the morphology of the electrospun fiber [30,35]. Generally, too low of a molecular weight for a polymer will form beads instead of fibers during the electrospinning process. While a high molecular weight results in fibers with a larger average diameter [58].

The viscosity of the polymer solution is another solution parameter that requires an optimal balance. If the viscosity of the polymer solution is too high, it is difficult for the polymer to traverse the needle and properly eject as a jet when an electric field is applied. The surface tension forces are too strong to be overcome by the electrostatic forces. Additionally, at a high viscosity, polymer solutions tend to exhibit longer stress relaxation times, which is suggested to prevent the fracturing of the jet during electrospinning, and create continuous fibers [30]. For the aforementioned reason, a low viscosity would reflect shorter stress relaxation times, and result in disturbances of the jet. These disturbances of the polymer jet will result in non-continuous fibers, as well as non-uniform fibers with "beads."

Most polymers are conductive, and the charged ions within the polymer solution are instrumental in jet formation. Typically the conductivity of a polymer solution is dictated by the polymer type, the solvent, and the availability of ionizable salts within the solution. With an increase in the electrical conductivity of the polymer solution, the applied electric field creates an electrical force that elongates the jet that emerges from

the Taylor cone so that the electrospun fibers have a smaller diameter. However, Hayati et al. demonstrated that polymer solutions that are too conductive are very unstable in the presence of an electric field, and will result in significant bending of the jet at the Taylor cone and create fibers with a broad range of fiber diameters [40]. Mathematically, it has been suggested that the jet radius varies inversely with the cube root of the electrical conductivity of the polymer solution [44].

1.5.3.2 Applied Voltage

The applied voltage is a crucial processing parameter that directly influences the dynamics of fluid flow. The electrospinning process requires a high voltage to be introduced to the polymer solution to induce charges within the fluid and create an electric field to propel the fibers along the potential difference that is created. Only once a threshold voltage is reached will fiber formation occur [30]. Literature has suggested in several studies that with higher applied voltages, there is an obvious increase in electric field strength that increases the electrostatic repulsive force on the jet that emerges from the Taylor cone and results in a smaller fiber diameter [30,41,44,53]. Due to the greater columbic forces within the jet, and the stronger electric field there is a greater stretching of the polymer solution and a more rapid evaporation of the solvent, which creates a reduction in fiber diameter size.

Jacobs et al. studied the effects of applied voltage on the morphology of electrospun fibers using a poly ethylene oxide (PEO) solution [59]. The group noted that with a low applied voltage of 5kV, there would be an irregular formation of fibers, bead like structures, a thicker fiber diameter, and a proper Taylor cone would not form [59]. The

same research group found that an applied voltage of 20kV would decrease the fiber diameter and offer more uniformity throughout the electrospun fibers. When the voltage was increased to above 25 kV the beads that formed at 5 kV were present again [59]. With the increase in voltage to above 25 kV the polymer solution droplet that would form at the end of the spinneret would recede completely. As a result the jet was initiated from within the capillary, without the formation of a Taylor cone. A similar observation was found by Larrondo et al., who also demonstrated that the fiber diameter would decrease by nearly half when the applied voltage was doubled [60]. Additionally, the group noticed that the aforementioned statement only held true up to a certain voltage, and that when the voltage was increased too high, there was a greater probability for large beads to form throughout the fibers.

1.5.3.3 Flow Rate

The flow rate or feed rate of the polymer solution from the syringe is a critical parameter that affects the jet velocity, Taylor Cone formation, and material transfer rate. It is important to strike a balance between the applied voltage and flow rate. Fundamentally, the applied voltage is stretching or pulling the polymer solution toward the collector, while the syringe pump is ejecting the polymer solution toward the collector. Hence, it is important that an optimal balance is found so that a Taylor cone is formed and uniform fibers are produced. A lower feed rate is more desirable as the solvent will get enough time for evaporation, and result in a smaller and more consistent fiber diameter [61]. Wannatong et al. studied the effect of flow rate on electrospinning as well, and found that when the flow rate is too high, the fibers form large beads, as there was not enough time for the solvent to dry prior to reaching the collector [62].

1.5.3.4 Gap Distance

Another component to the electrospinning process is the gap distance - the distance the grounded collector is placed from the tip of the spinneret. The space between the two offers the solvent time to evaporate before the polymer becomes dry and aggregates on the collector. The influence this parameter has on fiber morphology is not as significant as the other parameters discussed above. Zhang et al. studied the effects of this parameter while electrospinning poly vinyl alcohol (PVA) and found no noticeable trends with the gap distance parameter [63]. However, it has been suggested that flatter fibers are produced at closer gap distances, and that at larger gap distances the fibers tend to be more rounded [43]. Moreover, as discussed earlier it is important to find an optimal gap distance that allows the solvent enough time to evaporate before the polymer reaches the collector.

1.5.3.5 Ambient Parameters

Besides the solution and processing parameters there are ambient parameters such as temperature and humidity that can influence the electrospun fiber morphology. Mit-Uppatham et al. studied the effect of temperature on the electrospinning of polyamide-6 fibers ranging from 25˚C to 60˚C and discovered that an increase in temperature reduced the fiber diameter [64]. The group suggested that since there is an inverse relationship between temperature and viscosity, the increased temperature would decrease the viscosity of the polymer solutions, and as a result lead to smaller fiber diameter sizes [64].

Casper et al. investigated the influence of the ambient parameter humidity on electrospun polystyrene solutions [65]. The research group found that an increase in

humidity resulted in the appearance of small circular pores on the surface of the fibers, and that further increasing the humidity would lead to pores that would coalesce [65]. At a low humidity, the evaporation rate of the solvent would be faster, which could clog the spinneret within minutes. It is important to have an ambient humidity that will be conducive to the evaporation of the solvent as the polymer solution leaves the tip of the spinneret to the collector. Moreover, it is important to remain aware that the ambient parameters can also influence the electrospinning process.

All of the parameters discussed in the sections above influence the final fabrication product, the electrospun fiber. Since there are so many variables that can affect the process, it is important to be mindful of each parameter and find a balance. Typically through trial and error, many groups have succeeded in creating electrospun fibers that are consistent, uniform, and effectively enable cellular interactions for tissue engineering applications [30,31,41,52,65].

1.6 CELL INTERACTIONS WITH AN ELECTROSPUN SCAFFOLD

The physical and spatial architectural geometries of electrospun scaffolds are crucial to their application in tissue engineering strategies. Specifically, the pore size, surface topography, structural size-scale, and porosity are instrumental features of a scaffold that affect cell attachment, proliferation, migration, and/or differentiation [30]. Due to the complexity and intricacy of different cell types and behavior, there is the challenge of designing and fabricating the ideal scaffold for tissue engineering. The optimal pore size for cell attachment, proliferation, and migration is not constant across cell types but varies from 5 to 500 μm [46]. Pham et al. suggests that as electrospun fiber diameter is

increased, the average pore size is increased as well. This particular group measured the pore size using mercury porosimetry [31].

Eichhorn et al. investigated the influence of fiber diameter on pore size, and cell infiltration [35]. The group suggested that the decrease in electrospun fiber diameter resulted in more fiber-to-fiber contacts per unity length and lead to a reduced average pore radius. The smaller pore size decreased cell infiltration and attachment of cells, because of the physical size of fibroblasts, osteoblasts, and chondrocytes which have a mean size of 10 μm [35]. Pham et al. reported that electrospun microfiber meshes (approximately 5 - 10 μm in diameter) used with a dynamic flow perfusion culture resulted were ideal in terms of cellular infiltration and attachment [33].

With regard to tissue engineering, another challenge in using electrospun scaffolds and sheets is non-uniform cellular distribution as well as poor cellular infiltration within the scaffold under normal passive seeding conditions. Reasons for poor cellular distribution and infiltration include inconsistencies in the porosity of the scaffold and the diameter of the fiber [30]. According to Eichhorn et al. with the decrease of the electrospun fiber diameter there is an increase in the number of fiber to fiber contacts per unit length, and as a result a decrease in the mean pore radius [35]. Consequently, there is an inherent mismatch between the larger physical size of the cells and the small pores in the electrospun structure. This limits the ability of the cells to migrate and populate the interior of the scaffolds. Several methods have been developed in order to better promote cellular infiltration in three dimensional electrospun scaffolds. The co-deposition of a polymer solution with Heprasil has been found to be a very successful solution. Heprasil is a synthetic thiol modified hyaluronic acid, that has been developed for 3D cell culture

and tissue engineering [30]. The co-deposition using heprasil results in the creation of enzymatic degradable matrix pockets within the densely electrospun fibers in which cells can better migrate through the increasing depth of the scaffold [66]. In addition to these methods, manipulating the processing and solution parameters in the electrospinning process is the most practical means of developing a scaffold with specific characteristics.

Electrospinning is far from being an exact science, as there are countless variables to consider. However, by implementing an ideal set of parameters an electrospun scaffold with desired characteristics can be fabricated. Electrospun fibers offer several advantages: a high surface-to-volume ratio, tunable porosity, malleability to conform to a range of sizes and shapes, and the ability to control fiber composition. Tissue engineering blood vessels using electrospun scaffolds has demonstrated great promise [67]. Accordingly, the overall goal of this thesis is to characterize and develop an electrospun scaffold for use in a BBB model, which will be further discussed in the next section.

1.7 OVERALL OBJECTIVE AND AIMS OF THE THESIS

Developing an appropriate *in vitro* model of the BBB will prove to be a major advancement for future research into understanding CNS pathologies that result from BBB dysfunction. Additionally, the model will serve as a cost effective and high throughput alternative for the drug discovery process of CNS targeting pharmaceutical drugs. Currently, one of the most promising models is a DIV-BBB that implements polypropylene hollow fibers coated with ProNectin F as a scaffold [24]. To recreate and improve upon this model, work is being done in the Tissue Engineering lab at Cal Poly to develop a functional DIV-BBB. One aspect of creating a functional DIV-BBB is the

scaffold, and thus the Cal Poly lab needs the capabilities to create small diameter tubular polymers. Therefore, this thesis will focus on creation and characterization of an electrospun scaffold for the DIV-BBB. A protocol will be developed in order to produce a consistent and repeatable small diameter scaffold. Ultimately, the electrospun BBB scaffold developed in this thesis will be implemented in the DIV-BBB setup that is currently being created which utilizes an in-house perfusion bioreactor and is pressure sodded with BAEC and C6 glial cells.

Therefore the specific aims of this thesis are:

(i) To optimize, refine, and update the current electrospinner system employed by the Tissue Engineering group at California Polytechnic State University, San Luis Obispo.

(ii) To write a protocol with finalized processing and solution parameters that can be used to consistently fabricate 2 mm inner diameter scaffolds for a DIV-BBB setup.

(iii) To fabricate and characterize the 2 mm PLGA electrospun scaffolds using Scanning Electron Microscopy (SEM) and tensile testing.

CHAPTER 2 - OPTIMIZATION OF THE ORIGINAL ELECTROSPINNER SYSTEM

2.1 INTRODUCTION

A basic electrospinning system typically consists of three major components: a high voltage power supply, a spinneret (i.e. a needle), and a grounded collecting plate (i.e. a rotating metal mandrel) [45]. As the polymer solution is forced through the spinneret using a syringe pump, a high voltage power supply will be used to inject charge of a certain polarity into the polymer solution [30]. The power supply is connected to the metal spinneret, which will conduct the high voltage and induce a charge into the polymer solution [45]. Additionally, an electric field is created by the potential difference formed between the spinneret and the grounded collector.

Upon reaching the end of the spinneret, a suspended conical droplet of the polymer solution is formed. If formed properly, the surface tension of the droplet is in equilibrium with the electric field [68]. When the applied electric field is increased to a critical value, the repulsive electric force overcomes the surface tension force to produce a Taylor cone from which a small charged jet erupts from the surface of the droplet and is drawn towards the collecting plate. Because the jet is charged, its trajectory can be controlled by the electric field [53]. As the jet propagates towards the collecting plate, the solvent in the jet will gradually evaporate and leave behind a charged polymer fiber

which will lay itself on the collector [53]. Over a period of time, continuous fibers are laid to form a non-woven fabric.

The entire electrospinning process is governed by several parameters, which were discussed in Chapter 1. The processing parameters in particular, such as applied voltage and flow rate, are heavily dependent on the functionality and proficiency of the electrospinner system. Depending on the application, an electrospinner system will employ a variety of arrangements and equipment. The Tissue Engineering group at the California Polytechnic State University, San Luis Obispo implemented a robust and well-designed system in 2009 for the purposes of creating custom vascular scaffolds [69]. This system was refined and optimized in accordance to the first aim of this thesis. The majority of the modifications that were made to the electrospinner system at Cal Poly were necessary due to financial limitations when the system was first built and the several years that have passed since the system was first designed. This chapter will focus on the electrospinner system and its components before and after being optimized, as well as on a brief proof of concept study utilizing the new system.

2.2 ORIGINAL ELECTROSPINNER SYSTEM

The original electrospinner system was designed with the purpose of enabling in-house fabrication of Blood Vessel Mimic scaffolding. This system consisted of all the standard features found in a typical electrospinner: a high voltage power supply, a spinneret, syringe pump (to feed the polymer solution through the spinneret), and a collector. The system was constructed piece by piece from components supplied by various companies [69]. The isolation chamber, collection system, and syringe pump were

located within a fume hood since harmful solvent vapors are produced during the electrospinning process [70]. The rest of the electrospinning system resided outside of the hood, including: the collection system speed regulator, high voltage supply, amplifier, AC/DC transformer, and dual switch relay.

The unique aspect of the electrospinner system utilized at Cal Poly was the collection system. In order to produce tubular geometries of electrospun fibers, a rotating/ translating grounded mandrel collection system was developed. The apparatus was machined and assembled by Custom Design and Fabrication (Richmond, Virginia) [69]. A regulator connected to the apparatus controls the revolutions per minute (RPM) of the mandrel and the oscillations per minute (OPM) at which the metal mandrel translates back and forth as illustrated in Figure 7 [69]. Both translation and rotation of the metal mandrel (collector) allows for the electrospun fibers to create a layered tubular geometry on the cylindrical mandrel. These tubular geometries mimic the generally cylindrical shape of the vasculature found in the human body.

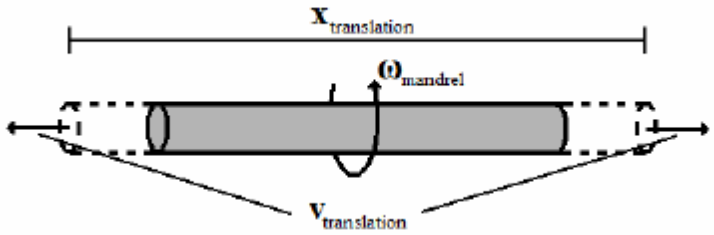

Figure 7: *Metal Mandrel translation and rotation capabilities.* The translation distance of $X_{translation}$ can be controlled as the apparatus is set on a swing arm wheel that allows for $X_{translation}$ to be adjusted. The angular velocity ($\omega_{mandrel}$) and translational velocity ($v_{translation}$) are both controlled by a regulator [69].

The original electrospinner system was well built, however, there were several aspects that could be improved upon. Specifically, the high voltage power supply, electrical safety, and the syringe pump setup were all in need of upgrading or refinement. The original power supply required several accessories in order to function, and had relatively limited capabilities. The electrical layout of the original electrospinner system required extensive electrical wiring and splices, all of which had the potential to introduce electrocution and fire hazards. Additionally, the original syringe pump became faulty, and required replacement as well as the stand it was set on. All of the aforementioned components that required improvement will be further discussed in the sections below.

2.3 HIGH VOLTAGE POWER SUPPLY

2.3.1 Original Power Supply

One of the most important components of any electrospinner system is the high voltage power supply. The original system at Cal Poly incorporated a K7-30R high voltage power supply from Matsusada Precision Inc. (Kusatsu-City, Japan), which was capable of output voltages from 0 to 30,000 V at a current of 250 µA [69]. A limitation of this power supply was that it required a separate DC power supply with a 1 to 10V range to act as an amplifier for high voltage output. Specifically, a Heathkit IP-2718 DC power supply provided an amplifying factor of 3000. Thus, a setting of 5 V on the external power supply would equate to a high voltage output of 15kV. In addition, as the power in the laboratory where the electrospinner is housed originates from a wall receptacle, the power is alternating current, approximately 110 V_{AC}. Since the K7-30R high voltage

power supply required 24 V_{DC} at 1.3 A, the system included a Kele PS5R-SC AC/DC transformer to convert the power. Also, a two switch array was setup to control the power supply, amplifier, and AC/DC transformer. The complete high voltage power supply and accessories of the original electrospinner can be seen in Figure 8.

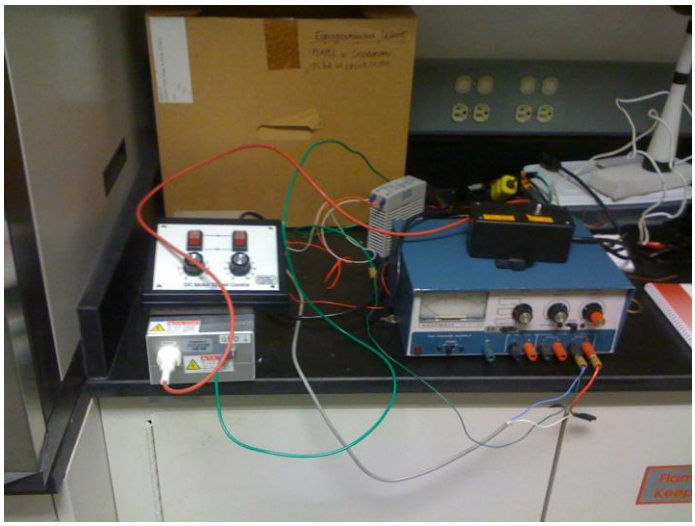

Figure 8: *Original High Voltage Power Supply setup*. The original power supply required an amplifier, an AC/DC transformer, and a dual switch relay to control all of the aforementioned components.

The original power supply necessitated several electrical components, a significant amount of wiring, and operator interaction. Specifically, the original system required a sequence of relay switches that needed to simultaneously be turned ON in order to function (see Appendix B, Original Electrospinning protocol). If the sequence of switches was not turned ON or OFF properly, it was highly probable that the equipment could be irreversibly damaged. For this reason, it was important that a new power supply be consolidated to a single unit that could utilize alternating current and not require an AC to DC transformer, switch relay, or an amplifier.

Additionally, while the original power supply was being utilized by a former master's student, he had reported that the external amplifier had overdrawn current and become faulty [69]. This malfunction resulted in the power supply only permitting a maximum voltage of 18kV instead of 30kV. Another noticeable problem that arose at the start of this thesis was that the voltage applied to the spinneret would fluctuate according to the voltage output meter located on the supply. A possible explanation for the faulty power supply could have been the multiple wire splits and components required (AC/DC transformer, amplifier, dual relay switch) had caused the system to overdraw current or perhaps create an electrical short circuit in the system due to damaged insulation or loose connections. Since the power supply is a sensitive electrical instrument, an electrical short could cause permanent damage to the power supply.

2.3.2 Criteria Used to Select New Power Supply

Besides the safety and maintenance issues of the original supply, new developments and strategies are actively transforming the standard technique used to electrospin [41,58,70,71]. With the guidance of Dr. Eugene Boland, Ph.D - a prominent figure in the electrospinning field- and current literature, it was within the first aim of this thesis to implement a power supply that would enable the electrospinner system to employ new electrospinning strategies [72,73,74,75,76]. Reversing the polarity of the applied voltage from positive to negative has been thoroughly investigated as a potential parameter that could affect the morphology and size of electrospun fibers [71,77,78,79]. Based on the conductive properties of a given polymer, Sutasinpromprae et al. suggested that the charged species within the polymer may react differently when the polarity of the charge injected is reversed [79]. Conflicting literature exists on whether the polarity truly influences fiber

morphology. Doshi and Reneker reported that the polarity of the electric potential did not have any effect on the electrospinning process [53]. Supaphol et al. reported that a negative polarity had resulted in larger and flatter fibers [78]. Dr. Eugene Boland had suggested that based on trial electrospins, a negative polarity could fine tune fiber morphology [80]. Moreover, depending on the conductive properties of the polymer solution being electrospun, the polarity of the applied voltage may create differences in fiber morphology and homogeneity. As a result, while searching for an adequate power supply, a reversible polarity function for the applied voltage was one of the top priorities.

Another electrospinning strategy involves a non-traditional setup that utilizes two power supplies simultaneously, one to create a positive applied voltage at the spinneret, and another supply to create a negative voltage at the collector. According to Subbiah et al., the idea behind this strategy is to alter the shape of the macroscopic electric field that extends from the spinneret to the collection target in such a way that the field lines converge to a point right above the collection target [37]. By controlling the electric field lines, the bending instability of the electrospun fibers could be dampened, and result in smaller fiber diameters. This theory was based on the results of electrospinning a poly(ethylene oxide) polymer solution using the aforementioned two power supply setup [81]. Accordingly, the capability to implement this non-traditional setup in the new Cal Poly electrospinner was another aspect used to select a power supply.

Since the original electrospinning equipment began demonstrating severe inconsistencies in providing a constant supply of applied voltage, and did not have the capacity to employ the strategies discussed above, several companies were contacted and consulted about purchasing a new high voltage power supply. Key criteria that were

considered included: operator safety, a self-contained unit that can utilize an input voltage from a standard wall outlet, reversible polarity, at least a 0-30kV capacity, and the potential to use two power supplies simultaneously in a non-traditional electrospinning setup. The options and cost estimates that were considered are summarized in Table 1.

Table 1: *Summary of options considered for the new high voltage power supply*. Several companies were consulted with and provide cost estimates for each of the power supplies described above. Ultimately, the Gamma High Voltage Model D-ES30R-10N-5W/M was selected.

	Manufacturer	Specifications	Input Voltage	Price
Gamma Model ES30R-5W	Gamma High Voltage	0-30kV, 166 µA REVERSIBLE polarity (open box to switch) Analog Voltage meter	90-240AC	$1,500.00
Gamma Model ES30R-5W	Gamma High Voltage	0-30kV, 166 µA REVERSIBLE polarity (open box to switch) Digital voltage and current output meters	90-240AC	$1,650.00
Gamma Model D-ES30R-10N-5W/M	Gamma High Voltage	Output #1: 0-30KV, 166uA REVERSIBLE polarity (front panel switch) Output fully adjustable via front panel potentiometer Analog meter to read output voltage and current Output #2: 0-10KV, 500uA Output polarity Negative Output fully adjustable via front panel potentiometer Analog meter to read output voltage only	90-240AC	$2,433.50
CZE1000R	Spellman High Voltage Electronics Corporation	0-30kV, 300 µA REVERSIBLE polarity (front panel switch) Analog Voltage and current meter Output fully adjustable via front panel potentiometer	115VAC	$3,645.00
SL30 P10	Spellman High Voltage Electronics Corporation	0-30kV, 300 µA SINGLE polarity Analog Voltage and current meter Output fully adjustable via front panel potentiometer	115VAC	$2,625.00
EL30R1.5	Glassman High Voltage	0-30kV, 1.5mA SINGLE polarity Analog Voltage and current meter Output fully adjustable via front panel potentiometer	105-125 VAC	$2,150.00

After careful consideration, the Gamma High Voltage Model D-ES30R-10N-5W/M was selected. The manufacturer agreed to custom design and build a high voltage power supply that could employ all of the strategies discussed above at an adequate cost. The details of the new power supply will be discussed in the next section.

2.3.3 New High Voltage Power Supply

The Gamma Model D-ES30R-10N-5W/M is a dual output power supply, that incorporates two individual supplies that can be independently controlled and used simultaneously. The first output has a range of 0 to 30kV, current of 166µA, and a reversible polarity. The second output has a range of 0 to 10kV, current of 500µA, and a negative polarity. This power supply has an amplifier built within the system, and has the ability to use a standard wall outlet. Hence, the new power supply did not require the transformer and external amplifier the original system required. Accordingly, this power supply was completely self-contained as seen in Figure 9. Overall, the new power supply has the capacity to function exactly like the original power supply, while also employing additional innovative electrospinning strategies that will surely be useful for scaffold fabrication for the BBB model, as well as future tissue engineering scaffold investigations.

Figure 9: *New high voltage power supply.* This new custom built voltage supply by Gamma High Voltage was selected for its reversible polarity capabilities, AC input power abilities, and the ability to use a negative polarity of up to 10kV instead of a ground wire on the mandrel collector in a non-traditional setup.

2.4 ELECTRICAL LAYOUT AND SAFETY

Electrostatic forces created by a potential difference using an applied voltage serves as the driving force for the electrospinning process. Consequently, the process requires a significant amount of electrical design and support that can pose electrocution and fire hazards. As mentioned in section 2.3.1, the high voltage power supply for the original electrospinner system required multiple components: an AC to DC transformer, an amplifier, a dual relay switch, and the high voltage power supply. Additional electrical requirements for the overall electrospinning setup include: grounding the rotating/ translating collection system (mandrel), directly applying the high voltage to the spinneret, and providing power for the syringe pump and speed regulator for the collection system. Under the guidance of Mr. Dave Laiho and Mr. Ralph Nicovich of the Biomedical Engineering department at Cal Poly, the new system's electrical wiring network was created with the intention of ensuring simplicity and safety.

The new self contained voltage supply immediately alleviated the electrical intricacy of the original power supply and its accessories. To reduce the footprint and increase isolation of the entire electrospinner system, all of the components were relocated to be contained within the fume hood. Furthermore, the original electrospinning system required all of the electrical equipment to be connected to individual wall outlets. To prevent damage to any of the electrical equipment of the electrospinner system from electrical spikes, dropouts, and surges that commonly occur from using a wall outlet, all of the electrical components were plugged into a single surge protector strip. Additionally, in order to prevent the electrical wiring from being tangled, to promote organization of the electrical network, and to reduce operator contact with electrical equipment, the isolation chamber was fitted with electrical bulkhead fittings for the ground wire and applied voltage (Figure 10). A 1 cm mouse hole was created in the isolation chamber to allow wiring from the collection system to connect with the speed regulator. Also, to ensure maintenance of the electrospinner system and operator safety, the high voltage power supply was grounded to the chassis of the fume hood.

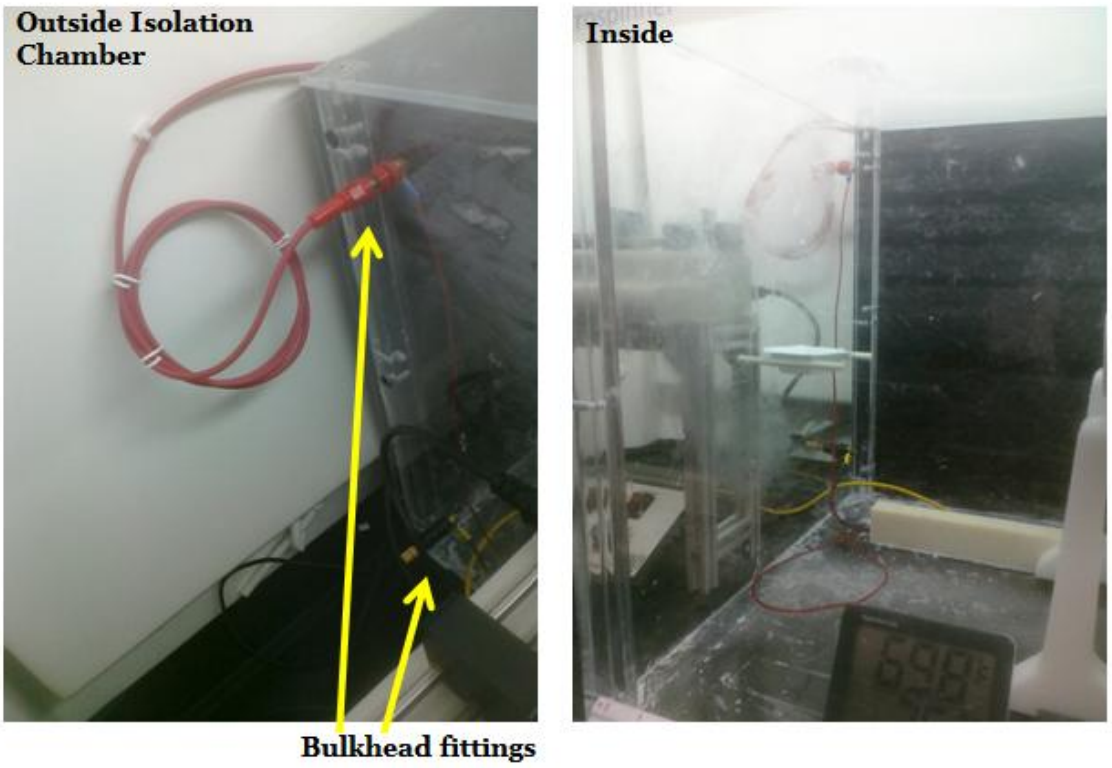

Figure 10: *Isolation chamber fitted with electrical bulkhead fittings.* Electrical bulkhead fittings were installed into the wall of the isolation chamber for the applied voltage (red) and the ground wire for the metal mandrel (black). In addition, a 1 cm mouse hole was drilled into the chamber below the ground bulkhead fitting to allow the translation and rotation wire of the collection system to reach the regulator (yellow wire).

2.5 SYRINGE PUMP SETUP

The original electrospinner system employed a KD Scientific Model 100 syringe pump (Holliston, MA) to eject the polymer solution through the spinneret. In order to inject charge into the polymer solution, an electrical alligator clip was wired from the high voltage power supply and attached to the spinneret exposed inside the isolation chamber. As discussed earlier, the syringe pump will feed the polymer solution through the spinneret at a controlled volumetric rate, the applied voltage induces charge and creates an electric field between the spinneret and the grounded collector, leading to the formation of a Taylor cone and a polymer jet. The syringe pump was elevated using a

stand so that the polymer jet produced from the spinneret was level with the metal mandrel.

The original syringe pump stand was improvised using particle board attached to four metallic rods held together by latex that provided limited assurance of a level platform (Figure 11A). Undisturbed proper Taylor cone formation is critical for consistent fiber production [77,82]. Accordingly, a four legged aluminum stand was custom built by Mr. Dave Laiho to fit the dimensions of the KD Scientific Model 100 syringe pump and securely situate it outside of the isolation chamber (Figure 11B), so that the spinneret would remain stable throughout the electrospinning process.

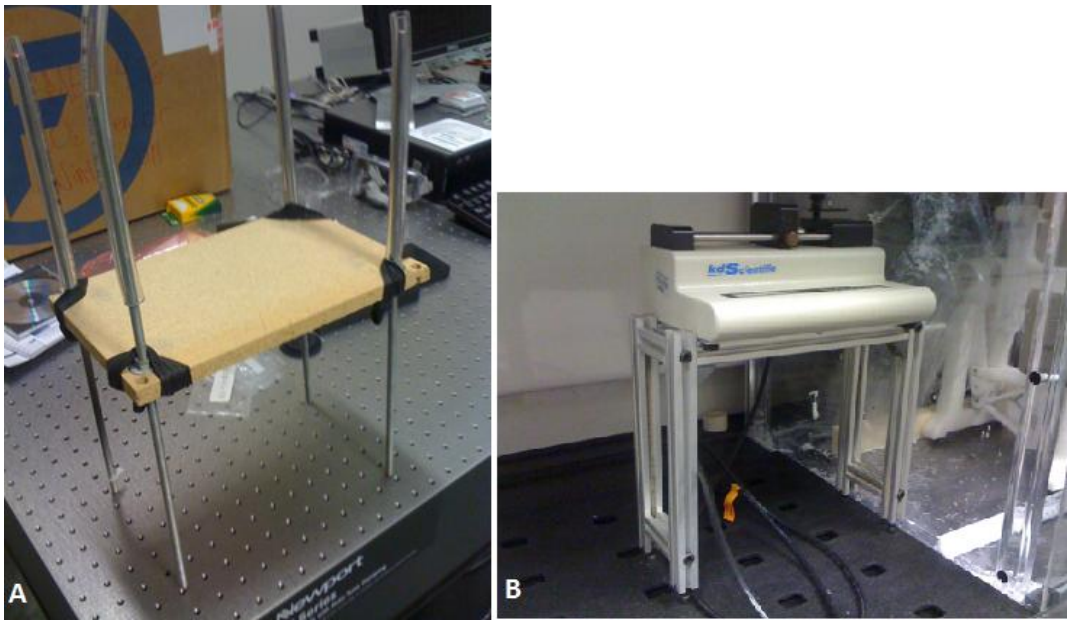

Figure 11: A) *Original Syringe Pump Stand.* Particle board raised with four metal columns and held together using latex. **B**) *New Syringe Pump Stand.* Custom built aluminum stand, designed to accommodate the dimensions of the KD Scientific Model 100 Syringe Pump.

Furthermore, the original syringe pump was inconsistent and would often display a POWER FAILURE error message. This error message signified an input power malfunction. In addition, on several occasions the stage used to apply pressure on the

syringe plunger would fail to move. As the syringe pump had been used considerably, and the lifespan for the motor can be as low as three to four years, it was determined that the faulty syringe pump should be replaced. Several options were considered, and summarized in Table 2.

Table 2: *Summary of Syringe pumps considered for replacement.* After careful consideration, the KDS 100 manufactured by KD Scientific was selected.

Model	Manufacturer	Syringe Size Range	Dimensions (inches)	Approx. Cost
Classic F100	Chemyx	0.5 µl to 60 ml	9.5 x 6.5 x 4.5	$925.00
KDS 100	KD Scientific	10µl to 60 ml	9 x 6 x 5	$1,100.00
Legato 100	KD Scientific	0.5 µl to 60 ml	9 x 7.5 x 5	$2,150.00
EW-74900-00	Cole-Parmer	0.5 µl to 60 ml	9 x 4 x 6	$1,371.00
Pump 11 Plus Single Syringe	Harvard Apparatus	0.5 µl to 60 ml	9 x 5 x 4.5	$1,895.00

The criteria used to select a new syringe pump included: reasonable cost, capability to eject volumes of as low as at least 2mL (volume of polymer solution used for BBB application), and the ability to fit the dimensions of the new syringe pump stand that was already custom built. Ultimately, the KDS 100 from KD Scientific was selected, as it was the only syringe pump to meet all of the requirements mentioned above.

2.6 COMPARISON OF THE ORIGINAL AND OPTIMIZED ELECTROSPINNER SYSTEMS

The improvements discussed in the previous sections can be clearly seen by comparing the original and optimized electrospinner systems in Figures 12 and 13 respectively. Noticeable differences include: the new power supply, the new syringe pump and stand, consolidation of the entire system within the fume hood, as well as the simplicity and safety of the electrical network.

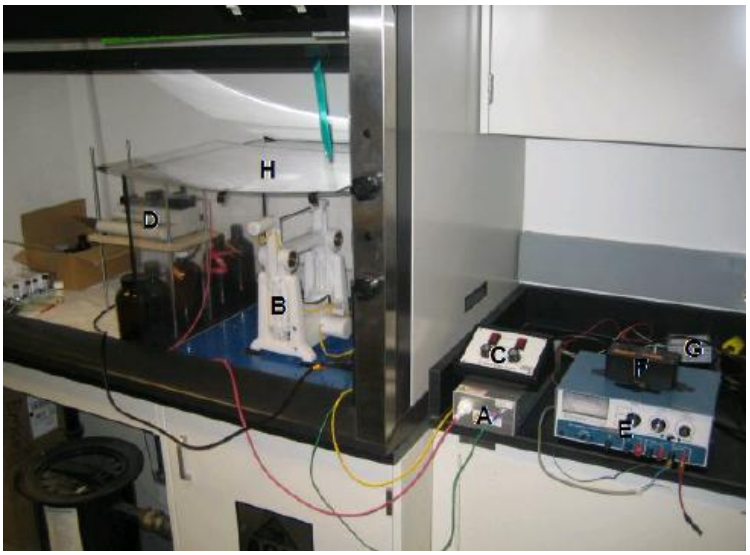

Figure 12: *Original Electrospinner System employed at Cal Poly*. Specific components included a high voltage power supply (A), a rotating/translating collection system that secures a grounded mandrel as a collector (B), a dual speed regulator (C), a syringe pump for polymer solution infusion (D), an external power supply (E), a dual switch array (F), an AC to DC power converter (G), and an isolation chamber (H) [69].

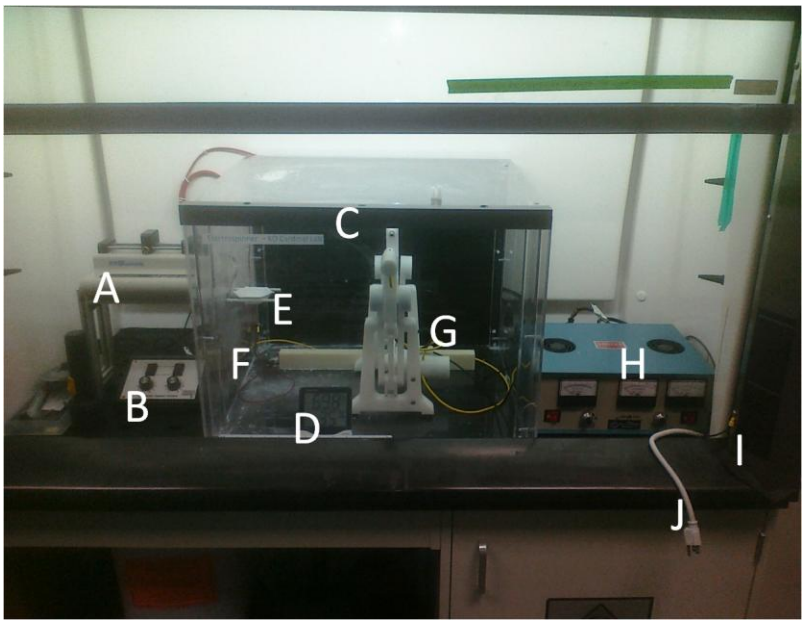

Figure 13: *Optimized Electrospinner System setup*. (A) Syringe pump for polymer infusion, (B) Regulator for rotation and translation of collection system, (C) Isolation chamber, (D) Electronic Thermometer and Hygrometer for ambient readings, (E) Polymer Drip tray, (F) Electric Bulkhead fittings, (G) Collection system- rotates and translate grounded mandrel, (H) High Voltage Power Supply, (I) System grounded to chassis of fume hood, (J) Surge Protector Power Strip.

In conclusion, the cost of implementing all of the modifications to the original electrospinner system totaled approximately $3,600.00. This included the new high voltage power supply, new syringe pump, and miscellaneous electrical wiring components. All of the modifications made enhanced the electrospinner system's capabilities and addressed issues concerning safety. Once the optimized electrospinner system was completely setup, a short proof of concept study was conducted in order to assess any possible differences in the electrospinning process and the resulting electrospun scaffold.

2.7 PROOF OF CONCEPT STUDY

In order to assess the modifications made to the original electrospinner system, a short proof of concept study was undertaken. The objective of this study was to qualitatively compare the electrospinning process and the fabricated scaffolds between the original and optimized electrospinner systems.

2.7.1 Materials and Methods

The original and optimized electrospinner systems were each used to fabricate a single BBB scaffold using the parameters listed below.

Polymer:	15wt% PLGA (75:25) in Chloroform ($CHCl_3$)
Flow Rate:	5.5ml/hr, 2ml of polymer solution was used
Needle:	18 gauge, beveled blunt (BD 305180)
Gap:	10 inches
Voltage:	+ 15,000V
Translate:	Distance set at 16cm, translation speed set at 3 or 55 OPM
Rotate:	Rotation speed at 6 or 3110 RPM
Mandrel Collector:	1.066mm diameter mandrel was used

These parameters were suggested by a colleague in the Cal Poly Tissue Engineering lab experienced in electrospinning [83]. The scaffold created using the optimized electrospinner, Scaffold A, was electrospun using the protocol outlined in Appendix C. While the scaffold fabricated using the original system, Scaffold B, was electrospun using the protocol developed by James described in Appendix B [69].

After being electrospun, each scaffold was placed in a desiccator to remove any residual solvent. After at least 24 hrs inside the desiccator, each scaffold was carefully sectioned radially using a carbon steel blade into proximal, middle, and distal fragments approximately 1cm in length. Each section was then cut longitudinally to expose the inner lumen. Then the inner lumen of each section was imaged at random locations with a range of magnifications using a Hitachi TM-1000 tabletop SEM (Tokyo, Japan). The complete protocol for SEM analysis is outlined in Appendix D. The scaffolds were then qualitatively evaluated for fiber morphology and uniformity.

2.7.2 Results and Discussion

The optimized electrospinner system was significantly more user friendly, and required very limited operator contact compared to the original electrospinner system. The original power supply demonstrated fluctuations in providing a constant supply of voltage to the spinneret. Additionally, disturbed Taylor cones were observed periodically for both original and optimized electrospinner processes. However, the polymer jet created using the original system appeared very erratic, and would often project large fragments of polymer towards the collector. In comparison, the optimized system produced more of a consistent polymer jet.

After evaluating the SEM images, Scaffold B from the original system consisted of several areas with large polymer blots instead of well rounded fibers typically found when electrospinning [30]. These polymer blots are highly disadvantageous as they are areas without any pores, or space for cells to infiltrate the scaffold (Figure 14B). A probable cause for the inconsistency in the electrospun fibers was the faulty power supply. This applied voltage fluctuation directly influences the strength of the electric field and the path the polymer jet takes to reach the collector [55]. Since a constant electric field may not have been applied, the typical fine fibers may not have been produced, and instead large polymer pieces aggregated on the collector. As illustrated in Figure 14A, the optimized system produced the typical rounded fibers expected. Additionally, Scaffold A was void of any major inconsistencies and appeared relatively uniform. Moreover, this proof of concept study demonstrated that the optimized electrospinner does indeed function properly. Further investigation would be required to statistically demonstrate any differences between the systems and would be outside the scope of this thesis.

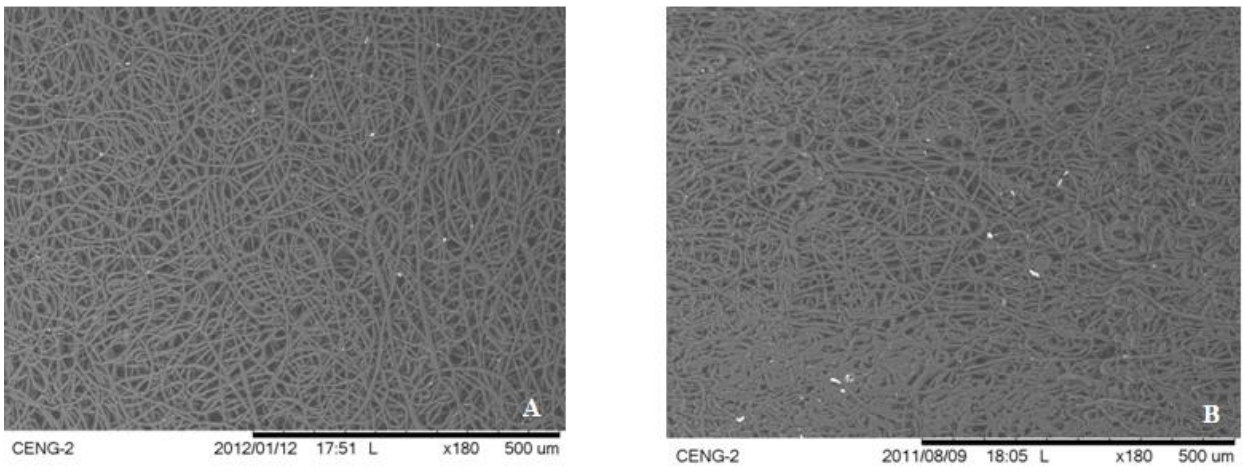

Figure 14: *SEM images at 180x of the inner lumen of a BBB scaffold electrospun using the optimized (A) and original (B) electrospinner systems.*

2.8 CONCLUSION

It was due time that the original electrospinner system be updated and optimized to ensure consistency, have the capabilities to employ new electrospinning strategies, and assure safety. In summary:

(i) A dual output high voltage power supply was custom designed and built. The first output permits reversible polarity, and a range of up to 30kV, while the second output has a negative polarity with a range of up to 10kV. Both outputs can be used simultaneously, and are self-contained to a single box. Additionally, the new power supply is powered by alternating current (AC), and as a result does not require an external transformer.

(ii) The syringe pump was replaced with the exact same model and situated on a new custom built stand.

(iii) The electrical layout was modified so that a surge protector is now being utilized, the isolation chamber was fitted with electric bulkhead fittings to reduce wiring and operator contact, the physical footprint of the system was reduced, and the entire system was grounded to the chasis of the fume hood.

These improvements are believed to facilitate success in electrospinning scaffolds for the Blood Brain Barrier application, and additional future tissue engineering investigations. The updated and optimized electrospinner system was then used to develop a protocol specific to electrospinning scaffolds for the BBB application, which will be further discussed in the next chapter.

CHAPTER 3 - BLOOD BRAIN BARRIER SCAFFOLD PROTOCOL DEVELOPMENT

3.1 INTRODUCTION

With the electrospinner updated and optimized, the next aim of this thesis was to find appropriate processing parameters for electrospinning a small diameter scaffold for tissue engineering an *in vitro* BBB vessel. As there are countless combinations of processing parameters that can be used for the electrospinning process, extensive literature research and advice from Dr. Eugene Boland, along with documented work by previous Cal Poly students [67,69], were used to strategize an approach for each of the electrospinning experiments presented in this chapter. In particular, focus was set on adjusting the gap distance, flow rate, and applied voltage parameters. Ultimately, the electrospinning experiments were used to develop a protocol for electrospinning tubular scaffolds using a specific polymer, PLGA, with a 2 mm inner diameter for the BBB application.

A major challenge in using electrospun scaffolds for tissue engineering is non-uniform cellular distribution and lack of cellular migration in the scaffold at increasing depths [30]. Eichhorn and Sampson reported that with the decrease of electrospun fiber diameter there was an increase in the number of fiber-to-fiber contacts per unit length, and hence a decrease in the mean pore radius of electrospun meshes [35]. A small mean pore size creates a mismatch with the larger physical size of the typical cells used for tissue engineering applications (approximately 10µm - whether it be an osteoblast, fibroblast, or chondrocyte) [84]. Moreover, too small of a fiber diameter limits the ability of

the cells to migrate and populate the interior of the scaffolds [66]. Pham et al. reported that microfibers (approx 5-10µm in diameter) in conjunction with dynamic flow perfusion culture resulted in excellent penetration and cellular distribution of rat mesenchymal stem cells (MSCs) on electrospun meshes [33]. Accordingly, the objective of the following electrospinning trial experiments was to explore the effects of different processing parameters on the electrospinning system's ability to fabricate uniform fibers with a diameter in the low micrometer range for a BBB tubular scaffold.

Poly(D,L-lactide-co-glycolide) [PLGA] was selected for the electrospinning work in this chapter based on evidence of adequate cell attachment [85], mechanical properties similar to a native vessel [86], controlled biodegradation [87], cost effectiveness [67], and excellent biocompatibility [88]. Additionally, various solution concentrations of PLGA dissolved in Chloroform ($CHCL_3$) was previously studied for use in electrospinning large diameter (approximately 4mm inner diameter) vascular scaffolds at Cal Poly prior to the work of this thesis [67]. Peña reported that electrospun solutions of 15 wt% PLGA in $CHCL_3$ resulted in continuous, uniform, un-beaded fibers with tensile properties (3-5 MPa) comparable to the native vessel [67]. Therefore, this solution concentration was selected for the current work.

3.2 MATERIALS AND METHODS

3.2.1 Polymer Mixing and Electrospinning

PLGA with a monomer to monomer molar ratio of 75:25 (D,L-lactic acid to Glycolic acid) obtained from Sigma Aldrich (St. Lous, MO) was used for every electrospin. The PLGA was dissolved in $CHCL_3$ to create a 15 wt% polymer (WPP) in

accordance to the protocol outlined in Appendix A. For every electrospin, three milliliters of polymer solution was prepared, of which 2 milliliters was used for the actual electrospinning process. After mixing on an orbital shake table for 48 hours the polymer solution was electrospun with a predetermined trial set of processing parameters using the protocol outlined in Appendix C. In brief, the applied voltage, gap distance, and flow rate were altered to some degree for each of the electrospinning trials. Additionally, all of the following experimentation was conducted using the new optimized electrospinner system with a 2mm metal mandrel.

3.2.2 SEM and Image Analysis

Consistency and uniformity of fiber morphology, as well as fiber diameter was assessed for each scaffold. After each electrospinning process, each metal mandrel layered with electrospun fibers was immediately removed from the collection system, and placed in a dessicator for at least 24 hours to remove any residual solvent. Then each scaffold was sectioned from the metal mandrel using a carbon steel blade to expose the inner lumen or surface that was in contact with the metal mandrel. Each SEM image was taken at random locations using a Hitachi TM-1000 tabletop SEM (Tokyo, Japan). In order to measure fiber diameter, ImageJ analysis software (National Institutes of Health, USA) was used in accordance to the protocol outlined in Appendix D.

3.3 RESULTS

The results for the individual electrospins will be presented in the following fashion: a purpose that includes the rationale for each electrospin, the process parameters used, observations made during the electropspin process, SEM image of the fiber

morphology, and an explanation regarding the process and resulting structure and morphology of the scaffold. Moreover, a probable explanation is provided for the variations noticed between each electrospin.

Electrospin #1

Purpose:

The following process parameters were reported by Peña as appropriate parameters for electrospinning scaffolds for a blood vessel mimic (BVM) on a mandrel that is approximately twice the size of the BBB model mandrel [67]. Therefore, these parameters were implemented using a 2mm diameter mandrel.

FLOW RATE:	5.5 ml/hr
APPLIED VOLTAGE:	+ 12,000V
GAP DISTANCE:	10"
TRANSLATIONAL SPEED OF COLLECTOR:	55 OPM or Setting 3
ROTATIONAL SPEED OF MANDREL:	3110 RPM or Setting 6

Process Observations:

Proper Taylor cone formation was clearly visible within the first few seconds of electrospinning, however, as the process continued, the expected conical shape was no longer present and the droplet at the tip of the spinneret fell to the drip tray. Immediately after, another conical droplet began to develop only to again fall into the drip tray. Throughout the electrospinning process, a significant amount of polymer was lost in the aforementioned fashion. Additionally, when the Taylor cone was present, the polymer jet appeared stable in the shape of a straight line for approximately 4-5cm, and then became very unstable and created a violent whipping movement as it shot towards the collector.

SEM Analysis:

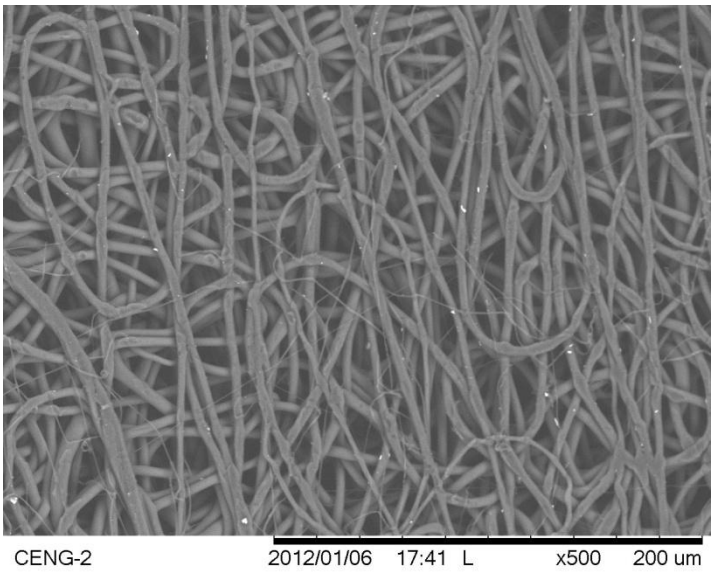

Figure 15 - *500x SEM image of the inner lumen of the tubular scaffold fabricated from Electrospin #1.* Many of the fibers on this electrospun scaffold appear flat, rather than rounded.

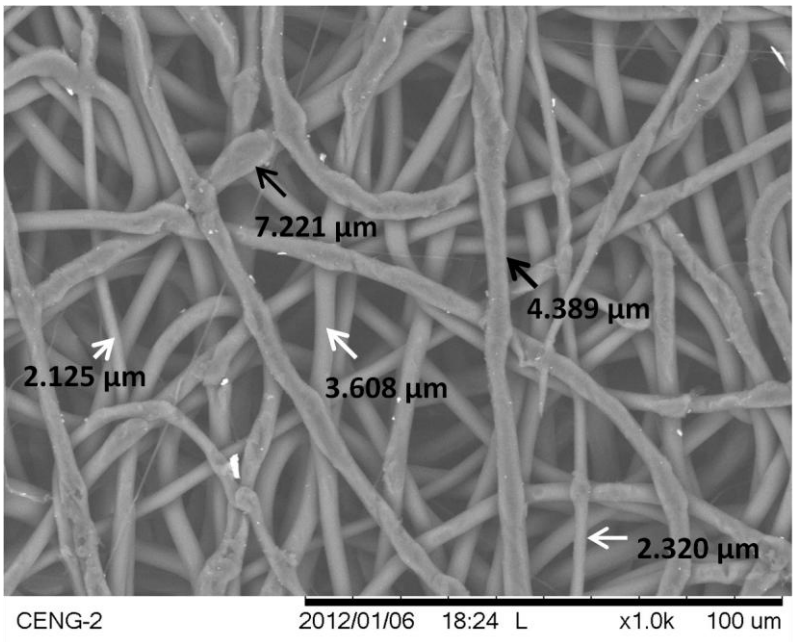

Figure 16 - *1000x SEM image of the inner lumen.* The flat fibers noticed in the previous figure can be clearly seen in this higher magnification image. All of the fibers measured are below 10 µm, several fibers take the expected well rounded fiber shape and have very low fiber diameters (white arrows), whereas some of the fibers appear flat, and are as a result larger in measured fiber diameter (black arrows).

Illustrated in Figure 15, most of the fibers on the interior surface of the scaffold appear flat. With further magnification, it is clear that the expected rounded fibers are present, however, the fibers that were in direct contact with the mandrel were the ones that appear flat. As demonstrated in Figure 16, most of the flattened fibers have larger fiber diameters than the rounded fibers. The flattened fibers may be a result of the contact that was made during sample preparation for SEM analysis. A major concern from this electrospin was the observation made during the electrospinning process in which the conical shape of the Taylor cone expected at the spinneret was rarely present. This resulted in a significant amount of polymer lost into the drip tray. Moreover, for the brief moments the Taylor cone was present, the expected jet dynamics including a stable and unstable phase were present. This indicated that the observed electrospinning process was similar to observations made by others in the field [55].

Electrospin # 2

Purpose:

According to Pham et al. electrospinning polysulfone at closer distances between the tip and collector yielded smaller and more uniform fibers [33]. Electrospin # 2 was performed with the intention of fabricating a scaffold with rounded fibers rather than flat fibers which could possibly decrease the pore size, and hence decrease cellular infiltration. The gap distance was reduced for Electrospin # 2. In addition, observed in the previous electrospin was a significant amount of polymer loss since a proper Taylor cone would not hold at the spinneret. To resolve this problem, the applied voltage was increased in an attempt to increase the strength of the electric field.

FLOW RATE:	5.5 ml/hr
APPLIED VOLTAGE:	+ 13,000V
GAP DISTANCE:	8"
TRANSLATIONAL SPEED OF COLLECTOR:	55 OPM
ROTATIONAL SPEED OF MANDREL:	3110 RPM

Process Observations:

Although a Taylor cone was present, after approximately one minute the conical shape was lost and the suspended polymer drop would fall into the drip tray. Occasionally, small fragments of polymer were launched toward the collector. Additionally, the polymer jet that was periodically formed appeared to shoot in an upward arc towards the collector, very close to the roof of the isolation chamber.

SEM Analysis:

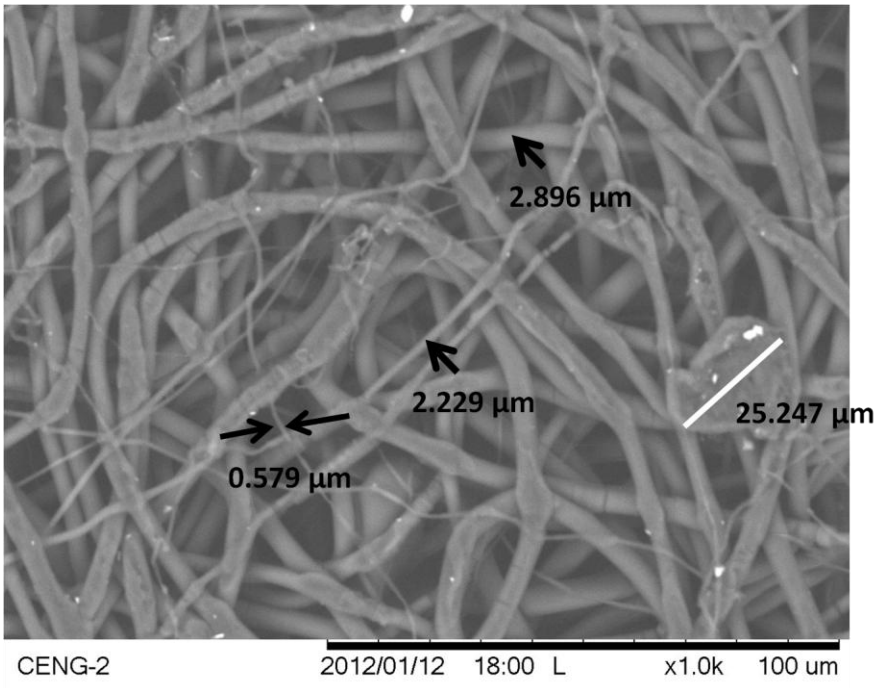

Figure 17:*1000x SEM image of the interior surface of the electrospun scaffold # 2.* Demonstrates fiber diameters that range from approximately 3µm to as lows as 0.579 µm. Additionally, fiber morphology is very inconsistent and includes large polymer blots (white line).

During the electrospinning process, the droplet of polymer at the tip of the spinneret formed the Taylor cone for longer periods of time than observed in Electrospin #1, however, the conical shape was short lived and would result in the loss of polymer solution into the drip tray below the spinneret. Moreover, significantly more inconsistent fiber morphology was present in this electrospin, including polymer drops which were as large as 25 microns squared (Figure 17). These areas are highly disadvantageous as they could potentially prevent cellular infiltration.

Electrospin # 3

Purpose:

This scaffold was spun immediately after Electrospin # 2 with the objective of understanding whether the gap distance would make a difference in creating rounder fibers. Conflicting literature exists on the affect gap distance has on fiber morphology. Contrary to the results reported by Pham et al., Buchko et al. reported flatter fibers at closer distances when electrospinning SLPF (Silk-Like Polymer with Fibronectin functionality) [43]. All of the processing parameters for this spin were held consistent with the parameters used in Electrospin # 2, except for the gap distance, which was changed from 8" to 12".

FLOW RATE:	5.5 ml/hr
APPLIED VOLTAGE:	+ 13,000V
GAP DISTANCE:	12"
TRANSLATIONAL SPEED OF COLLECTOR:	55 OPM
ROTATIONAL SPEED OF MANDREL:	3110 RPM

Process Observations:

The Taylor cone was disrupted often, and would result in an inconsistent polymer jet. A noticeable amount of polymer solution was present in the drip tray at the end of the electrospinning process. In addition, there was a considerable build of electrospun mesh on the walls of the isolation chamber.

SEM Imaging:

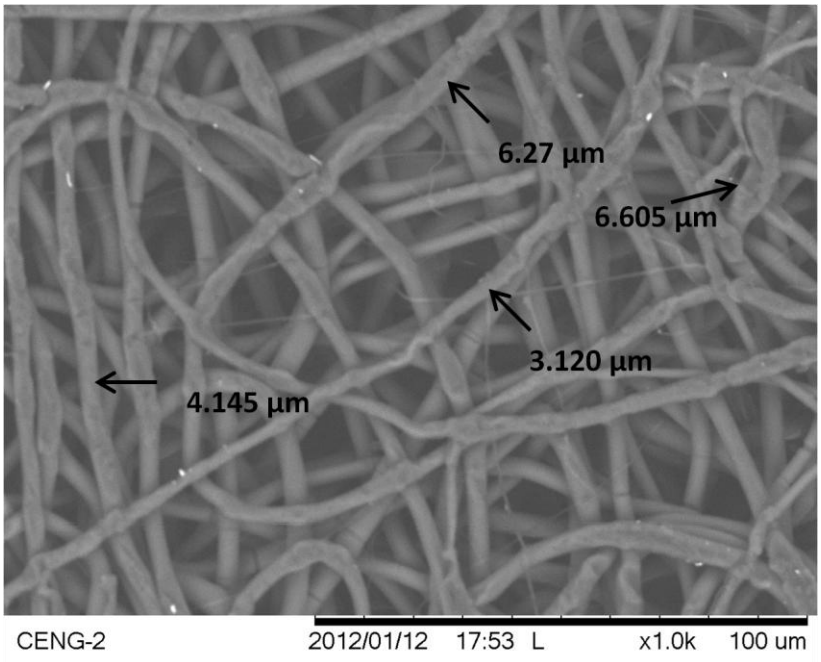

Figure 18: *SEM image of the interior surface of a Electrospun #3 scaffold (1000x).* Fibers are in the low micron range, however, continue to display flat morphology.

Fibers continued to demonstrate flattened fiber morphology as illustrated in Figure 18. In addition, fiber diameters ranged from approximately 3 to 7 µm. The scaffold lacked any significant polymer drops on the interior surface. Although the flat fibers are still all under approximately 7 microns, the objective of these electrospins is to find processing parameters that will result in the uniform rounded fibers reported by others in the electrospinning field [30,53,74,89]. Additionally, in this electrospin a noticeable

amount of polymer mesh had collected along the walls of the isolation chamber. The increase in gap distance to 12" may result in fewer polymers that collect on the metal mandrel. The last three electrospins revealed no noticable correlation between the gap distance and fiber morphology. Also, in order to maximize the collection of polymer fibers on the mandrel collector rather than the isolation chamber's walls, the gap distance was brought back to 10".

A cause for concern continues to be the considerable loss of polymer solution during the electrospinning process. This is a direct result of an improper Taylor cone from forming. According to Liang et al. the surface tension of the droplet should be in equilibrium with the electric field, until the applied voltage is increased to a critical point where the repulsive electric force overcomes the surface tension force, and a small charged jet emerges from the tip of the droplet and is drawn towards the collecting plate [68]. Accordingly, with the next electrospins a balance needed to be found between the applied voltage, and the flow rate of the polymer solution at the tip of the spinneret.

Electrospin # 4

Purpose

In an attempt to address the issue of polymer loss, the applied voltage was increased in order to increase the strength of the electric field. The applied voltage was raised to 18kV in an attempt to resolve the issue of the polymer Taylor cone from being disrupted and falling to the drip tray.

FLOW RATE:	5.5 ml/hr
APPLIED VOLTAGE:	+ 18,000V
GAP DISTANCE:	10"
TRANSLATIONAL SPEED OF COLLECTOR:	55 OPM
ROTATIONAL SPEED OF MANDREL:	3110 RPM

Process Observations

The Taylor cone was formed once the high voltage was applied to the polymer droplet at the tip of the spinneret, however, the polymer drop extended to approximately 2 cm from the tip of the spinneret, until it was eventually projected towards the base of the collection system. As the electrospinning continued, elongated polymer drops were periodically shoot towards the collector.

SEM Analysis:

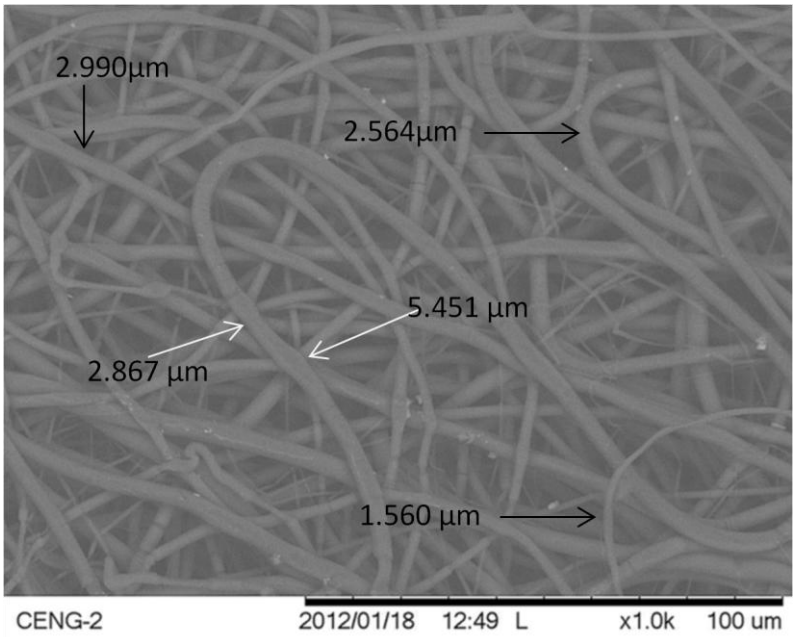

Figure 19: *1000x SEM image of the interior surface of Electrospun scaffold #4.* Most fiber diameters are in low the micron range. However, fiber diameter variations are present for the same fiber (white arrows).

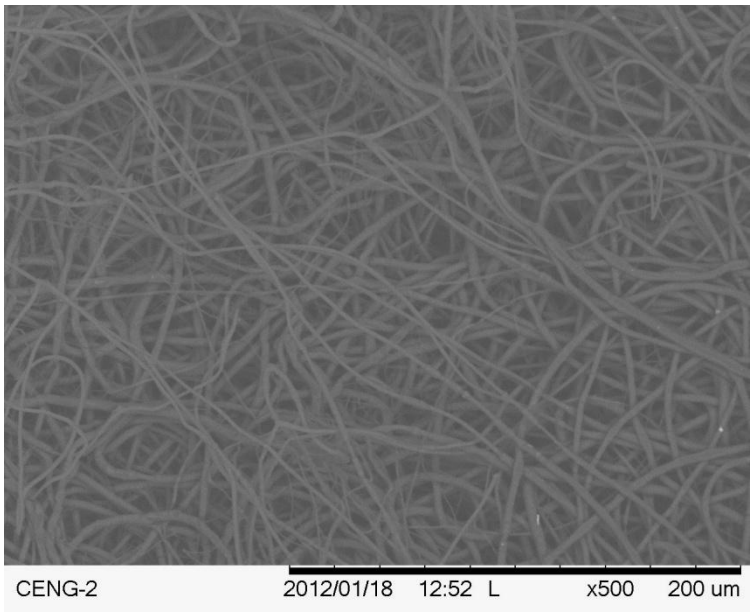

Figure 20: *SEM image of interior surface at 500x.* Scaffold is void of any large polymer drops, however, fibers do not possess uniformity.

By increasing the applied voltage, the observations made in the previous electrospins regarding the polymer Taylor cone being disrupted and falling to the drip tray was no longer present. Additionally, the interior surface was well covered with continuous fibers; however, within the same fiber there were variations in the fiber diameter as illustrated in Figure 19. The irregularity of the fibers can be better seen in Figure 20. Although this electrospin resolved the issue of the polymer solution from falling to the drip tray, the increase in the applied voltage caused the polymer Taylor cone to elongate and eventually shoot towards the collector. Further investigation into balancing the rate at which the polymer is being ejected from the spinneret and the applied voltage was therefore required.

Electrospin # 5

Purpose:

Investigation into finding a balance between the applied voltage and the polymer ejection flow rate was continued with this electrospin. The flow rate was reduced to 4ml/hr, and the applied voltage was left at 18kV. Additionally, upon suggestion by Dr. Eugene Boland, the polarity of the applied voltage was switched from positive to negative.

FLOW RATE:	4.0 ml/hr
APPLIED VOLTAGE:	- 18,000V (neg. polarity)
GAP DISTANCE:	10"
TRANSLATIONAL SPEED OF COLLECTOR:	55 OPM
ROTATIONAL SPEED OF MANDREL:	3110 RPM

Process Observations:

Once the electrospinning process was started, a Taylor cone formed, and a stable jet was visible for approximately 5cm, the jet then entered an unstable phase. The unstable portion looked like a transparent cone, with the tip of the cone emerging from the end of the stable polymer jet region. Past the cone like shape, the fibers were no longer visible; however, white fibers were seen collecting on the mandrel.

Occasionally, the Taylor cone was disrupted, and the polymer appeared to shoot from within the spinneret.

SEM Analysis:

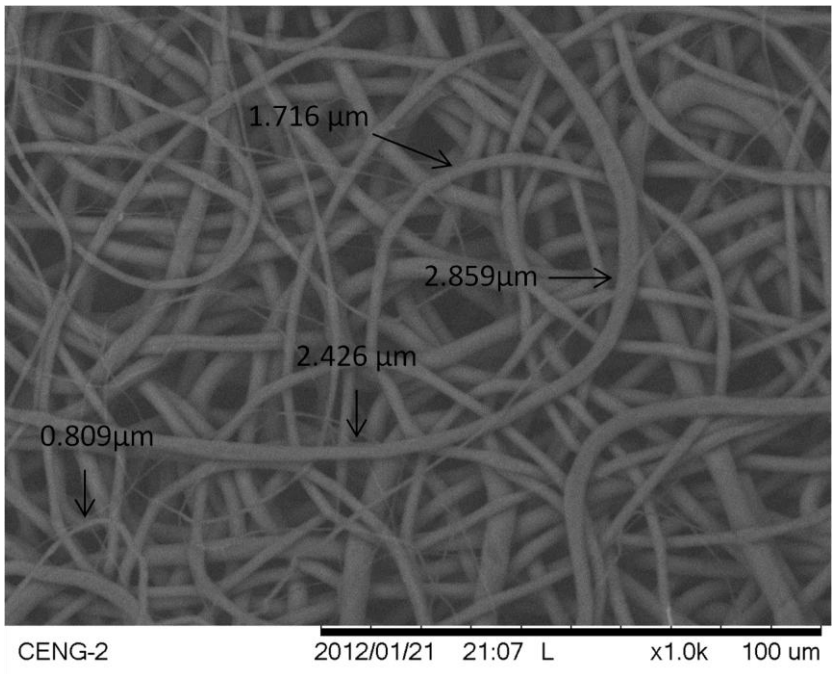

Figure 21: *SEM image (1000x) of the interior surface of Electrospun scaffold #5.* Fiber diameter ranged from approximately 3µm to 800 nm.

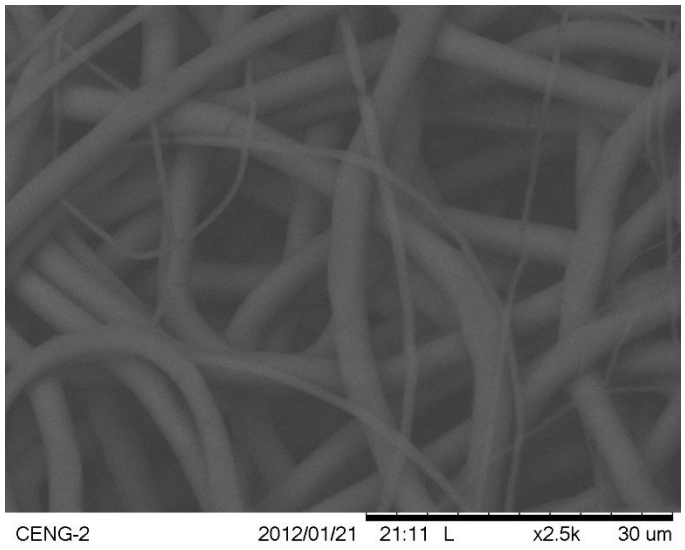

Figure 22: *SEM image of the interior surface of Electrospun scaffold #5 at 2500x.*

Taylor cone formation was significantly better than any of the previous electrospins. However, occasionally the Taylor cone was disrupted and the polymer jet

was shot from within the spinneret. The most probable explanation for this is that the polymer solution was being ejected too slowly, or the electric field was too strong. The strong electric field can cause the electrostatic forces to be significantly greater than the surface tension forces of the polymer solution, hence resulting in the polymer solution being pulled from within the spinneret.

This electrospin was a success, uniform fibers were present with fiber diameters predominantly around 2 µm, as illustrated in Figure 21. Dr. Eugene Boland suggested using negative polarity as a tool to fine tune the uniformity of the fibers produced by electrospinning [80]. As illustrated in Figure 22, the fibers at 2500x are clearly very uniform and consistent with the expected ideal electrospun fiber morphology. Therefore the next electrospin continued to adjust the applied voltage and flow rate parameters.

Electrospin # 6

Purpose:

This electrospin implemented a minor adjustment in the flow rate in an attempt to prevent the polymer jet from receding within the spinneret. The flow rate was increased to 4.5 ml/hr. Due to the success in uniform fiber morphology from the previous electrospin, a negative polarity was maintained for the applied voltage.

FLOW RATE:	4.5 ml/hr
APPLIED VOLTAGE:	- 18,000V (neg. polarity)
GAP DISTANCE:	10"
TRANSLATIONAL SPEED OF COLLECTOR:	55 OPM
ROTATIONAL SPEED OF MANDREL:	3110 RPM

Process Observations:

Proper Taylor cone formation was clearly visible once the applied voltage was applied. Rarely was the conical polymer droplet disturbed. Additionally, the Taylor cone extended approximately 2mm from the spinneret. A stable polymer jet erupted from the Taylor cone for approximately 5cm, then became unstable.

SEM Analysis:

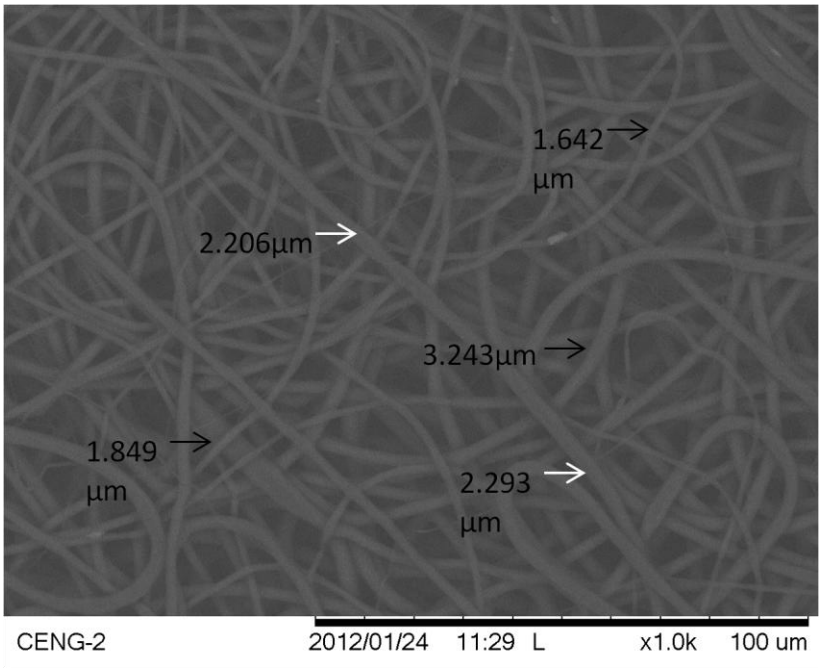

Figure 23: *SEM image of the interior surface of electrospun scaffold # 6*. Fiber morphology demonstrates continuous uniform fibers. Fiber diameter measurements were taken twice for the same fiber (white arrows) to demonstrate uniformity.

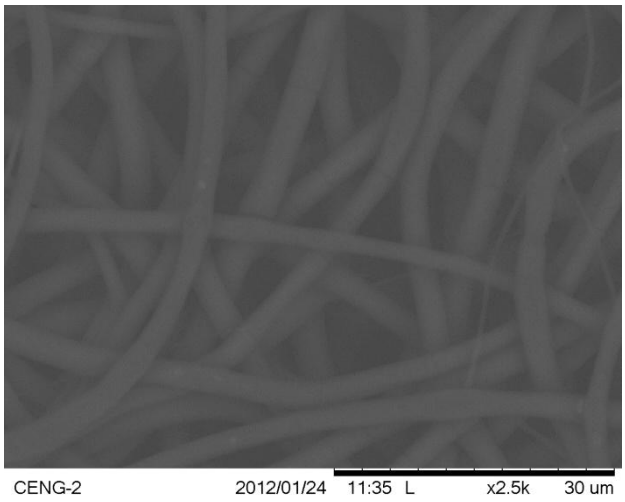

Figure 24: *2500x SEM image of the interior scaffold of Electrospin #6.*

The consistency and uniformity desired in an electrospun scaffold for the DIV-BBB application is clearly visible in Figure 23 and 24. In addition, the fiber diameter was measured to be in the low micron range that was suggested to be ideal for a scaffold implemented in an dynamic flow perfusion culture [33]. Moreover, during the electrospinning process, the Taylor cone was rarely disrupted. Proper Taylor cone formation is critical for influencing the polymer jet dynamics and consistency of the fibers that gather on the collector [55]. The next electrospin was undertaken to see if any refinements could be made by adjusting the flow rate.

Electrospin # 7

Purpose:

Taylor cone formation is an integral element to consistency of electrospun fibers [53,57,77]. The previous electrospin demonstrated a balance between applied voltage and flow rate. It resulted in proper Taylor cone formation that created uniform rounded fibers

on the collector. The following electrospin was conducted to see if another adjustment in flow rate would make a difference to the fibers produced.

FLOW RATE:	5.0 ml/hr
APPLIED VOLTAGE:	- 18,000V (neg. polarity)
GAP DISTANCE:	10"
TRANSLATIONAL SPEED OF COLLECTOR:	55 OPM
ROTATIONAL SPEED OF MANDREL:	3110 RPM

Process Observations:

Once the high voltage was applied, a Taylor cone was clearly visible. As time passed, the Taylor cone progressively elongated until eventually a large polymer fragment was projected towards the collector. This continued to occur approximately every 6 minutes.

SEM Analysis:

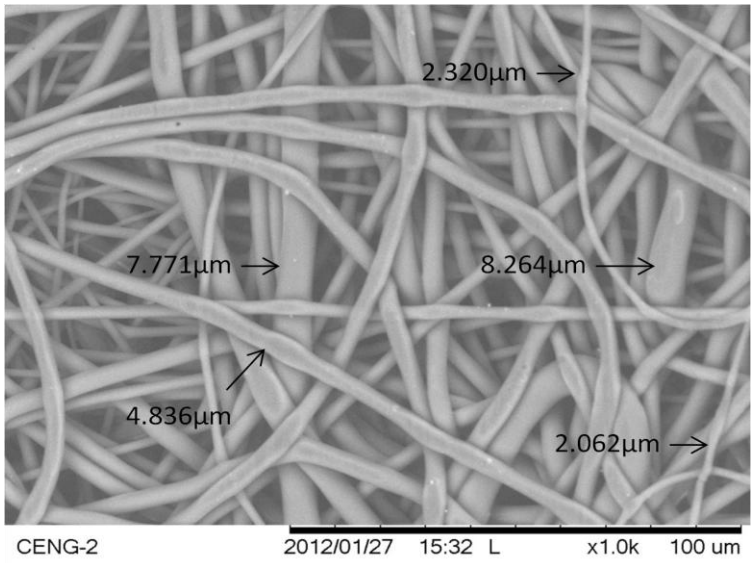

Figure 25: *SEM image of the interior surface of scaffold fabricated from Electrospin # 7.* Irregularities are visible in fibers, as well as inconsistency in fiber diameters.

By increasing the flow rate to 5.0ml/hr, the polymer was ejected faster than the electrostatic forcers were able to attract the polymer jet towards the collector. It most likely resulted in the elongation of the Taylor cone that was noticed during the electrospinning process. The elongated Taylor cone seems to have resulted in irregularities in the fibers (Figure 25), rather than well rounded consistent fibers seen in the previous electrospin. Therefore the next electrospin focused on the effects of increasing the applied voltage.

Electrospin # 8

Purpose:

The new high voltage power supply has an upper limit of 30kV. To determine the effects of the applied voltage on fiber morphology the following series of electrospins was performed with increasing applied voltages. Jacobs et al. reported that an increased applied voltage resulted in more uniform fibers with smaller diameters when electrospinning poly ethylene oxide (PEO) [59].

FLOW RATE:	5.5 ml/hr
APPLIED VOLTAGE:	- 20,000V (neg. polarity)
GAP DISTANCE:	10"
TRANSLATIONAL SPEED OF COLLECTOR:	55 OPM
ROTATIONAL SPEED OF MANDREL:	3110 RPM

Process Observations:

After around 0.4ml of polymer solution was ejected, multiple polymer jets appear to arise from the single Taylor cone. One of the jets shot towards the roof of the isolation chamber, while a second jet projected towards the collector. Only for limited periods of

time was a proper Taylor cone formed. Occasionally large drops of polymer solution were projected towards the collector. In addition, it was clear that there was very little stability of the polymer jet at the tip of the spinneret.

SEM Analysis:

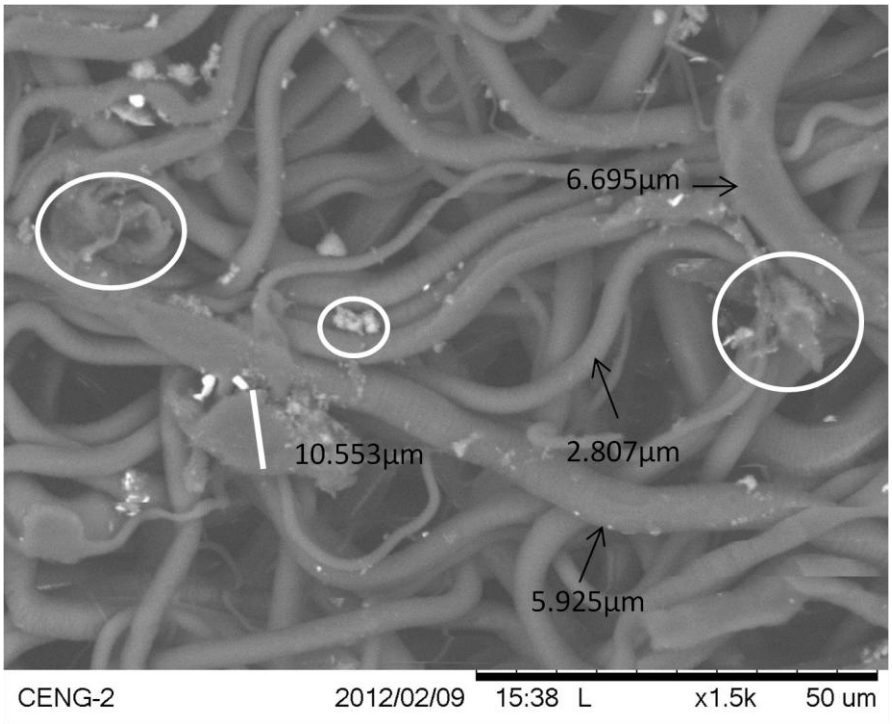

Figure 26: *SEM image (1500x) of the interior surface of scaffold fabricated from Electrospin # 8.* Inconsistencies in the fiber morphology are clearly visible, as well as polymer drops (white line). In addition. polymer debris is extensive throughout the scaffold (white circles).

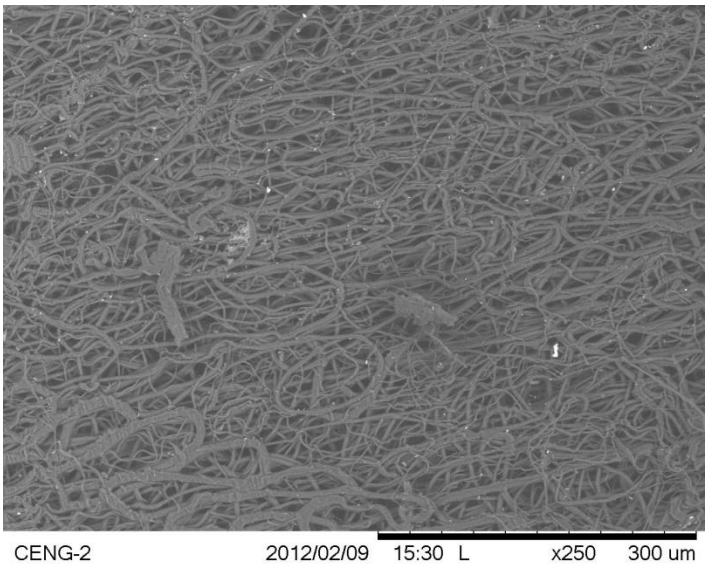

Figure 27: *SEM image of the interior surface at 250x.* Significant amounts of polymer blots are present on the scaffold, and there is no uniformity to the fibers.

The increased applied voltage greatly reduced the consistency and uniformity of the fibers. There were extensive polymer blots (illustrated in Figure 27). Additionally, significant amount of polymer debris was visible throughout the scaffold (Fig. 26). The most probable explanation for this is the improper Taylor cone formed during the electrospinning process as a result of an imbalance between the flow rate and the applied voltage. Since a correct fiber jet was not formed, large polymer drops were projected towards the collector and are clearly visible on the interior surface of the scaffold. The imbalance between the applied voltage and flow rate resulted in improper jet dynamics. A possible explanation for the polymer blots could also be the insufficient time for the solvent ($CHCL_3$) to evaporate as the polymer is being jetted towards the collector [69].

Electrospin # 9

This electrospin was performed with an increased applied voltage, in an attempt to balance the 5.5ml/hr flow rate.

FLOW RATE:	5.5 ml/hr
APPLIED VOLTAGE:	- 22, 000V (neg. polarity)
GAP DISTANCE:	10"
TRANSLATIONAL SPEED OF COLLECTOR:	55 OPM
ROTATIONAL SPEED OF MANDREL:	3110 RPM

Process Observations:

Once the electrospinning process was started, there was very limited formation of the Taylor cone and the polymer jet was initiated from within the spinneret. The jet that did emerge from inside the spinneret appeared very unstable and erratic. The polymer was directed primarily towards the roof of the isolation chamber and towards the collector. Significant amounts of large pieces of polymer solution were projected towards the collector.

SEM Analysis:

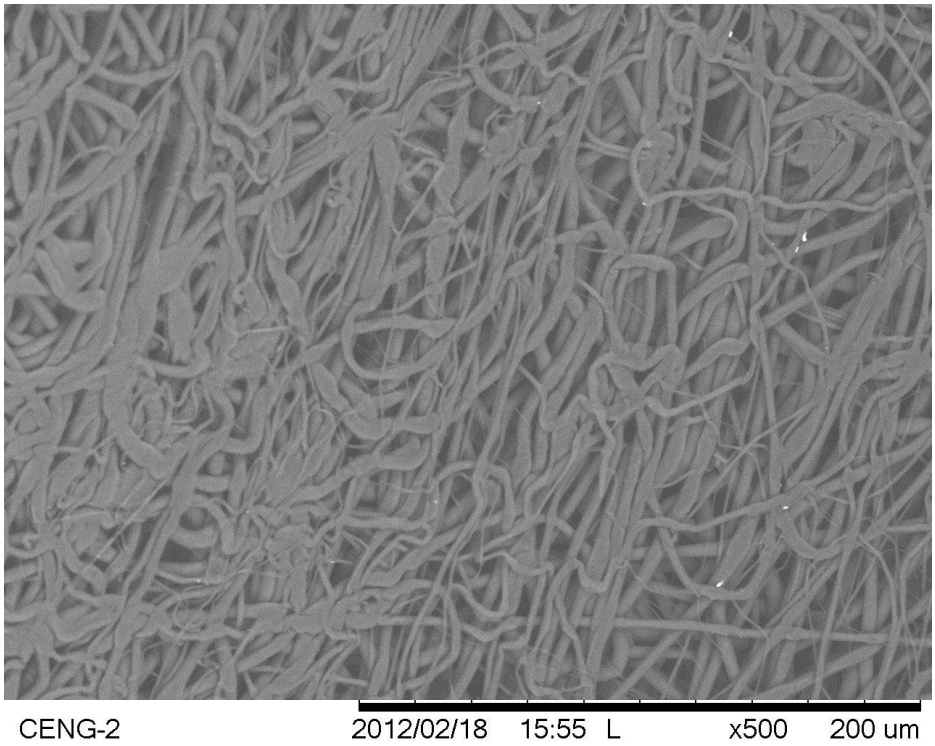

Figure 28: *SEM image (500x) of the interior surface of scaffold fabricated in Electrospin #9.* Extensive polymer clumps are visible throughout the scaffold.

The fiber morphology from this electrospin was very inconsistent. The large polymer fibers that appear flat in Figure 28 are most likely a result of the jet dynamics not allowing the polymer solution to fully develop into a fiber before aggregating on the collector. There are very limited numbers of pores that can be seen, which would place the scaffold at a major disadvantage for cellular infiltration and attachment. During the electrospinning process it was clear that the increased applied voltage had resulted in instability of the polymer solution within the spinneret, causing the polymer jet to emerge

in an unstable manner. It is clear that increasing the applied voltage to 21kV is detrimental for the consistency and uniformity of continuous fibers.

Electrospin # 10

Purpose:

This electrospin was an attempt to find an applied voltage that would balance the 5.5ml/hr flow rate that was used for the previous two electrospins. Specifically, the applied voltage was set to 19 kV. Ideally, a balance would be present between the flow rate and the electric field produced by the applied voltage, and continuous uniform fibers would emerge from a properly formed Taylor cone.

FLOW RATE:	5.5 ml/hr
APPLIED VOLTAGE:	- 19, 000V (neg. polarity)
GAP DISTANCE:	10"
TRANSLATIONAL SPEED OF COLLECTOR:	55 OPM
ROTATIONAL SPEED OF MANDREL:	3110 RPM

Process Observations:

Taylor cone formation was present for limited periods of time. The conical shape elongated, and eventually resulted in the polymer drop to be projected towards the collector. Occasionally, the polymer jet receded to within the spinneret. Everything appeared very erratic. Additionally, there was a noticeable amount of instability in the polymer jet at the tip of the spinneret.

SEM Analysis:

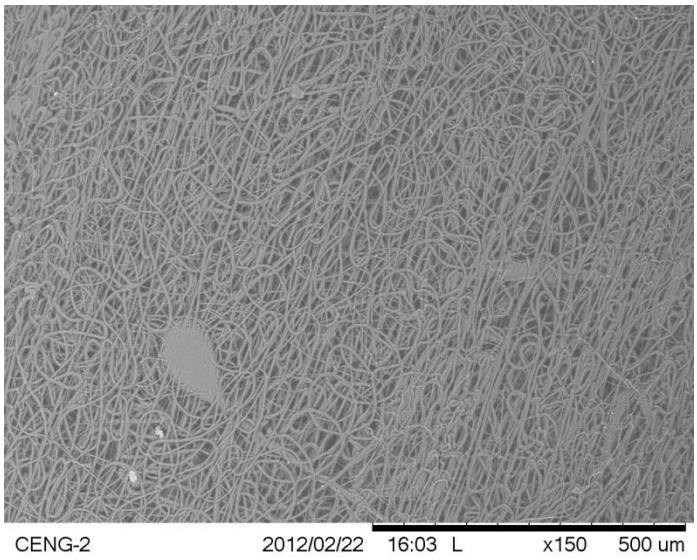

Figure 29: *SEM image (150x) of the interior surface of the scaffold fabricated in Electrospin #10.* Several polymer blots are clearly visible, and could potentially limit cellular infiltration of the scaffold.

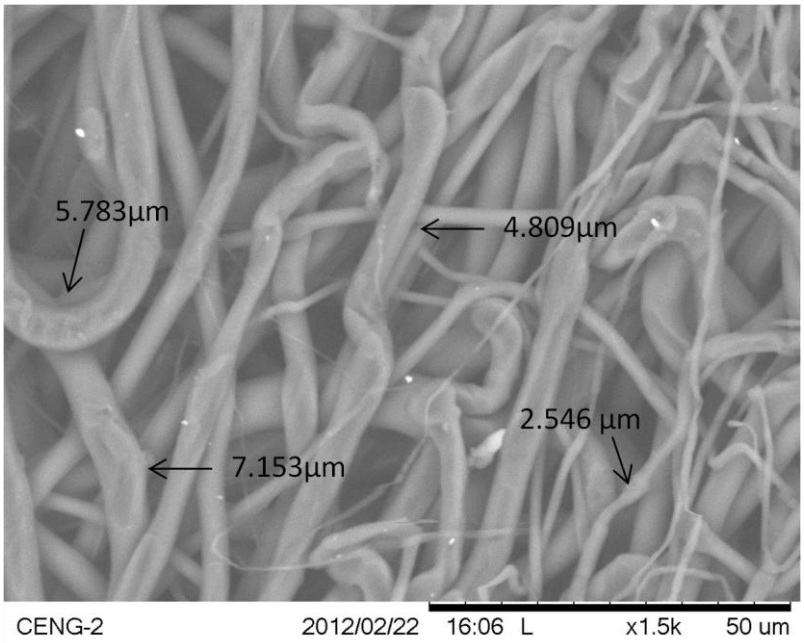

Figure 30: *1500x SEM image of the interior surface of Electrospun scaffold #10*. Fibers appear very non-uniform.

According to Reneker et al. if the electrospinning process is performed effectively, a Taylor cone will form at the tip of the spinneret, with a single polymer jet emerging from the tip of the cone that is stable for some distance before entering an unstable phase in which the fiber is whipped towards the collector [55]. During the electrospinning process in the current studies, a high applied voltage (above 20 kV) seemed to cause very erratic movement of the polymer jet. In addition, there was no consistency throughout the electrospinning process. As a polymer jet would emerge from within the spinneret, the expected Taylor cone at times, and occasionally from a severely elongated Taylor cone. The processing parameters used for this electrospin did not produce a scaffold with continuous and uniform fibers. As illustrated in Figure 29 there are several locations on the interior surface that consist of large polymer blots, and very inconsistent fibers that consist of irregularities (Fig. 30). This electrospun scaffold did not fit the criteria of a desired scaffold for the DIV-BBB model.

3. 4 DISCUSSION AND CONCLUSION

The 10 trial electrospins provided a better understanding of the gap distance, applied voltage (including positive and negative polarity), and flow rate processing parameters. The gap distance did not demonstrate any noticeable effect on the fiber morphology. Several other groups have also reported that the effect of the distance from the spinneret to the collector on fiber morphology is insignificant when compared to other parameters. This has been observed when electrospinning PVA[63], gelatin [90], chitosan [91], and poly (vinylidene fluoride) [92].

One of the new capabilities of the optimized electrospinner system was the ability to apply a high voltage of negative polarity. This technique was suggested by Dr. Eugene Boland as a method for fine tuning the consistency of the fabricated fibers [80]. Depending on the conductive properties of the polymer being electrospun, the polarity of applied voltage has demonstrated importance in fabricating uniform continuous fibers [71]. Once the applied voltage was changed to a negative polarity, and a proper balance was found between the flow rate and the electric field, consistent uniform fibers were fabricated. Jacobs et al. reported fibers with a smaller diameter with increased voltages up to a certain point. Thereafter, at too high of an applied voltage the fibers would demonstrate irregularities and inconsistencies[59]. The higher voltages tested in these electrospin experiments demonstrated incredible instability in the polymer jet, and resulted in non-uniform fibers similar to those reported by Jacobs et al [59].

Applied voltage and flow rate proved to be the most important processing parameters in controlling fiber morphology. When an effective balance between these processing parameters was found, a Taylor cone emerged from the suspended droplet at the tip of the spinneret. From the tip of the Taylor cone an electrically charged jet emerged and traveled a few centimeters in a straight line, also known as the stable phase of the jet dynamics [55]. After this straight segment, a transparent shape, also conical, was seen with its vertex at the end of the straight segment. This transparent cone is actually the complicated set of paths taken by the polymer jet, which is continuously bending rapidly towards the collector, and referred to as the unstable phase [55]. The jet dynamics from Taylor cone to stable phase to unstable phase is integral for consistency in electrospun fibers [44]. Accordingly, finding a balance between the applied voltage and

flow rate was imperative for creating proper jet dynamics. If the applied voltage was too high, the resulting electric field would be so strong that it would pull the polymer directly from within the spinneret. Hence, the polymer jet would emerge from inside the spinneret rather than from the Taylor cone at the tip of the spinneret. Additionally, if the flow rate was too high and the applied voltage was not adequate enough to create a polymer jet from the Taylor cone, a significant amount of polymer was simply lost and not collected on the grounded mandrel.

From the trial electrospins presented in this chapter, it was determined that Electrospin # 6 produced the most desirable scaffold characteristics. Therefore, the parameters from this spin were used to develop a protocol with appropriate processing parameters for electrospinning scaffolds with an inner diameter of 2 mm for an *in vitro* BBB vessel (see Appendix C). The resulting protocol was therefore implemented in a study described in the next chapter to further characterize the electrospun BBB scaffolds and determine the consistency of the electrospinning process.

CHAPTER 4 - CHARACTERIZATION AND CONSISTENCY STUDY OF THE BBB SCAFFOLD

4.1 INTRODUCTION

The Cal Poly Tissue Engineering lab is in the process of implementing a DIV-BBB system to construct *in vitro* BBB vessels. The PLGA electrospun scaffold was selected for this application because it is biocompatible, would promote cellular attachment and infiltration, and is mechanically sound [67]. In order to ensure consistency of the scaffolds used in this system, the in-house electrospinning fabrication process needed to be assessed for reproducibility.

The electrospinning experimentation in the previous chapter was used to develop a protocol with appropriate parameters to fabricate scaffolds with a suitable interface for cellular attachment and infiltration for tissue engineering a BBB vessel. This protocol was then used to fabricate multiple scaffolds, which were utilized for characterization and consistency assessment, as described in this chapter.

4.2 MATERIALS AND METHODS

4.2.1 Electrospinning Parameters for the Characterization and Consistency Study

All of the scaffolds that were electrospun for this study were fabricated using the parameters listed below.

Polymer: 15wt% PLGA in Chloroform ($CHCl_3$)
Flow Rate: 4.5ml/hr, 2ml of polymer solution used
Needle: 18 gauge, beveled, blunt (BD 305180)

Gap:	10 inches
Voltage:	- 18,000V (negative polarity)
Translate:	Distance set at 16cm, translation speed set at 3 or 55 OPM
Rotate:	Rotation speed at 6 or 3110 RPM

A total of 5 scaffolds were created using the BBB electrospinning protocol outlined in Appendix C. After each scaffold was electrospun on a metal mandrel, the scaffold was left entact on the mandrel and placed into a dessicator for at least 24 hours to remove any residual solvent that did not evaporate during the electrospinning process.

4.2.2 Sampling Method

After the electrospun scaffolds had dessicated for at least 24 hours, each scaffold was sectioned away from the metal mandrel using a carbon steel blade in the manner illustrated in Figure 31.

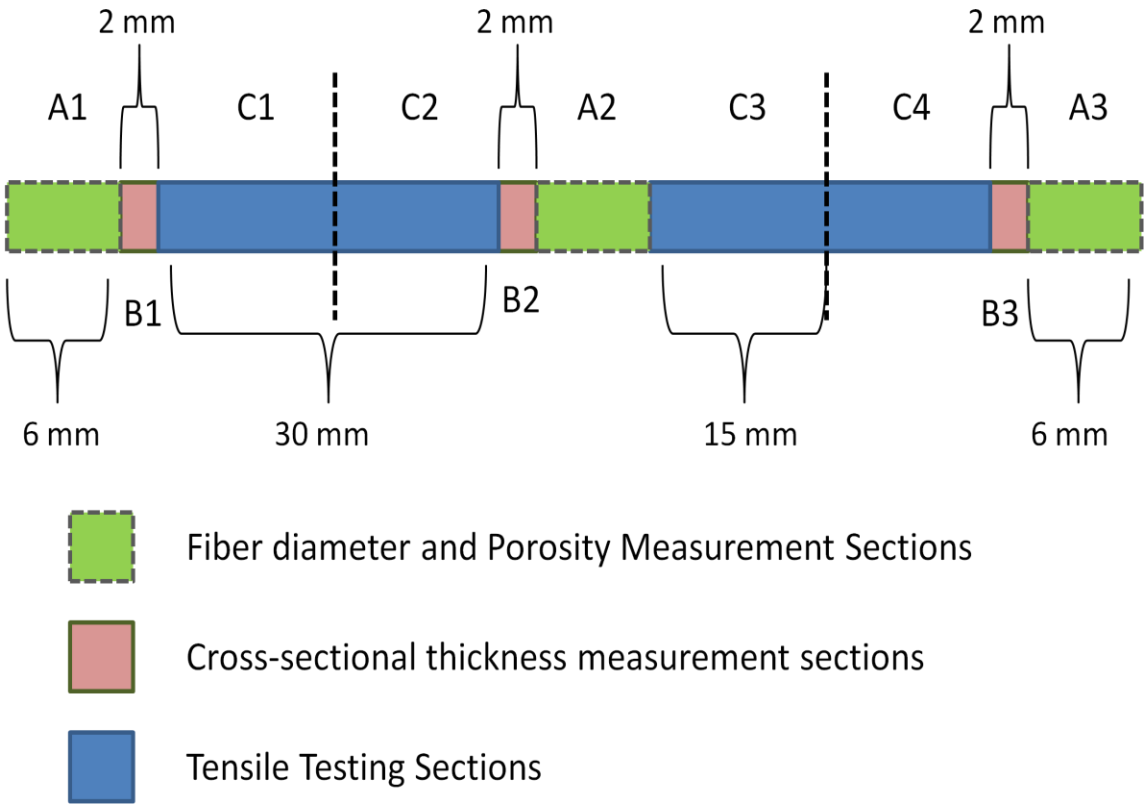

Figure 31: Each individual electrospun scaffold was sectioned for analysis in the fashion illustrated above. The letter A represents all sections used for fiber diameter and porosity measurements (A1, A2, A3). The letter B represents all the sections used for determining the cross-sectional thickness (B1, B2, B3). And the letter C signifies the sections used for tensile testing (C1, C2, C3, C4). Section A1 was the area closest to the collectors rotation motor, while section A3 was the opposite end.

4.2.3 Fiber Diameter Measurement

The fiber diameters of the electrospun scaffolds were measured to evaluate the morphological consistency of the electrospinning process. For each electrospun scaffold, sections A1, A2, and A3 were cut radially while on the metal mandrel with a carbon steel blade. Once the radial incisions were made to create three sections (A1, A2, and A3), a single longitudinal cut was made to expose the luminal surface of each section. Then, all three sections were mounted with the luminal surface up onto an SEM sample stage using

double sided adhesive tape. All three sections for each scaffold were imaged using a Hitachi TM-1000 tabletop SEM (Tokyo, Japan) at a 1000x magnification. Three random locations were chosen on each section (A1, A2, A3) as described below for a total of 9 images saved as jpeg files.

In order to select the fibers that were to be measured, a fixed fiber selection mask was applied to each image as demonstrated in Figure 31. The fixed mask permitted 9 measurements per image, for a total of 27 fiber diameter measurements per section, and a total of 81 measurements per scaffold. The measurements were made using ImageJ analysis software (National Institutes of Health, USA) as outlined in Appendix D.

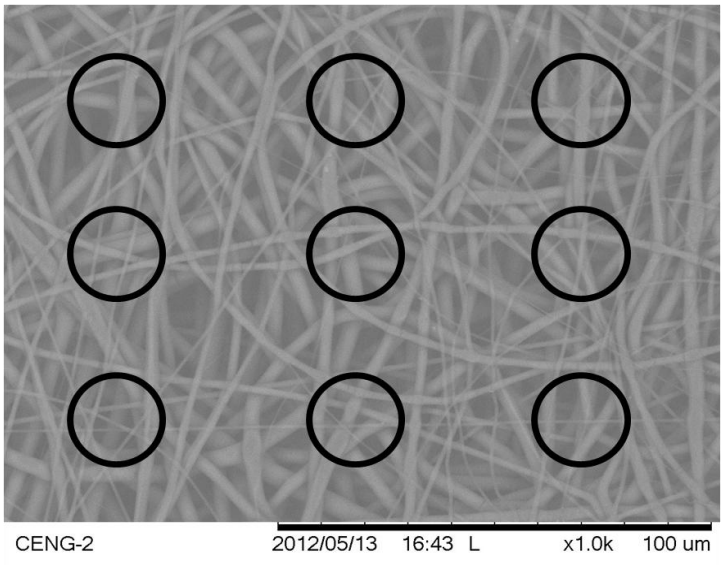

Figure 32: *Example image of fiber diameter measurement with a fixed selection mask.* The fiber closest to the center of the circle was selected for fiber diameter measurement.

4.2.4 Porosity Measurement

Each of the SEM images that were used to determine fiber diameter were also used to measure porosity as well. As mentioned in the previous section each image was

fitted with a fixed selection mask. In addition, each image used for porosity measurements was contrast enhanced to 10% pixel saturation in order to increase the prominence of each pore. The same selection mask was used to randomly select 9 pores to be measured using ImageJ. The pore closest to the center of each circle on the selection mask was outlined using the "freehand selection" tool in the ImageJ analysis software as seen in Figure 33. Each pore that was outlined was automatically calculated into an area in μm^2 by the software. The full protocol used is outlined in Appendix E.

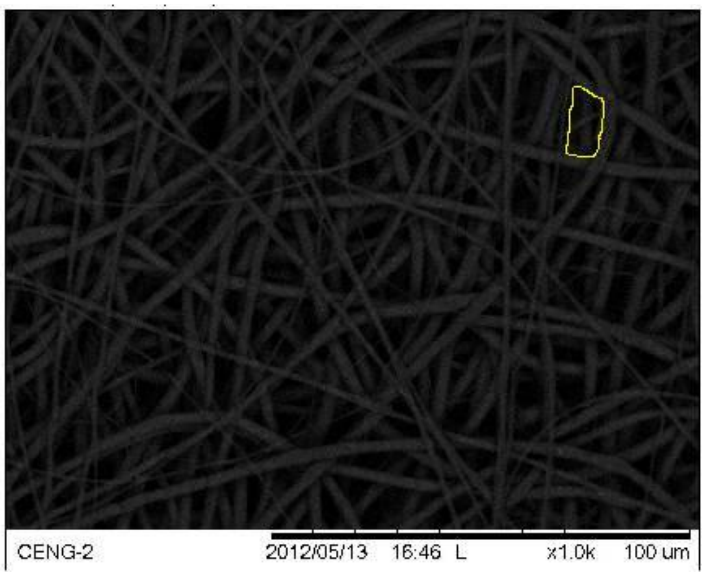

Figure 33: *Example image of porosity measurement.* The filtration mask is not shown as it is difficult to see the outlined pore in this example image with the mask present. The pore closest to the center of the circle of the filtration mask (same mask used in fiber diameter measurements) was selected for porosity measurement. Prior to measuring the pore of each image, the contrast was enhanced (10% pixel saturation) in order to see the pore more clearly.

4.2.5 Thickness Measurement

The wall thickness of each scaffold was also measured in order to evaluate the consistency of the electrospinning process. This assessment was performed to assist in

determining if the polymer fibers are aggregating on the collector uniformly. Additionally, this test was significant because a scaffold of varying wall thickness could alter the scaffold's mechanical properties. Thicker scaffolds would be less compliant that those with thinner walls [69]. The wall thickness was also vital for the tensile testing that was undertaken as part of this consistency study. Specifically, the wall thickness would be used for calculating the cross-sectional area for stress calculations when creating stress-strain curves for each scaffold sample.

The wall thickness measurements were obtained by taking the radial cross sections B1, B2, and B3 and placing them on the SEM sample stage so that the circumference or cross-section of the scaffold could be seen using SEM, as illustrated in Figure 33. The Hitachi TM-1000 tabletop SEM was used to capture scaffold wall thickness images at a magnification of 40x. A total of four measurements were made for each section, at locations corresponding to the four quarters of a circle (Fig. 34). Each SEM image was analyzed using ImageJ software in order to measure the thickness.

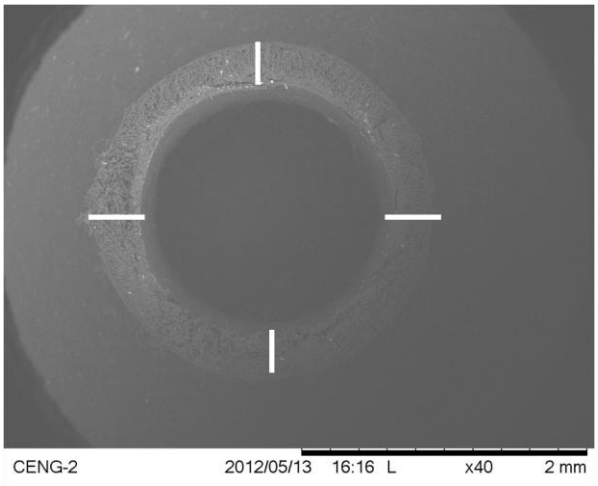

Figure 34: *Example image of SEM image used to measure wall thickness.* The white lines represent the four locations wall thickness measurements were made for each section (B1, B2, and B3)

4.2.6 Uniaxial Tensile Testing

Another assessment used to determine consistency of the scaffolds was uniaxial tensile testing. This testing was undertaken primarily for determining if the mechanical properties remained consistent with each in-house electrospun scaffold. Since the scaffold is to be implemented into a dynamic flow bioreactor, it is important that each scaffold has the tensile properties to withstand the fluidic pressure applied within the bioreactor. In particular, because the scaffold will potentially endure peristaltic flow it is important that as the scaffold may stretch circumferentially, that it returns to its original dimensions [69]. This property denotes stress in the linear elastic region of the material properties of the scaffold and is characterized by Young's modulus [69,93]. Hence, for this study the Young's modulus was of interest, rather than other properties like yield or ultimate tensile strength.

To calculate Young's modulus the relationship defined by Hooke's law was used. Specifically, Hooke's law is the relationship between the stress that a material experiences and the strain that it exhibits. Typically, the initial linear segment of a stress-strain curve is characterized by Equation 1. By calculating the strain (ε) and the stress (σ) using equations 2 and 3 respectively, the values can then be used in Eqn. 1 to find the Young's modulus (E), typically measured in Pascals.

$$\sigma = E\epsilon \qquad \text{Equation 1}$$

$$\epsilon = \frac{Extension\ (mm) + Length\ (mm)}{Length\ (mm)} \qquad \text{Equation 2}$$

$$\sigma = \frac{Load\ (N)}{Cross\text{-}Sectional\ Area\ (mm^2)} \qquad \text{Equation 3}$$

An Instron In-Spec 2200 benchtop tensile tester (Norwood, MA) was used for tensile testing for all of the samples. Sections C1, C2, C3, and C4 from each scaffold were cut longitudinally to create flattened rectangular sheets with lengths of approximately 15mm (see Figure 30). Each rectangular sheet section was measured for width and gauge length prior to testing using a digital caliper with a resolution of 0.01 mm. The width used for cross-sectional area calculations was the average wall thickness for each scaffold that was measured in the manner described in the previous section. Each sample was pulled at 0.5 mm/sec until the sample was visibly broken at the center. The Instron tensile tester provided data points for time, extension, and load. Using this data, stress-strain curves were generated using Microsoft Excel 2010. The linear elastic region of each curve was isolated, and a Trendline was calculated to determine a Young's modulus for each sample. All tensile testing stress-strain curves are available in Appendix G.

4.2.7 Statistical Analysis

All of the data for fiber diameter, porosity, wall thickness, and tensile properties was analyzed using JMP 10 statistical analysis software. In addition, all of the figures and statistical tests presented in the following section were generated using this software. A one-way analysis of variance (ANOVA) test was performed to test for statistical difference between the five electrospun scaffolds for each respective test (fiber diameter, porosity, wall thickness, and tensile properties). In addition, a Tukey HSD (Honestly Significance Difference) test was used to highlight the differences between each scaffold.

Intrascaffold sample data was also analyzed using ANOVA testing to determine if any differences in fiber diameter, porosity, and wall thickness were present within a scaffold.

4.3 RESULTS

4.3.1 Results and Statistical Analysis of Fiber Diameter

A statistical difference ($P < 0.0001$) amongst the fiber diameter of scaffolds 1 thru 5 was found with regards to the fiber diameter as illustrated in Figure 35. Although the scaffolds were statistically different in fiber diameter, an average of all the fiber diameter measurements made was approximately 2.556 µm. Figure 36 illustrates the variation amongst the scaffolds and respective sections with regards to fiber diameter.

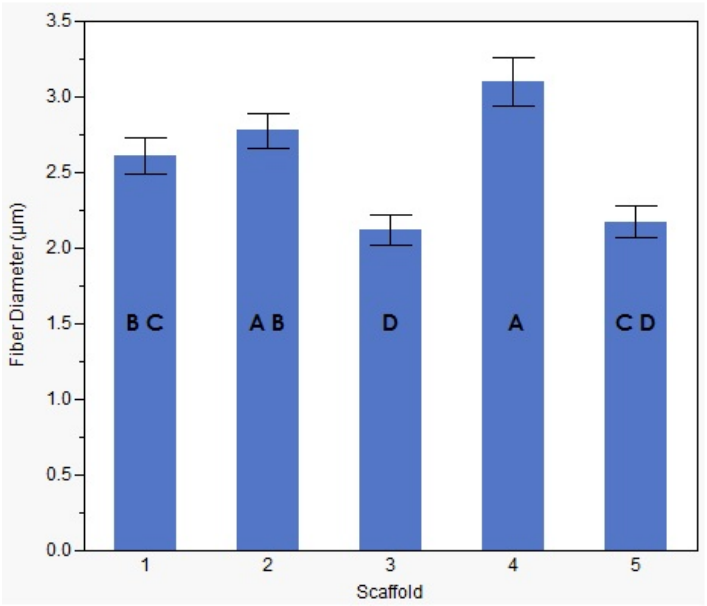

Figure 35: *Mean Fiber Diameter (µm) by Scaffold.* The ANOVA analysis demonstrated statistical difference ($P < 0.0001$) with regards to fiber diameter between the five scaffolds using a 95% confidence interval. Standard error bars are included for each scaffold. Tukey HSD test revealed specific scaffolds that were statistically different (scaffolds not connected by the same letter are statistically different).

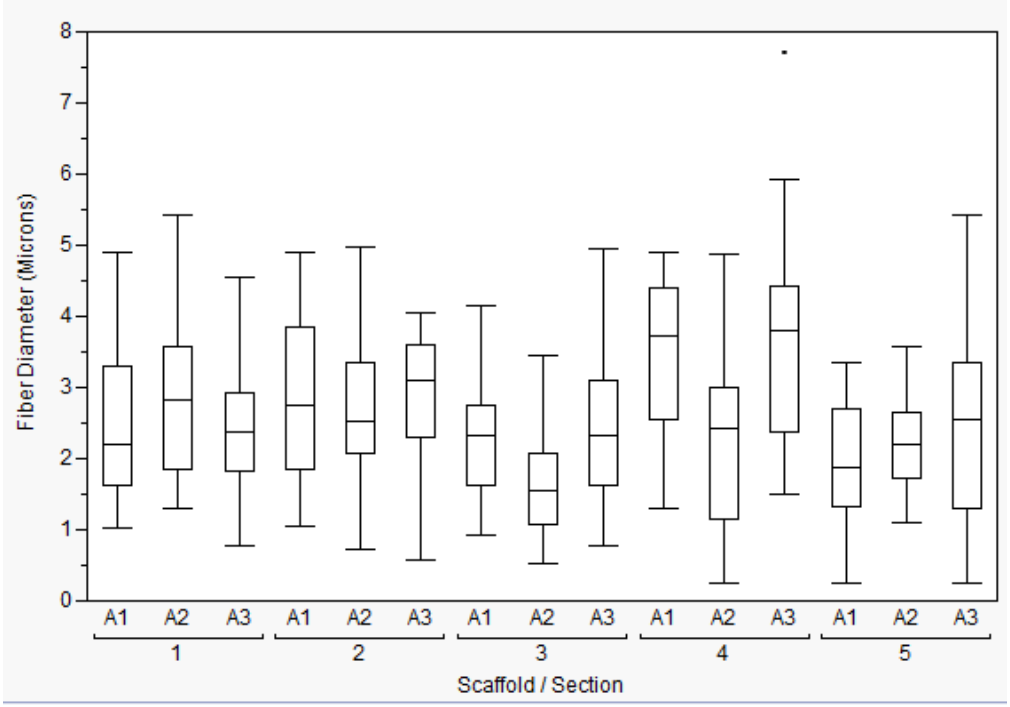

Figure 36: *Boxplots of the fiber diameters data illustrates how the fiber diameter varied between each scaffold and respective intrascaffold section*. The vertical lines demonstrate the non-outlier range, and the rectangle on each line represents the interquartile range of each data set. The horozontal line through each interquartile range box marks the median of each data set. The black points represent outliers.

Intrascaffold ANOVA testing was conducted to determine the consistency within each scaffold at the different sections (A1, A2, and A3). The sections imaged for scaffold 3 and 4 contained fibers of statistically different diameters as demonstrated in Table 3.

Table 3: *Intrascaffold ANOVA fiber diameter results.* Sections A1, A2 and A3 were all analyzed to determine if fiber diameter was statistically different within each scaffold. An * signifies statistical difference using a 95% confidence interval.

	Mean Fiber Diameter per section (µm)			
	A1	**A2**	**A3**	**P-VALUE**
Scaffold 1	2.52	2.85	2.49	0.3615
Scaffold 2	2.81	2.64	2.87	0.6884
Scaffold 3	2.21	1.67	2.47	**0.0039***
Scaffold 4	3.43	2.26	3.59	**0.0005***
Scaffold 5	1.96	2.16	2.40	0.2222

Ultimately, statistical analysis revealed that the fiber diameter was statistically different between scaffolds 1 thru 5. Additionally, intrascaffold ANOVA analysis indicated that scaffolds 3 and 4 demonstrated regions of statistically different fiber diameters within the scaffold, and that scaffolds 1, 2, and 5 were statistically similar.

4.3.2 Results and Statistical Analysis of Scaffold Porosity

Using JMP statistical software, the porosity data was analyzed in the same fashion as the fiber diameter. The average size of a pore amongst the five scaffolds was 71 μm^2 with a standard deviation of 52.6 μm^2. ANOVA testing indicated that the porosity between scaffolds 1 thru 5 was statistically different ($P < 0.0001$). However, Tukey HSD testing revealed that only scaffold 5 was statistically different from the rest as demonstrated in Figure 37. The variation in porosity between each scaffold and respective sections can be seen in Figure 38.

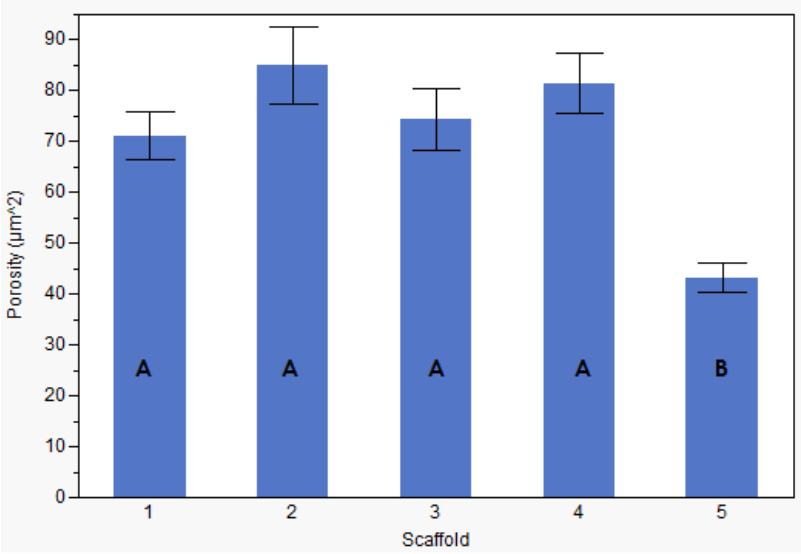

Figure 37: *Mean Porosity (μm^2) versus Scaffold.* The ANOVA analysis demonstrated statistical difference ($P < 0.0001$) with regards to porosity between the five scaffolds using a 95% confidence interval. Standard error bars are included for each scaffold. Tukey HSD test revealed specific scaffolds that were statistically different (scaffolds not connected by the same letter are statistically different).

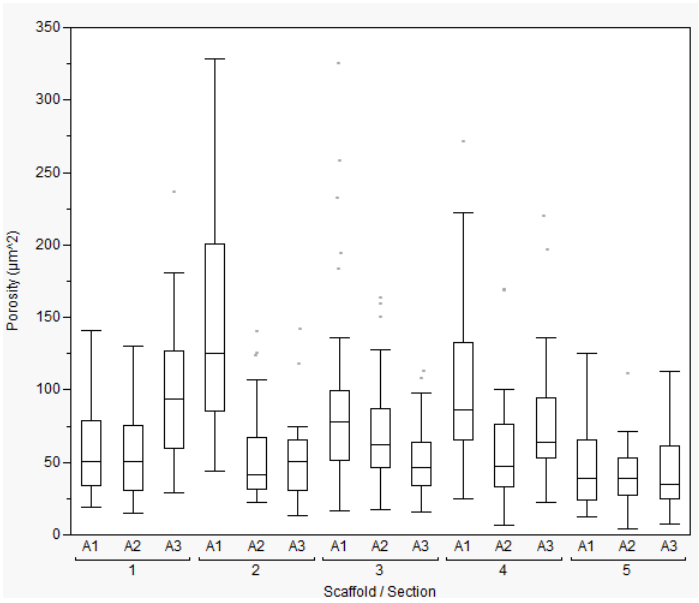

Figure 38: *Boxplots of the porosity data illustrates how the porosity varied between each scaffold and respective intrascaffold section*. The. The vertical lines demonstrate the non-outlier range, and the rectangle on each line represents the interquartile range of each data set. The horozontal line through each interquartile range box marks the median of each data set. The black points represent outliers.

Intrascaffold porosity of sections A1, A2, and A3 within each scaffold was also compared using oneway ANOVA testing. Analysis indicated that porosity varied within each scaffold except for one (scaffold 5). Calculated P-values are summarized in Table 4.

Table 4: *Intrascaffold ANOVA porosity results.* Sections A1, A2 and A3 were all analyzed to determine if porosity was statistically different within each scaffold. An * signifies statistical difference using a 95% confidence interval.

	Mean Porosity per section (μm^2)			
	A1	**A2**	**A3**	**P-VALUE**
Scaffold 1	59.83	54.36	99.32	**< 0.0001***
Scaffold 2	148.17	55.05	51.79	**< 0.0001***
Scaffold 3	98.37	72.24	52.76	**0.0074***
Scaffold 4	103.49	59.73	81.23	**0.0080***
Scaffold 5	48.51	39.94	41.17	0.4314

4.3.3 Results and Statistical Analysis of Wall Diameter

Wall thickness data was analyzed with ANOVA and Tukey HSD testing. Results indicated that the wall thickness between scaffolds 1 thru 5 was statistically different ($P < 0.0001$) as illustrated in Figure 39. Intrascaffold wall diameter was also analyzed using ANOVA testing. Analysis revealed that within each scaffold at the three sections (B1, B2, and B3) the wall diameter was statistically consistent for scaffolds 1,2,3, and 5. Scaffold 4 was the only scaffold to demonstrate intrascaffold statistical difference in wall diameter.

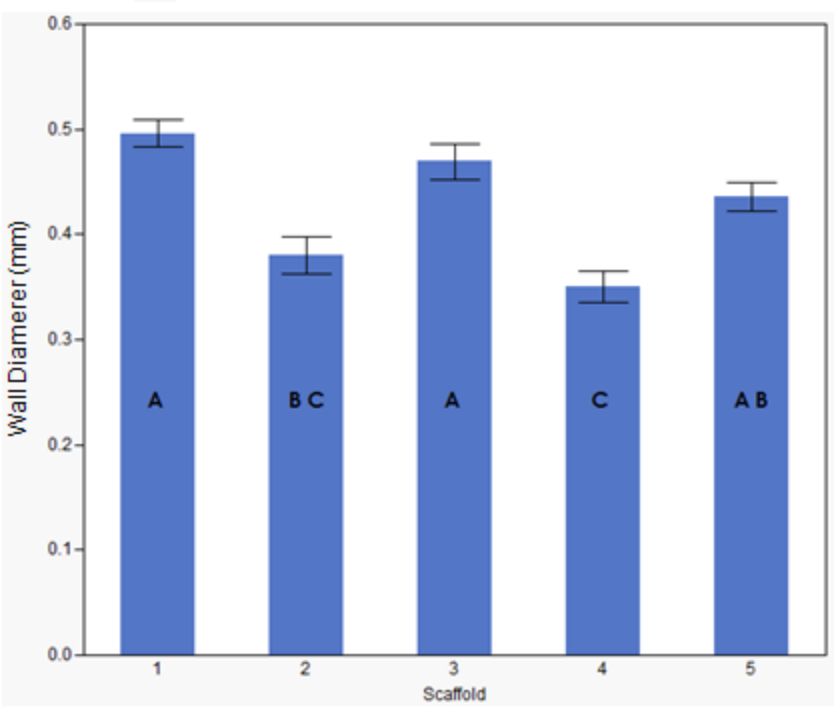

Figure 39: *Mean Wall Diameter (mm) versus Scaffold.* The ANOVA analysis demonstrated statistical difference ($P < 0.0001$) with regards to porosity between the five scaffolds using a 95% confidence interval. Standard error bars are included for each scaffold. Tukey HSD test revealed specific scaffolds that were statistically different (scaffolds not connected by the same letter are statistically different).

Table 5: *Intrascaffold ANOVA Wall Diameter results*. Sections B1, B2 and B3 were all analyzed to determine if wall diameter was statistically different within each scaffold. An * signifies statistical difference using a 95% confidence interval.

	Mean Wall Thickness per section (mm)			
	B1	**B2**	**B3**	**P-VALUE**
Scaffold 1	0.47	0.49	0.52	0.4089
Scaffold 2	0.32	0.43	0.39	**0.0210***
Scaffold 3	0.52	0.42	0.46	0.0523
Scaffold 4	0.38	0.34	0.33	0.2803
Scaffold 5	0.44	0.41	0.45	0.4992

4.3.4 Results and Statistical Analysis of Tensile Testing

The Young's modulus for each section of every scaffold is reported in Table 6. It should be noted that a modulus was not calculated for section C4 of scaffold 4 because of operator error while collecting data. An ANOVA test of the recorded values for Young's modulus was used to compare whether the value was consistent from scaffold to scaffold. Results indicated no statistical difference in the Young's modulus between scaffolds 1 thru 5 (P-value of 0.6134). A Tukey HSD test was generated as well and is illustrated in conjunction with the ANOVA test in Figure 40.

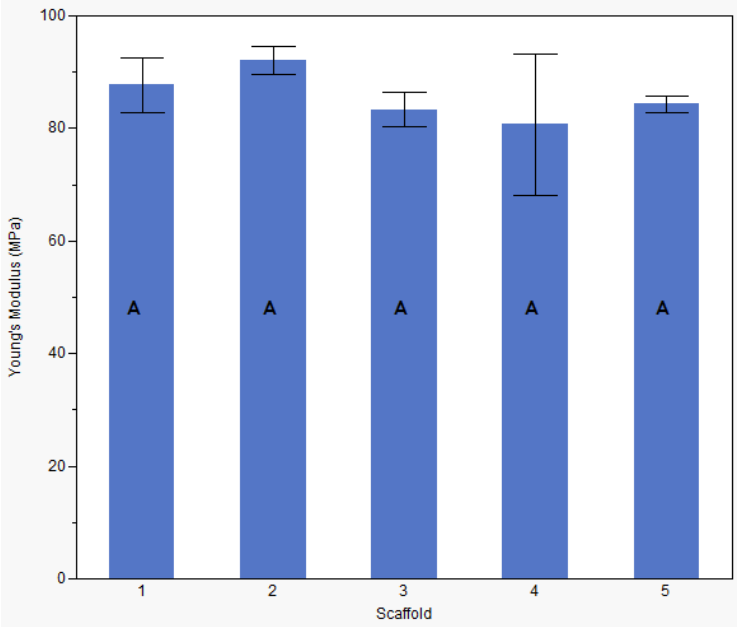

Figure 40: *Mean Young's modulus (MPa) versus Scaffold.* ANOVA analysis indicated no statistical difference (P-value of 0.6134) with regards to Young's modulus between the five scaffolds using a 95% confidence interval. Standard error bars are included for each scaffold. Tukey HSD test revealed specific scaffolds that were statistically different (scaffolds not connected by the same letter are statistically different).

Table 6: *Young's Modulus (MPa) per section of each scaffold.* The Young's modulus for scaffold 4, section C4 is not available because of operator error while collecting data.

	Young's Modulus (MPa) per Section			
	C1	**C2**	**C3**	**C4**
Scaffold 1	87.79	92.787	96.337	74.071
Scaffold 2	87.95	87.809	95.242	97.485
Scaffold 3	81.546	90.238	86.018	75.656
Scaffold 4	62.618	74.349	105.05	NA
Scaffold 5	82.257	87.556	91.726	85.667

In order to assess whether the location of the of the section had any effect on the mechanical properties of the scaffold, ANOVA testing was conducted by aggregating the Young's modulus values per section for all of the scaffolds. Results demonstrated that the different locations on the scaffolds had no statistically significant difference on the mechanical properties (P -value of 0.2313) as illustrated in Figure 41.

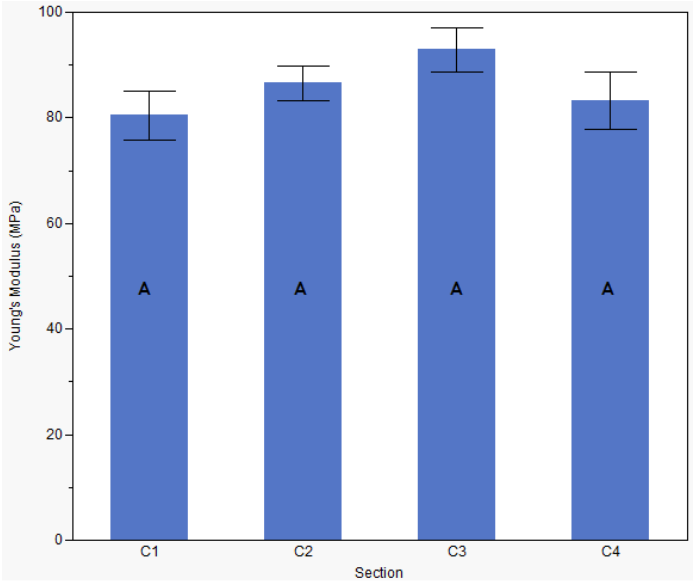

Figure 41: *Mean Young's modulus (MPa) by Section.* The ANOVA analysis indicated no statistical difference (P -value of 0.2313) with regards to Young's modulus between the four sections (C1,C2,C3, and C4) with a 95% confidence interval. Tukey HSD test revealed specific scaffolds that were statistically different (scaffolds not connected by the same letter are statistically different).

4.4 DISCUSSION AND CONCLUSIONS

In-house fabrication of electrospun scaffolds for the BBB application requires a certain level of consistency to ensure that the tissue engineered vessels do not differ from one another. As a result, the objective of the consistency studies presented in this chapter was to assess the reproducibility of the electrospinning protocol developed in the previous chapter, and better characterize the electrospun BBB scaffold. Specific measurements included: fiber diameter, porosity, wall thickness, and mechanical properties (Young's modulus). Besides comparing the scaffolds with one another, consistency throughout the length of the scaffold was evaluated as well.

Statistically, the fiber diameter varied between the scaffolds. However, data does indicate that the vast majority of fiber diameters were between 2 and 3 µm. The reason for the variation in the fiber diameter is unknown. Although a possible resolution could be to decrease the solution concentration of PLGA: $CHCL_3$. The solution concentration has been suggested to greatly influence fiber morphology up to a certain concentration [94]. Too low of a solution concentration can limit the uniformity of the fibers and result bead formation[30]. Within each scaffold the fiber diameter was consistent, except for scaffolds 3 and 4. Consistency within the scaffold demonstrates that along the length of the tubular scaffold, the fiber diameter is consistent from the proximal to distal end. Yet again, improving solution parameters may improve intrascaffold fiber consistency.

One of the major advantages of electrospinning is the ability to control the porosity by adjusting the electrospun fiber diameter through electrospinning processing and solution parameters [30]. Since the pores enable cellular infiltration and are physical areas that promote cellular attachment, the porosity of a scaffold used for tissue engineering is an important property [65]. Statistical analysis demonstrated that the pore size varied between the scaffolds, however, a Tukey HSD revealed that only scaffold 5 was statistically different from the other scaffolds. With a higher sample size, an ANOVA analysis of the pore size may reveal no statistical difference between the scaffolds. Moreover, an average pore size of 70.06 μm^2 with a standard deviation of 52.60 μm^2 was calculated for all pore size measurements (n = 405). Although cellular interactions with the electrospun scaffolds was not the objective of this thesis, the mean pore size measured in this study indicates that the cells used in the DIV-BBB model should have more than adequate space to infiltrate the scaffold. Intrascaffold analysis of

the pore size revealed that within each scaffold the pore size was inconsistent for four of the five scaffolds. These results are surprising since intrascaffold fiber diameter was mostly statistically similar. Moreover, the reason for the inconsistency in pore size within each scaffold is unknown. However, since the mean pore size within each scaffold section was never lower than 39 μm^2. There should be adequate space for the cells to infiltrate, especially since the cells used for the BBB application, glial and endothelial cells, are typically around 10μm[84].

The wall thickness was statistically inconsistent between the electrospun scaffolds. The wall thickness ranged from 0.31 to 0.54 mm. Sample preparation post-electrospinning may have contributed to the inconsistent data. Although the sectioning and assessment of wall thickness was conducted with great diligence and carefulness, removing the scaffold sections from the metal mandrel is an arduous process with a great deal of operator contact that could have influenced the wall thickness as the scaffold was being removed. Intrascaffold analysis indicated that within the length of each tubular scaffold, the wall thickness was statistically consistent for all of the scaffolds except for scaffold 2. Areas of lower resistance along the length of the grounded mandrel may result in preferential fiber collection sites resulting in differences within the scaffold [69]. However, since only one of the five scaffolds demonstrated intrascaffold variation it is highly unlikely that the grounded mandrel was demonstrating any areas of lower resistance.

The data aggregated from tensile testing revealed that there was no statistical difference between the mechanical response and the consistency between the electrospun scaffolds. It was also determined that the location of the section was insignificant on the

mechanical properties of the scaffold. These results are unusual since the structure (fiber diameter in this case) determines the mechanical properties (Young's modulus) [69]. Statistical analysis revealed a difference in fiber diameter between all of the scaffolds. A possible explanation may be that although a statistical difference was found, the difference of approximately one micrometer between the average fiber diameters of all five scaffolds was not significant enough structurally to alter the scaffold's mechanical properties.

Overall, the consistency study conducted and reported in this chapter demonstrated statistical inconsistencies in fiber diameter, porosity, and wall thickness between each scaffold fabricated using electrospinning. However, the process did indicate statistically consistent scaffolds mechanically. A major limitation to this study was the sample size was only five scaffolds. Since the DIV-BBB is not yet completely developed, it was not cost appropriate or logical to undergo an expansive study without truly understanding the biological cellular interaction with the electrospun scaffolds. With future experimentation, a larger sample size may greatly influence the statistical analysis and demonstrate less variation between each scaffold. Further research into reassessing the solution parameters may also promote uniformity and result in less variation.

Since there are several processing, solution, and ambient parameters that can influence the morphology of an electrospun scaffold, this process is far from being an exact science. There are countless combinations of parameters that can be used to electrospin. The data presented in this thesis can be used as a foundation for future

research and improvements to the electrospinning process and the fabrication of scaffolds for the BBB application once the DIV-BBB system at Cal Poly is fully developed.

CHAPTER 5 - DISCUSSION AND CONCLUSION

5.1 OVERVIEW

As the scope of the Tissue Engineering group at Cal Poly expanded to include BBB models, scaffolding for a vessel of approximately 2 mm in diameter was required. While the work of this thesis was being conducted, a DIV-BBB system was concurrently being developed. Accordingly, the system required scaffolding that would promote uniform cellular attachment, infiltration, and proliferation of C6 glial and BAECs (bovine aortic endothelial cells). Scaffolding for larger vessels, *in vitro* blood vessel mimics (BVM), was already being fabricated using an in-house electrospinner system. Subsequently, it was a logical decision to pursue electrospinning as a process that could be used for fabricating scaffolds for tissue engineering an *in vitro* BBB vessel, as illustrated in Figure 42.

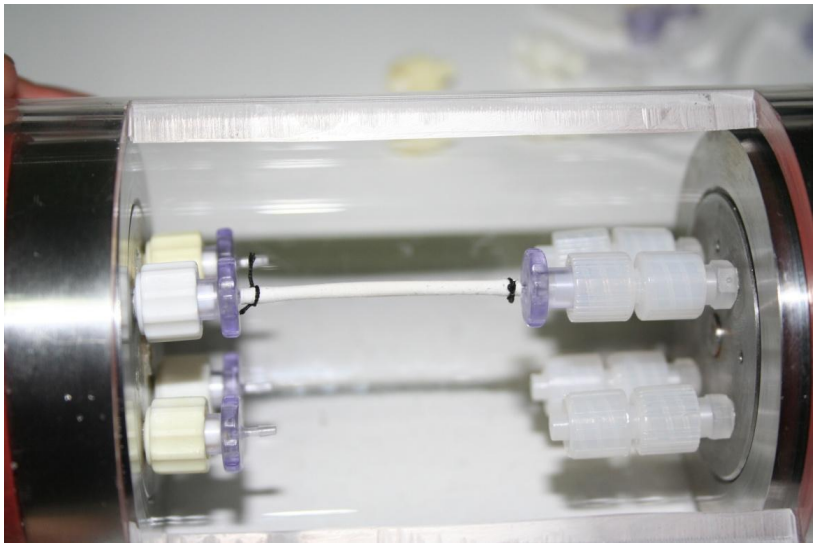

Figure 42: *Electrospun PLGA scaffold installed in the Cal Poly DIV-BBB model bioreactor.*

Electrospinning is a widely used technology that utilizes electrical forces to produce fine polymer fibers using a broad variety of both natural and synthetic polymers[30]. Moreover, electrospinning scaffolds for tissue engineering applications offers several major advantages, including: a high surface-to-volume ratio, tunable porosity, malleability to conform to a wide range of sizes and shapes, and the ability to control the fiber composition to achieve desired results from its properties and functionality [30]. As a result, this thesis hypothesized that a protocol could be developed to electrospin a scaffold that would consistently offer properties that would be conducive to an *in vitro* BBB model. Specific characteristics that were desired included: fiber uniformity and consistency, mechanical strength that could endure pulsatile flow from the bioreactor, a fiber diameter that would be in the low micrometer range, and an average pore size that would permit cellular infiltration. In order to develop a scaffold that would meet the aforementioned criteria, extensive research was undertaken to understand the electrospinning process and the broad list of processing, solution, and ambient parameters that can influence the technique. The literature research that was carried out was summarized and presented in Chapter 1.

The original electrospinner system was well-built with a careful attention to detail [69]. However, several years had passed since the system was first developed, and financial limitations that were present at the time restricted the capabilities of the system. Consequently, the first aim of this thesis was to optimize and refine the original electrospinner system. The improvements made were presented in Chapter 2 of this thesis. Specific modifications included replacing the power supply, creating an electrical

layout that would ensure operator safety and equipment longevity, and improving the syringe pump setup. In brief, the optimized electrospinner system enabled the ability to employ new electrospinning strategies such as electrospinning with a negative polarity applied voltage, and the ability to employ a non-traditional setup that utilizes a positive applied voltage at the spinneret, and a negative applied voltage at the collector. All of the changes were made with the intention of improving the fabrication of electrospun scaffolds for the BBB application and for other future tissue engineering investigations.

Once the electrospinner system had been refined, a series of ten electrospin trials were used to better understand the influence of several processing parameters, and develop a protocol for BBB scaffold fabrication. The methodology and qualitative results of each trial electrospin were presented in Chapter 3. The final set of processing parameters that were selected for the electrospinning BBB scaffolding was then evaluated for consistency. Accordingly, five scaffolds were electrospun using the developed protocol, and assessed for consistency in: fiber diameter, pore size, wall thickness, and mechanical properties (Young's modulus). In addition, intrascaffold sections at different locations were studied to determine if consistency was present throughout the length of each tubular electrospun scaffold. The methodology, results, and statistical analysis were presented in Chapter 4. Results indicated that the fiber diameter, pore size, and wall thickness varied statistically between all of the scaffolds. Additionally, intrascaffold results revealed at least one scaffold was inconsistent along its length with regards to fiber diameter, wall thickness, and pore size. The mechanical properties of each electrospun scaffold were statistically similar.

The variations discovered with the electrospun scaffolds did demonstrate statistically significant differences; however, the range at which these differences were found may have no practical importance. For instance, the range in the average fiber diameter found for each scaffold varied by approximately a single micrometer. Since cellular studies were not conducted, there is no certainty on whether the inconsistencies found on the scaffolds will have a direct influence on cellular attachment, proliferation, or infiltration. However, as the DIV-BBB system is in its final developmental stages, the results that were arrived upon from this thesis can be used as a foundation for future work concerning BBB scaffolding.

5.2 LIMITATIONS AND FUTURE WORK

5.2.1 Sample Size and Biological Cellular Assessment

After discussing the results with the California Polytechnic State University, San Luis Obispo Statistics consulting group, the sample size used (n = 5) for the consistency study may not have been large enough to come up with an accurate conclusion. Power analysis of the data currently available determines that a sample size of 25 scaffolds would permit a 90% power level. Larger sample sizes typically lead to increased precision when estimating unknown parameters in an empirical study [95]. However, since the DIV-BBB system is not completely developed, it was not logical or cost appropriate to conduct a study with a sample size of 25 scaffolds without the ability to assess the biological interaction with the electrospun scaffold in detail.

Furthermore, once the DIV-BBB system is completely developed, it would be prudent to conduct a consistency study that includes cellular attachment, proliferation,

and infiltration assessments using immunohistochemistry (IHC) and histology with a greater number of scaffolds to truly assess the reproducibility and effectiveness of the electrospinning process.

Another important assessment will include the difference between fiber diameter at the nano- and micrometer scale. As the protein protrusions that extend from a cell are on the nano scale, it may be worth exploring the use of a scaffold with fiber diameters in the nanometer range. However, Pham et. al has reported success in terms of cellular infiltration and attachment with dynamic perfusion culture using electrospun scaffolds with fiber diameters in the low micron range[33]. As conflicting literature does exist, it will be imperative once the DIV-BBB system at Cal Poly is completely developed to assess any potential differences with regards to cellular attachment and infiltration.

5.2.2 Improving Wall Thickness Assessment

In order to measure the wall thickness of the scaffold, sections of the scaffold were cut using a carbon steel blade and placed on an SEM sample stage so that the circumference or cross-section of the tubular scaffold was exposed. The samples were then imaged using a Hitachi TM-1000 tabletop SEM, and analyzed for thickness using ImageJ. A noticeable problem with this method was that while cutting the sections and removing them from the metal mandrel, an incredible amount of operator contact is required with the scaffold. Accidental pressure from the contact by the operator may have decreased the true cross-sectional thickness. Alternative thickness measurement techniques should be explored to address this problem in sample preparation. Preferably, the wall thickness should be measured with the scaffold still on the mandrel. Future work

may involve using ultrasonic imaging which could be a possible technique that could be used to save time and increase the accuracy of the wall thickness measurements [69].

5.2.3 Tensile Testing Assessment

In order to determine the mechanical properties of the electrospun scaffold, the tubular scaffold was first sectioned into 15 mm pieces in length with two radial cuts. A longitudinal cut was then made and the scaffold was flattened out resulting in a rectangular sheet. By unfolding the electrospun scaffold and flattening it out, compressive and tensile forces are applied to the exterior and interior surfaces of the scaffold respectively. These opposing forces may cause separation of the fibers in the scaffold, and alter the true mechanical properties of the scaffold [96]. In addition, a limitation to the tensile testing was that only longitudinally oriented samples were mechanically tested, since the tubular scaffold was too small to test radially oriented samples. Future work may explore methods for testing radial mechanical properties of the scaffold that are not influenced by sample preparation. Berry implemented a custom fixture which utilized two rods that could be inserted into the lumen of a BVM scaffold. Each rod could then be pulled in opposite directions to pull the scaffold apart [97]. Future work could use a similar idea for the smaller BBB scaffold in order to prevent disruption of the mechanical properties via sample preparation. Furthermore, it may be important to assess the mechanical properties of scaffolds with inconsistent fiber morphology in order to compare with the electrospun scaffolds using the protocol developed in Chapter 4.

5.2.4 Reassessment of the Solution Parameters

The work in this thesis was able to produce scaffolds with fiber diameters in the low micron range, with pores that enable adequate space for cells to infiltrate and attach. However, the consistency studies revealed that the scaffolds fabricated using electrospinning were statistically inconsistent. The variation in fiber morphology could be resolved by adjusting the solution parameters [94]. Peńa studied the solution parameters in great detail, and evaluated scaffolds fabricated from various PLGA solution concentrations [67]. As a newly optimized electrospinner system is being used with new processing parameters, future work may investigate using different solvents such as tetrahydrofurane (THF) [98] or using a different solution concentration [45].

Furthermore, it may be worth assessing different blends or molecular weights of PLGA as both influence the co-polymer's material properties. The blend currently used is a 75:25 (Lactide: Glycolide) and has a molecular weight of 66,000 to 107,000. Future work may investigate the effect of different blends of PLGA, to determine if a difference is present in the fiber morphology and mechanical properties of the electrospun scaffolds. The molecular weight has a considerable effect on the rheological and electrical properties such as viscosity, surface tension, conductivity, and dielectric strength [30]. The molecular weight of the polymer reflects the number of entanglements of polymer solution chains in a solution, and hence the solution viscosity. It is key to maintain a sufficient number of entanglements of the polymer chains to ensure a level of solution viscosity to produce a uniform jet during electrospinning that restrains the antagonistic effects of surface tension at the tip of the spinnerert. Accordingly, assessing the molecular weight of PLGA may be another area worth exploring.

5.2.5 Modifying the Ambient Parameters

Several research groups have conducted studies with regards to the influence of ambient parameters on the electrospinning process. Future work may explore the effect temperature or humidity has on jet dynamics and fiber morphology of electrospun scaffolds. Investigation into whether a different media within the isolation chamber may be another possibility. Currently, atmospheric gas is contained within the isolation chamber of the electrospinner system at Cal Poly. Fang et al. utilized an isolation chamber filled with argon. This novel setup was reported to have resulted in an efficient, continuous, and highly productive fiber fabrication technique [99]. If possible, this type of setup may be worth investigating.

5.2.6 Improving Scalability of Electrospun Scaffold Fabrication

Currently, the electrospinner collector system limits a single scaffold to be electrospun at a time. One of the major disadvantages of electrospinning is scalability, especially since a single jet is not very feasible for applications that require large quantities of fibers [30]. Research groups have used a porous hollow tube instead of a single spinneret in order to produce multiple jets that permit faster and larger fabrication of fiber meshes [41]. Future work may explore developing a collection system that allowed several mandrels to be grounded, rotated, translated, and all be used at once. This could increase scaffold production, however, may result in significant variation.

5.2.7 New Electrospinning Strategies

Once the DIV-BBB system is completely developed, and cellular interactions with the BBB electrospun scaffold can be assessed, future work may explore the multilayering electrospinning technique. This method fabricates layered scaffolds by electrospinning sequentially different polymers [100], or by creating a scaffold with alternating layers of micro- and nanofibers [33]. Using different polymers or adjusting the processing parameters to create alternating layers of micro- and nanofibers may result in better cellular interactions with the scaffold, or enable fabrication of scaffolds with certain desired mechanical properties. In particular, as the BBB scaffold is to be sodded with two different cell types, it may be advantageous to initially layer larger fibers then after some time smaller fibers. This would result in larger fibers at the interior surface of the lumen, and smaller diameter fibers at increasing depths of the scaffold. As larger fibers tend to result in larger pores [35], this sort of multilayered scaffold could potentially enable better infiltration of the C6 glial cells which are to be sodded prior to the BAECs in the DIV-BBB model at Cal Poly.

Another electrospinning technique that may be investigated in the future is using two power supplies at once in a non-traditional setup. The current optimized electrospinner system permits applying a voltage with a positive polarity to the spinneret and a negative polarity applied voltage to the collector. This strategy would permit one to adjust the electric field lines and influence fiber morphology [37]. Investigating this technique would require a tremendous amount of time and money since there are countless combinations of voltages, and flow rates that would need to be tested to determine the effects.

5.3 CONCLUSION

The DIV-BBB system that is currently being developed at Cal Poly has great potential to be used for pre-clinical testing for pharmaceutical drugs that target the CNS, as well as a model that can be utilized to study pathologies that result from BBB dysfunction. The scaffold is one of several key components needed to successfully create a tissue engineered vessel. The optimized in-house electrospinner system demonstrates great promise to fabricate scaffolds for the BBB application and other future tissue engineering investigations. Moreover, further research is required to assess the consistency of the scaffolds being produced using electrospinning. Additionally, it will be important to assess cellular interactions with the electrospun scaffold once the DIV-BBB system is completely developed. The work presented in this thesis establishes a BBB scaffold electrospinning protocol, and a preliminary assessment of consistency that can be used as a baseline for future studies.

LIST OF REFERENCES:

1 Cucullo, L., Aumayr, B., Rapp, E. & Janigro, D. Drug delivery and in vitro models of the blood-brain barrier. *Curr Opin Drug Discov Devel* **8**, 89-99 (2005).

2 Jolliet-Riant, P. & Tillement, J. P. Drug transfer across the blood-brain barrier and improvement of brain delivery. *Fundam Clin Pharmacol* **13**, 16-26, doi:S0767398199800036 [pii] (1999).

3 Deli, M. A., Abraham, C. S., Kataoka, Y. & Niwa, M. Permeability studies on in vitro blood-brain barrier models: physiology, pathology, and pharmacology. *Cell Mol Neurobiol* **25**, 59-127 (2005).

4 Cucullo, L. *et al.* A new dynamic in vitro model for the multidimensional study of astrocyteâ€“endothelial cell interactions at the bloodâ€“brain barrier. *Brain Research* **951**, 243-254 (2002).

5 Dehouck, M. P. *et al.* Drug transfer across the blood-brain barrier: correlation between in vitro and in vivo models. *J Neurochem* **58**, 1790-1797 (1992).

6 Abbott, N. J. Evidence for bulk flow of brain interstitial fluid: significance for physiology and pathology. *Neurochem Int* **45**, 545-552, doi:10.1016/j.neuint.2003.11.006 S0197018603002675 [pii] (2004).

7 Abbott, N. J., Ronnback, L. & Hansson, E. Astrocyte-endothelial interactions at the blood-brain barrier. *Nat Rev Neurosci* **7**, 41-53, doi:nrn1824 [pii] 10.1038/nrn1824 (2006).

8 Lundquist, S. *et al.* Prediction of drug transport through the blood-brain barrier in vivo: a comparison between two in vitro cell models. *Pharm Res* **19**, 976-981 (2002).

9 Kortekaas, R. *et al.* Blood–brain barrier dysfunction in parkinsonian midbrain in vivo. *Annals of Neurology* **57**, 176-179, doi:10.1002/ana.20369 (2005).

10 Liebner, S. *et al.* Claudin-1 and claudin-5 expression and tight junction morphology are altered in blood vessels of human glioblastoma multiforme. *Acta Neuropathol* **100**, 323-331 (2000).

[11] Abbott, N. J. Prediction of bloodâ€“brain barrier permeation in drug discovery from in vivo, in vitro and in silico models. *Drug Discovery Today: Technologies* **1**, 407-416 (2004).

[12] Grant, G. A., Abbott, N. J. & Janigro, D. Understanding the Physiology of the Blood-Brain Barrier: In Vitro Models. *News Physiol Sci* **13**, 287-293 (1998).

[13] Stanness, K. A. *et al.* Morphological and functional characterization of an in vitro blood-brain barrier model. *Brain Res* **771**, 329-342, doi:S0006-8993(97)00829-9 [pii] (1997).

[14] Berzin, T. M. *et al.* Agrin and microvascular damage in Alzheimer's disease. *Neurobiol Aging* **21**, 349-355, doi:S0197-4580(00)00121-4 [pii] (2000).

[15] Ballabh, P., Braun, A. & Nedergaard, M. The blood-brain barrier: an overview: structure, regulation, and clinical implications. *Neurobiol Dis* **16**, 1-13, doi:10.1016/j.nbd.2003.12.016 S0969996103002833 [pii] (2004).

[16] de Boer, A. G. & Gaillard, P. J. Blood–brain barrier dysfunction and recovery. *Journal of Neural Transmission* **113**, 455-462, doi:10.1007/s00702-005-0375-4 (2006).

[17] Axiotis, C. A., Guarch, R., Merino, M. J., Laporte, N. & Neumann, R. D. P-glycoprotein expression is increased in human secretory and gestational endometrium. *Laboratory investigation; a journal of technical methods and pathology* **65**, 577-581 (1991).

[18] Cecchelli, R. *et al.* In vitro model for evaluating drug transport across the blood-brain barrier. *Adv Drug Deliv Rev* **36**, 165-178, doi:S0169-409X(98)00083-0 [pii] (1999).

[19] Naik, P. & Cucullo, L. In vitro blood–brain barrier models: Current and perspective technologies. *Journal of Pharmaceutical Sciences* **101**, 1337-1354, doi:10.1002/jps.23022 (2011).

[20] Santaguida, S. *et al.* Side by side comparison between dynamic versus static models of bloodâ€“brain barrier in vitro: A permeability study. *Brain Research* **1109**, 1-13 (2006).

[21] Parkinson, F. E., Friesen, J., Krizanac-Bengez, L. & Janigro, D. Use of a three-dimensional in vitro model of the rat bloodâ€“brain barrier to assay nucleoside efflux from brain. *Brain Research* **980**, 233-241 (2003).

[22] McAllister, M. S. *et al.* Mechanisms of glucose transport at the bloodâ€“brain barrier: an in vitro study. *Brain Research* **904**, 20-30 (2001).

[23] O. Ogunshola, O. In Vitro Modeling of the Blood-Brain Barrier: Simplicity Versus Complexity. *Current Pharmaceutical Design* **17**, 2755-2761 (2011).

[24] Jin Ho, L., Jong Woo, P. & Hai Bang, L. Cell adhesion and growth on polymer surfaces with hydroxyl groups prepared by water vapour plasma treatment. *Biomaterials* **12**, 443-448 (1991).

[25] Nago, S. & Mizutani, Y. Microporous polypropylene hollow fibers with double layers. *Journal of Membrane Science* **116**, 1-7 (1996).

[26] Yeow, M. L., Liu, Y. & Li, K. Preparation of porous PVDF hollow fibre membrane via a phase inversion method using lithium perchlorate (LiClO4) as an additive. *Journal of Membrane Science* **258**, 16-22 (2005).

[27] Deshmukh, S. P. & Li, K. Effect of ethanol composition in water coagulation bath on morphology of PVDF hollow fibre membranes. *Journal of Membrane Science* **150**, 75-85 (1998).

[28] Loeb, S. & Sourirajan, S. in *Saline Water Conversion?II* Vol. 38 *Advances in Chemistry* 117-132 (AMERICAN CHEMICAL SOCIETY, 1963).

[29] Jansen, J. C., Macchione, M. & Drioli, E. High flux asymmetric gas separation membranes of modified poly(ether ether ketone) prepared by the dry phase inversion technique. *Journal of Membrane Science* **255**, 167-180 (2005).

[30] Bhardwaj, N. & Kundu, S. C. Electrospinning: a fascinating fiber fabrication technique. *Biotechnol Adv* **28**, 325-347, doi:S0734-9750(10)00006-6 [pii] 10.1016/j.biotechadv.2010.01.004 (2010).

[31] Bhattarai, S. R. *et al.* Novel biodegradable electrospun membrane: scaffold for tissue engineering. *Biomaterials* **25**, 2595-2602, doi:S0142961203007816 [pii] (2004).

[32] Min, B. M. *et al.* Electrospinning of silk fibroin nanofibers and its effect on the adhesion and spreading of normal human keratinocytes and fibroblasts in vitro. *Biomaterials* **25**, 1289-1297, doi:S0142961203006574 [pii] (2004).

[33] Pham, Q. P., Sharma, U. & Mikos, A. G. Electrospun poly(epsilon-caprolactone) microfiber and multilayer nanofiber/microfiber scaffolds: characterization of scaffolds and measurement of cellular infiltration. *Biomacromolecules* **7**, 2796-2805, doi:10.1021/bm060680j (2006).

[34] Yoshimoto, H., Shin, Y. M., Terai, H. & Vacanti, J. P. A biodegradable nanofiber scaffold by electrospinning and its potential for bone tissue engineering. *Biomaterials* **24**, 2077-2082, doi:S014296120200635X [pii] (2003).

[35] Eichhorn, S. J. & Sampson, W. W. Statistical geometry of pores and statistics of porous nanofibrous assemblies. *J R Soc Interface* **2**, 309-318, doi:M9LGNT8L9379J0WE [pii] 10.1098/rsif.2005.0039 (2005).

[36] Thandavamoorthy Subbiah, G. S. B., R.W. Tock, S. Parameswaran, S.S. Ramhumar. Electrospinning of Nanofibers. *Journal of Applied Polymer Science* **96**, 557-569 (2004).

[37] Subbiah, T., Bhat, G. S., Tock, R. W., Parameswaran, S. & Ramkumar, S. S. Electrospinning of nanofibers. *Journal of Applied Polymer Science* **96**, 557-569, doi:10.1002/app.21481 (2005).

[38] Reneker, L. W., Silversides, D. W., Xu, L. & Overbeek, P. A. Formation of corneal endothelium is essential for anterior segment development - a transgenic mouse model of anterior segment dysgenesis. *Development* **127**, 533-542 (2000).

[39] Luu, Y. K., Kim, K., Hsiao, B. S., Chu, B. & Hadjiargyrou, M. Development of a nanostructured DNA delivery scaffold via electrospinning of PLGA and PLA-PEG block copolymers. *J Control Release* **89**, 341-353, doi:S016836590300097X [pii] (2003).

[40] Hayati, I., Bailey, A. I. & Tadros, T. F. Investigations into the mechanisms of electrohydrodynamic spraying of liquids: I. Effect of electric field and the environment on pendant drops and factors affecting the formation of stable jets and atomization. *Journal of Colloid and Interface Science* **117**, 205-221 (1987).

[41] Dosunmu, O. O., Chase, G. G., Kataphinan, W. & Reneker, D. H. Electrospinning of polymer nanofibres from multiple jets on a porous tubular surface. *Nanotechnology* **17**, 1123-1127, doi:S0957-4484(06)08401-7 [pii]10.1088/0957-4484/17/4/046 (2006).

[42] Taylor. Electrically Driven Jets. *Proceedings of the Royal Society of London. Series A, Mathematical and Physical Sciences* **313**, 453-475.

[43] Buchko, C. J., Chen, L. C., Shen, Y. & Martin, D. C. Processing and microstructural characterization of porous biocompatible protein polymer thin films. *Polymer* **40**, 7397-7407 (1999).

[44] Peter K, B. Electrostatic spinning of acrylic microfibers. *Journal of Colloid and Interface Science* **36**, 71-79 (1971).

[45] Teo, W. E. & Ramakrishna, S. A review on electrospinning design and nanofibre assemblies. *Nanotechnology* **17**, R89-R106, doi:S0957-4484(06)22291-8 [pii] 10.1088/0957-4484/17/14/R01 (2006).

[46] Yang, S., Leong, K. F., Du, Z. & Chua, C. K. The design of scaffolds for use in tissue engineering. Part I. Traditional factors. *Tissue Eng* **7**, 679-689, doi:10.1089/107632701753337645 (2001).

[47] Yang, J. *et al.* Cell sheet engineering: Recreating tissues without biodegradable scaffolds. *Biomaterials* **26**, 6415-6422 (2005).

[48] Matthews, J. A., Wnek, G. E., Simpson, D. G. & Bowlin, G. L. Electrospinning of collagen nanofibers. *Biomacromolecules* **3**, 232-238, doi:bm015533u [pii] (2002).

[49] Um, I. C., Fang, D., Hsiao, B. S., Okamoto, A. & Chu, B. Electro-spinning and electro-blowing of hyaluronic acid. *Biomacromolecules* **5**, 1428-1436, doi:10.1021/bm034539b (2004).

[50] Stankus, J. J., Guan, J. & Wagner, W. R. Fabrication of biodegradable elastomeric scaffolds with sub-micron morphologies. *J Biomed Mater Res A* **70**, 603-614, doi:10.1002/jbm.a.30122 (2004).

[51] Ma, Z., Kotaki, M. & Ramakrishna, S. Electrospun cellulose nanofiber as affinity membrane. *Journal of Membrane Science* **265**, 115-123 (2005).

[52] Chen, Z., Mo, X. & Qing, F. Electrospinning of collagenâ€“chitosan complex. *Materials Letters* **61**, 3490-3494 (2007).

[53] Doshi, J. & Reneker, D. H. Electrospinning process and applications of electrospun fibers. *Journal of Electrostatics* **35**, 151-160 (1995).

[54] Ltd, T. N. Z. I. f. P. a. F. R. (2008).

[55] Reneker, D. H. Bending instability of electrically charged liquid jets of polymer solutions in electrospinning. *Journal of Applied Physics* **87**, 17 (2000).

[56] Sukigara, S., Gandhi, M., Ayutsede, J., Micklus, M. & Ko, F. Regeneration of Bombyx mori silk by electrospinningâ€”part 1: processing parameters and geometric properties. *Polymer* **44**, 5721-5727 (2003).

[57] Fong, H., Chun, I. & Reneker, D. H. Beaded nanofibers formed during electrospinning. *Polymer* **40**, 4585-4592 (1999).

[58] Haghi, A. K. & Akbari, M. Trends in electrospinning of natural nanofibers. *physica status solidi (a)* **204**, 1830-1834, doi:10.1002/pssa.200675301 (2007).

[59] Jacobs, V., Anandjiwala, R. D. & Maaza, M. The influence of electrospinning parameters on the structural morphology and diameter of electrospun nanofibers. *Journal of Applied Polymer Science* **115**, 3130-3136, doi:10.1002/app.31396 (2009).

[60] Larrondo, L. & St. John Manley, R. Electrostatic fiber spinning from polymer melts. I. Experimental observations on fiber formation and properties. *Journal of Polymer Science: Polymer Physics Edition* **19**, 909-920, doi:10.1002/pol.1981.180190601 (1981).

[61] Yuan, X., Zhang, Y., Dong, C. & Sheng, J. Morphology of ultrafine polysulfone fibers prepared by electrospinning. *Polymer International* **53**, 1704-1710, doi:10.1002/pi.1538 (2004).

[62] Wannatong, L., Sirivat, A. & Supaphol, P. Effects of solvents on electrospun polymeric fibers: preliminary study on polystyrene. *Polymer International* **53**, 1851-1859, doi:10.1002/pi.1599 (2004).

[63] Zhang, C., Yuan, X., Wu, L., Han, Y. & Sheng, J. Study on morphology of electrospun poly(vinyl alcohol) mats. *European Polymer Journal* **41**, 423-432 (2005).

[64] Mit-uppatham, C., Nithitanakul, M. & Supaphol, P. Ultrafine Electrospun Polyamide-6 Fibers: Effect of Solution Conditions on Morphology and Average Fiber Diameter. *Macromolecular Chemistry and Physics* **205**, 2327-2338, doi:10.1002/macp.200400225 (2004).

[65] Casper, C. L., Stephens, J. S., Tassi, N. G., Chase, D. B. & Rabolt, J. F. Controlling Surface Morphology of Electrospun Polystyrene Fibers:â€‰ Effect of Humidity and Molecular Weight in the Electrospinning Process. *Macromolecules* **37**, 573-578, doi:10.1021/ma0351975 (2003).

[66] Prestwich, G. D. Simplifying the extracellular matrix for 3-D cell culture and tissue engineering: a pragmatic approach. *J Cell Biochem* **101**, 1370-1383, doi:10.1002/jcb.21386 (2007).

[67] Pena, T. *Preparation and Characterization of Electrospun Poly(D,L-Lactide-Co-Gylcolide) Scaffolds for Vascular Tissue Engineering and the Advancement of an In Vitro Blood Vessel Mimic* Master of Science thesis, California Polytechnic State University, (2009).

[68] Liang, D., Hsiao, B. S. & Chu, B. Functional electrospun nanofibrous scaffolds for biomedical applications. *Advanced Drug Delivery Reviews* **59**, 1392-1412 (2007).

[69] James, C. *Assesment of Electrospinning as an In-House Fabrication Technique for Blood Vessel Mimic Cellular Scaffolding* Master of Science thesis, California Polytechnic State University, (2009).

[70] Agarwal, S. & Greiner, A. On the way to clean and safe electrospinning—green electrospinning: emulsion and suspension electrospinning. *Polymers for Advanced Technologies* **22**, 372-378, doi:10.1002/pat.1883 (2011).

[71] Kilic, A. Effects of Polarity on Electrospinning Process. *Textile Research Journal* **78** (2008).

[72] Boland, E. D. *et al.* Electrospinning polydioxanone for biomedical applications. *Acta Biomaterialia* **1**, 115-123 (2005).

[73] Boland, E. D., Telemeco, T. A., Simpson, D. G., Wnek, G. E. & Bowlin, G. L. Utilizing acid pretreatment and electrospinning to improve biocompatibility of poly(glycolic acid) for tissue engineering. *Journal of Biomedical Materials Research Part B: Applied Biomaterials* **71B**, 144-152, doi:10.1002/jbm.b.30105 (2004).

[74] Boland, E. D., Wnek, G. E., Simpson, D. G., Pawlowski, K. J. & Bowlin, G. L. TAILORING TISSUE ENGINEERING SCAFFOLDS USING ELECTROSTATIC PROCESSING TECHNIQUES: A STUDY OF POLY(GLYCOLIC ACID) ELECTROSPINNING. *Journal of Macromolecular Science, Part A* **38**, 1231-1243, doi:10.1081/ma-100108380 (2001).

[75] McManus, M. C. *et al.* Mechanical properties of electrospun fibrinogen structures. *Acta Biomaterialia* **2**, 19-28 (2006).

[76] McManus, M. C., Boland, E. D., Simpson, D. G., Barnes, C. P. & Bowlin, G. L. Electrospun fibrinogen: Feasibility as a tissue engineering scaffold in a rat cell culture model. *Journal of Biomedical Materials Research Part A* **81A**, 299-309, doi:10.1002/jbm.a.30989 (2007).

[77] Reneker, D. H. & Yarin, A. L. Electrospinning jets and polymer nanofibers. *Polymer* **49**, 2387-2425 (2008).

[78] Supaphol, P., Mit-uppatham, C. & Nithitanakul, M. Ultrafine Electrospun Polyamide-6 Fibers: Effects of Solvent System and Emitting Electrode Polarity on Morphology and Average Fiber Diameter. *Macromolecular Materials and Engineering* **290**, 933-942, doi:10.1002/mame.200500024 (2005).

[79] Sutasinpromprae, J., Jitjaicham, S., Nithitanakul, M., Meechaisue, C. & Supaphol, P. Preparation and characterization of ultrafine electrospun polyacrylonitrile fibers and their subsequent pyrolysis to carbon fibers. *Polymer International* **55**, 825-833, doi:10.1002/pi.2040 (2006).

[80] Boland, E. (ed Deven Patel) (San Luis Obispo, 2011).

[81] Deitzel, J. M., Kleinmeyer, J. D., Hirvonen, J. K. & Beck Tan, N. C. Controlled deposition of electrospun poly(ethylene oxide) fibers. *Polymer* **42**, 8163-8170 (2001).

[82] Yarin, A. L., Koombhongse, S. & Reneker, D. H. Taylor cone and jetting from liquid droplets in electrospinning of nanofibers. *Journal of Applied Physics* **90**, 4836-4846 (2001).

[83] Castillo, Y. (ed Deven Patel) (San Luis Obispo, 2011).

[84] Alberts, B. (Garland Science, New York, 2002).

[85] In Jeong, S. *et al.* Tissue-engineered vascular grafts composed of marine collagen and PLGA fibers using pulsatile perfusion bioreactors. *Biomaterials* **28**, 1115-1122 (2007).

[86] Shin, H. J. *et al.* Electrospun PLGA nanofiber scaffolds for articular cartilage reconstruction: mechanical stability, degradation and cellular responses under mechanical stimulation in vitro. *Journal of Biomaterials Science, Polymer Edition* **17**, 103-119 (2006).

[87] Makadia, H. K. Poly Lactic-co-Glycolic Acid (PLGA) as Biodegradable Controlled Drug Delivery Carrier. *Polymers* **3**, 1377-1397 (2011).

[88] Anderson, J. M. & Shive, M. S. Biodegradation and biocompatibility of PLA and PLGA microspheres. *Advanced Drug Delivery Reviews* **28**, 5-24 (1997).

[89] Fischer, T. & Hampp, N. A. Encapsulation of purple membrane patches into polymeric nanofibers by electrospinning. *IEEE Trans Nanobioscience* **3**, 118-120 (2004).

[90] Ki, C. S. *et al.* Characterization of gelatin nanofiber prepared from gelatinâ€“formic acid solution. *Polymer* **46**, 5094-5102 (2005).

[91] Geng, X., Kwon, O.-H. & Jang, J. Electrospinning of chitosan dissolved in concentrated acetic acid solution. *Biomaterials* **26**, 5427-5432 (2005).

[92] Zhao, Z. *et al.* Preparation and properties of electrospun poly(vinylidene fluoride) membranes. *Journal of Applied Polymer Science* **97**, 466-474, doi:10.1002/app.21762 (2005).

[93] Ho Joon, S. *et al.* Electrospun PLGA nanofiber scaffolds for articular cartilage reconstruction: mechanical stability, degradation and cellular responses under mechanical stimulation in vitro. *Journal of Biomaterials Science -- Polymer Edition* **17**, 103-119 (2006).

[94] Mo, X. M., Xu, C. Y., Kotaki, M. & Ramakrishna, S. Electrospun P(LLA-CL) nanofiber: a biomimetic extracellular matrix for smooth muscle cell and endothelial cell proliferation. *Biomaterials* **25**, 1883-1890 (2004).

[95] Bartlett, J. E., II, Kotrlik, J. W., & Higgins, C. Orginizational research: Determining the appropriate sample size for survey research. *Information Technology, Learning and Prformance Journal* **19**, 43-50 (2001).

[96] Mller, R. Size-dependent elastic properties of nanosized structural elements. *Nanotechnology* **11** (2000).

[97] Berry, C. *Design and Development of Two Test Fixtures to Test the Longitudinal and Transverse Tensile Properties of Small Diameter Tubular Polymers* Master's thesis, California Polytechnic State University - San Luis Obispo, (2011).

[98] Lee, K. H., Kim, H. Y., Bang, H. J., Jung, Y. H. & Lee, S. G. The change of bead morphology formed on electrospun polystyrene fibers. *Polymer* **44**, 4029-4034 (2003).

[99] Jian Fang, L. Z., David Sutton, Xungai Wang, Tong Lin. Needleless Melt-Electrospinning of Polypropylene Nanofibres. *Journal of Nanomaterials* **2012**, 9 (2012).

[100] Kidoaki, S., Kwon, I. K. & Matsuda, T. Mesoscopic spatial designs of nano- and microfiber meshes for tissue-engineering matrix and scaffold based on newly devised multilayering and mixing electrospinning techniques. *Biomaterials* **26**, 37-46 (2005).

APPENDIX A: MIXING PLGA SOLUTIONS FOR ELECTROSPINNING

Protocol was taken from Tiffany R. Pena's thesis.

Table 1: Bill of Materials

Materials/Equipment	Vendor	Part Number	Quantity
Poly (DL-lactide-co-glycolide) (PLGA) Lactide: Glycolide (75:25) Mol wt 66,000 - 107,000	Sigma-Aldrich	P1941	5 grams
Chloroform, extra dry, water <50ppm, stabilized	Fisher Scientific, Inc	326820010	1 Liter
10 ml Syringe, Luer-Lok tip	BD	309604	100/Pack
Blunt Fill Needle, 18G 1 ½ (1.2 mm x 40 mm)	BD	305180	100/Pack
Analytical Balance	Acculab	ALC-80.4	1
Orbital Shaker [check new shaker]			1
Vacuum-Pressure Pipette Aid	Drummon Scientific Co.	P-80991	1
Serological Pipet 5 x 1/10 ml	VWR International	53283-706	NA
Clear Glass Vial 20 ml	VWR International	15900-002	72/CS

Procedure

1. Calculate the amount of PLGA resin necessary for the desired weight percent polymer solution using the following equation. (Density of chloroform is 1.48 g/ml.)

$$WPP = m1/ (m1 + m2b)$$

WPP = Weight percent polymer solution

m1 = mass of polymer (g)

m2 = mass of solvent (ml)

b = density of solvent (g/ml)

2. Put on safety gloves. (*WARNING: Chloroform can have serious side-effects if it comes in contact with skin, eyes or is inhaled or swallowed. Target organs to be effected are kidneys, heart, central nervous system, liver, eyes, reproductive system and skin. Always open chloroform in a hood and wear protective clothing!!*

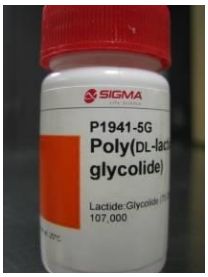

Figure 1: Bottled PLGA

3. Remove PLGA (Figure 1) from the freezer and allow it to reach room temperature (5-10 minutes). Doing so prevents condensation when the polymer is exposed to air.
4. Weigh out the calculated amount of PLGA using the Acculab Balance (Figure 2) and place the polymer in a 20 ml clear vial. Close the lid immediately.
5. Return unused PLGA to the freezer.

Figure 2: Acculab Balance

6. Retrieve the chloroform (Figure 3) for the hazardous chemical cabinet and place it in the fume hood immediately.
7. Gather the Pipette-Aid, a 10 ml disposable pipette and the vial of weighed PLGA and place in the hood with the chloroform.
8. Pipette the desired volume of chloroform into the vial with PLGA. Immediately cap the vial as well as the chloroform container to prevent evaporation of chloroform since it is highly volatile.
9. Properly label the solution vial with the WPP, date and your initials.
10. Wrap vial in aluminum foil to prevent light from entering the solution (chloroform is highly sensitive to light).

Figure 3: Bottled chloroform

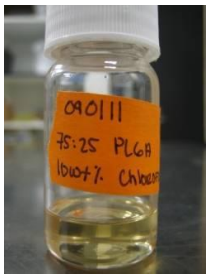

Figure 4: Labeled vial of WPP

11. Place the vial on the shake table. Set the shake table to approximately 3 revolutions per second. Use tape to ensure that the vial will stay upright while on the shake table. Turn the table on.
12. Allow the solution to mix for 24 hours. After mixing is complete, the solution is usable for up to 48 hours.
13. Remove chloroform container from hood and place back into chemical cabinet.
14. Properly dispose of the pipette tip.
15. Clean up work area.

APPENDIX B: ORIGINAL ELECTROSPINNING PROTOCOL

Protocol used taken Yvette Castillo's Thesis. Protocol originally developed by Colby James, and was later modified by Tiffany Pena and Yvette Castillo.

<u>WARNING:</u> This electrospinning process requires extremely high voltages! Always wear shoes, gloves, and be mindful of what you are touching. Do not attempt to use the electrospinner unless you have been trained by a qualified user.

1. Put on safety gloves and protective clothing. (*<u>WARNING</u>: Chloroform can have serious side-effects if it comes in contact with skin, eyes or is inhaled or swallowed. Target organs to be effected are kidneys, heart, central nervous system, liver, eyes, reproductive system and skin. It is possible for residual chloroform to be present on and around the electrospinner during and after a spin!! Make sure to read the MSDS for all chemicals you are working with and know the necessary emergency procedures.)*
2. The green ground wire located on the backside of the collector can be removed by pulling it straight out. Unplug the green ground wire from the collector (Figure).
3. The yellow power wire connects the collector to the DC motor control box. The yellow power wire comes off the DC motor control box by unscrewing the connection head. Unscrew the yellow power wire from the DC motor control box (Figure).

Figure 1: Green ground wire location on back of the collector

Figure 2: Location of the yellow power wire on the DC motor control box

4. The collector can now be removed from the containment chamber. Remove the collector from the containment chamber and place it on the counter outside the fume hood (Figure).

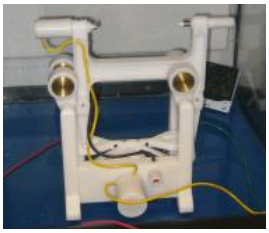

Figure 3: Entire electrospinner in the containment chamber

5. During a spin, stray polymer preferentially builds up on exposed metal, wires and the motor casing. Cleaning before each spin is necessary to remove any residual polymer or dust from the collector that may potentially interfere with the next spin process. Clean the collector using IPA and paper towels. Ensure all residues from both the front and back of the collector including the wires are removed (Figure).

Figure 4: Polymer build up on collector that needs cleaning

6. During a spin, stray polymer can attach to any wall of the containment chamber and even form webs of polymer between walls. If necessary, clean the inside of the containment chamber with IPA.
7. Replace the collector back inside the containment chamber and reconnect the green ground and yellow power wires.
8. Prepare the mandrel for spinning. Clean the mandrel with IPA to remove any dust, residual polymer from a previous spin, or metal particles. If the mandrel surface is scratched, fine grit sand paper can be used to re-smooth the surface of the mandrel. If sanding is necessary, clean the mandrel with IPA when finished.
9. Attach the mandrel to the collector. When inserting the mandrel, rotate the turn knob until most of the metal chuck is covered, you will feel some resistance. If you go too far the turn knob will spring back.

10. There are three power cords to the right of the fume hood; one for the external power supply, one for the main power and one for the DC motor control box. Plug in all the equipment.
11. Using a multimeter, check the resistance between the ground connection and the mandrel. Verify that there is some conductivity. Record your measurements (Figure).

Figure 5: Multimeter lead placement to measure resistance

12. In the fume hood, prepare a 10 ml syringe with an 18GA fill needle.
13. Remove aluminum foil from the PLGA solution vial for better visibility when working with the solution.
14. Solutions may be highly viscous and filling the syringe may take time and require some strength. Make sure to not release pressure on the plunger when drawing solution into the syringe. Acquire just over 3 ml of the polymer solution into the prepared 10 ml syringe (Figure).

Figure 6: Syringe usage to acquire polymer solution

15. Once the solution has been acquired in the syringe, replace the fill needle with an 18GA Blunt needle.
16. Push the plunger back into the syringe until most of the air is removed and the solution is just in the needle. *<u>WARNING:</u> If you push too hard too fast the polymer melt may squirt out. If this happens you will need to attach a new needle.*
17. Place the filled 10 ml syringe into the syringe pump. The needle should go through the needle tip hole in the containment chamber wall (Figure).

Figure 7: Position of collector for electrospinning

18. Re-position the collector in the containment chamber so that the mandrel and the needle tip are the desired amount of inches apart and perpendicular to each other, by lining the collector against the marked ruler (Figure). *NOTE: The side of the collector with green ground wire connection should face away from the needle.*

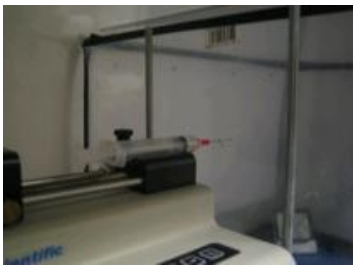

Figure 8: Syringe/needle placement on syringe pump and within needle hole on containment chamber.

19. Hang the exposed metal of the red high voltage wire on the needle tip inside the containment chamber. You can secure the wire on the needle by taping the wire to the containment chamber wall (Figure). *<u>WARNING</u>: If the wire falls off the needle during the spin, the external 10 V power source used to regulate high voltage output will burn out. Be sure to hang the wire on the needle securely!*

Figure 9: Attachment of red high voltage wire on needle tip

20. The power switch for the syringe pump is located on the back of the pump. Turn the syringe pump on.
21. Enter the desired flow rate and solution volume. The solution volume will determine when the pump will stop. Make sure the screen remains on volume. NOTE: Syringe pump instructions are located in a cabinet close to the fume hood if you need further instructions.

22. Turn on the “Rotate” and “Slide” functions of the collector at the DC motor control box. Ensure the collector is now oscillating back and forth and the mandrel is rotating. If the mandrel is not rotating, you can tap it gently to get it started (Figure).

Figure 10: DC motor control box

23. Secure the containment chamber by sliding close the front wall.
24. Turn on the external power source and set it to the desired voltage. Turn the external power source off (Figure).


Figure 11: External power source

Read Steps 25-40 BEFORE beginning the electrospinning process. The following steps for turning ON and OFF the electrospinning system must be followed in the exact order listed.

25. Press the “Run” button on the syringe pump. The volume count will begin on the screen and an arrow will flash meaning the solution is now being pushed through the needle.
26. When a droplet forms on the tip of the needle, the process is ready to begin.
27. Turn on the “Main Power” (left switch). Power is on if the light on the AC/DC power converter turns green (Figure).
28. Turn on the external source.
29. Prepare to turn on the High Voltage (right switch) (Figure). Look at the droplet of polymer on the end of the syringe and turn High Voltage on. The droplet should disappear.

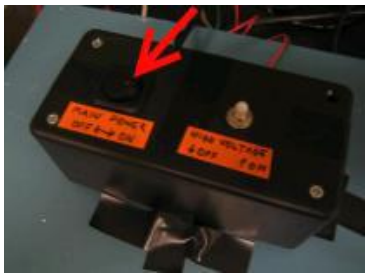
Figure 12: Main power switch

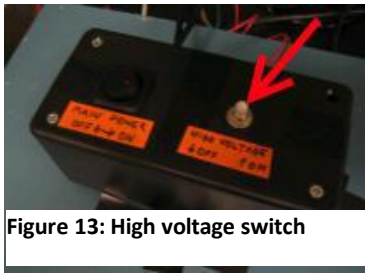
Figure 13: High voltage switch

30. Monitor the process for the entire spin. The mandrel should slowly start to become coated with the polymer.
31. When the entire polymer solution has been spun, the process should be shut down in the following order.
    a. Press the RUN/STOP button on the syringe pump.
    b. Turn the HV switch to OFF
    c. Turn the Main Power OFF
    d. Turn the ROTATE and SLIDE functions on the DC Motor Control box OFF.
32. In order to allow the solvent to fully evaporate, wait a few minutes before removing the mandrel from the containment chamber.
33. Remove the front containment chamber wall.
34. Remove the mandrel with PLGA scaffold.
35. Touch the red high voltage wire to the green ground wire to remove any residual charge.
36. Remove syringe from syringe pump and dispose in sharps container.
37. Unplug all equipment.
38. Properly dispose of all waste and clean up your work station.
39. Transfer the mandrel with the PLGA scaffold to the desiccators for further drying of the scaffold. Allow the scaffold to remain on the desiccators for 24 hours.
40. Remove the scaffold from the mandrel using gauze and carefully twist the scaffold off.

APPENDIX C: BBB ELECTROSPINNING PROTOCOL

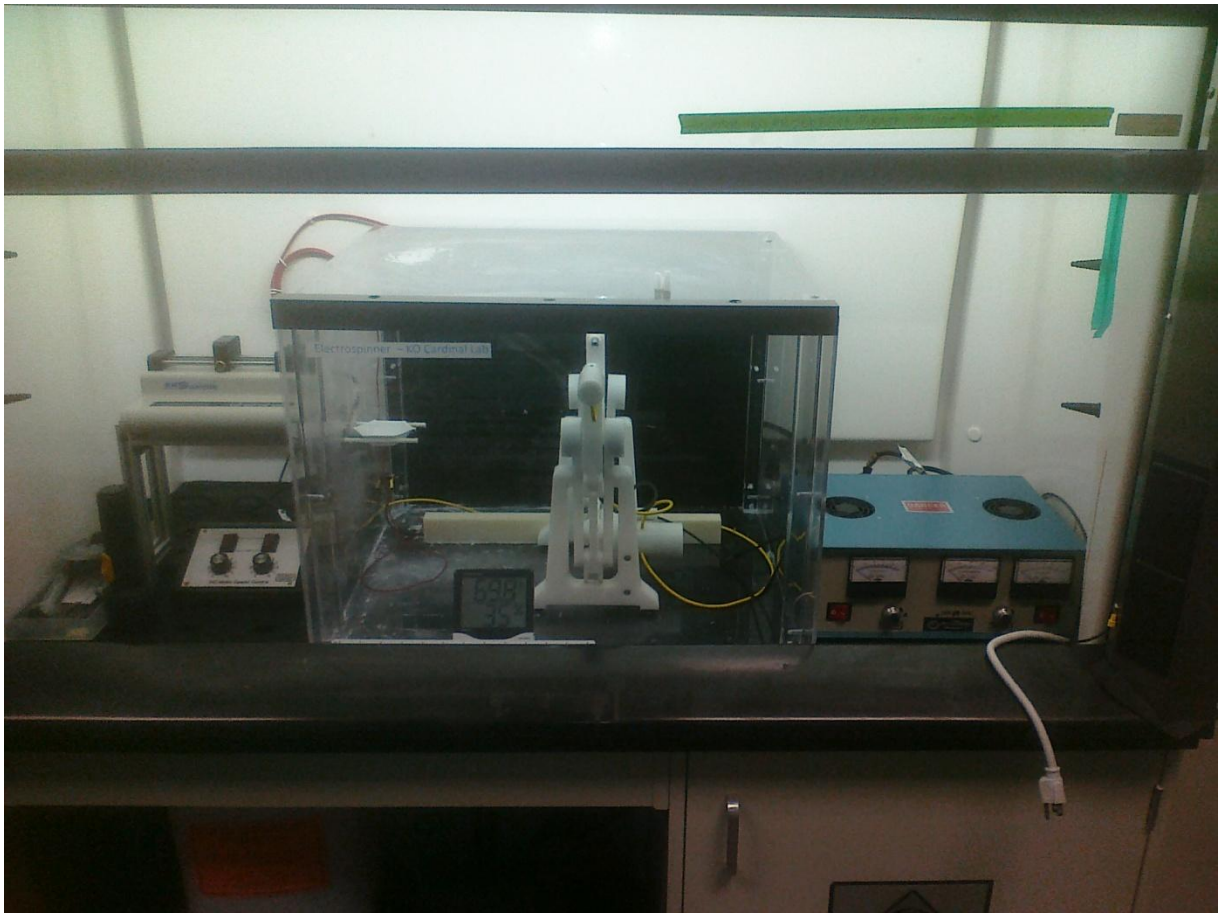

<u>WARNING:</u> This process utilizes extremely high voltages. Always wear shoes, gloves, and be careful of what you are contacting. To use the electrospinner, you must be trained by a qualified user and be approved by an appropriate faculty member.

BBB Parameters are in red

Polymer:	15wt% PLGA in Chloroform ($CHCl_3$)
Flow Rate:	4.5ml/hr, 2ml of polymer solution used
Needle:	18 gauge, beveled, blunt (BD 305180)
Gap:	10 inches
Voltage:	- 18,000V (negative polarity)
Translate:	Distance set at 16cm, translation speed set at 3 or 55 OPM
Rotate:	Rotation speed at 6 or 3110 RPM

1) Put on latex gloves.
2) Clean debris left from previous spins using paper towels and isopropal alcohol (IPA). Be sure to clean polymer collection system (Figure 1) and inside walls of the isolation chamber.
3) Sand mandrel with 1200 grain sandpaper (Figure 2), then spray and clean off with IPA.
4) Insert mandrel into collector.
5) Attach a 18 gauge BD needle to a BD 10ml plastic syringe.
6) Inside the fume hood, pull the desired amount of polymer solution into the syringe - 2mL for BBB scaffolds. The polymer solution is very viscous, so this will take some time. Be sure that there is no air within the syringe.
7) Place needle through the small hole drilled in the isolation chamber and set the syringe onto the syringe pump (Figure 3).

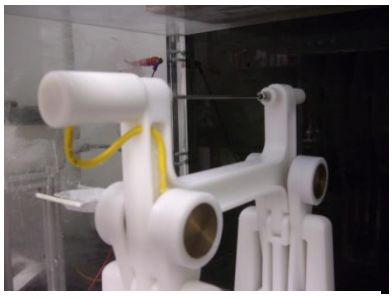

Figure 1: Clean collection system

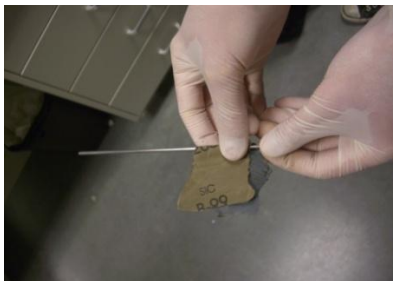

Figure 2: Sand mandrel with sand paper

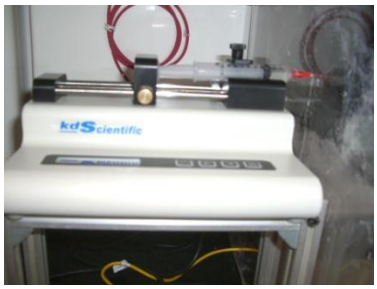

Figure 3: Secure syringe on syringe pump, and place needle into the isolation chamber

8) Secure the syringe into position using the black clamp on the syringe pump.

9) Clip the red high voltage alligator clip to the needle inside the isolation chamber, see Figure 4.

Figure 4: Attach high voltage alligator clip to needle.

10) Position the collection system in the isolation chamber so that the metal mandrel and needle tip are at the desired gap distance and perpendicular to each other - 10 inches or 25.4 cm for BBB scaffolds.

11) Take the black ground banana plug and connect to the collector system as seen in Figure 5.

Figure 5: Connect black ground wire to collection system.

12) Using a multimeter, check the resistance between the ground connection and the aluminum mandrel to verify conductivity. One should see very little resistance (fractions of an ohm) if the mandrel is properly grounded. If a very high resistance is detected, the mandrel is no longer maintaining continuity with the ground wire.

13) Close the front panel of the isolation chamber.

14) Next, plug in the surge protector into the wall outlet of the fume hood.

15) Flip the green switch on the surge protector to turn it on, and as a result provide power to the syringe pump, rotation and translation regulator, and power supply.

16) Switch on the syringe pump, and enter the desired settings (syringe type, volume, flow rate, etc.). The syringe pump will maintain the same settings that were used previously. So if no one has used the apparatus since, there is no need to make any changes to the syringe pump programming.

Syringe Type: BD 10 ml Plastic syringe (select from syringe pump library)
Volume: 2mL
Flow Rate: 4.5 ml/hr

17) Turn on the "Rotate" and "Slide" functions of the collector at the regulator box. The speed at which the mandrel rotates and translates is controlled from this box. Settings 3 for slide, and 6 for rotate.

18) Press the "Run" button on the syringe pump so that the polymer solution will begin ejecting at a controlled volumetric rate.

19) Once a polymer droplet forms at the tip of the spinneret, the electrospinning process is ready to start. Immediately turn on the power supply (Figure 6), press red button, and adjust output voltage knob to the desired applied voltage (-18kV).

Figure 6: High Voltage Power supply.

20) Observe the process of the entire spin, slowly the metal mandrel will become visibly coated with polymer (white color).

Figure 7: Detach polymer coated mandrel from collection system

21) Once the desired amount of polymer solution has been electrospun, the process should be shut down in the following manner.

22) Turn the high voltage power supply off, by flipping the red switch to "off."

23) Next, press the "Run/Stop" button on the syringe pump to stop the pump. Then turn the syringe pump off.

24) Turn the "Rotate" and "slide" switches off on the regulator box.

25) Flip the green switch of the surge protector to "off." And then unplug the surge protector from the wall outlet of the fume hood.

26) Slide open the front panel of the isolation chamber and wait for a few minutes to allow the evaporated solvent to leak out and be taken up by the fume hood.

27) Detach the polymer coated mandrel from the collector system, see Figure 7.

28) Contact the red high voltage alligator clip to the black ground wire to remove any residual charge.

Figure 8: Dispose any material that came in contact with chloroform into Hazardous Waste bucket.

29) Clean any polymer fiber debris using paper towels and isopropal alcohol (IPA). Be sure to clean polymer collection system (Figure 1) and inside walls of the isolation chamber.

30) Dispose of the syringe needle in the sharps container.

31) Dispose syringe and polymer solution vials into Hazardous Waste bucket, Figure 8.

32) Take the polymer coated mandrel to the desiccator and leave for at least 24 hours before sectioning, Figure 9.

33) Cut polymer scaffold off of metal mandrel between 24-48 hours later (once polymer is completely dry) and place onto glass rod in desiccator; be sure rod is labeled clearly (with tape).

34) Return metal mandrel to top of desiccator box.

Figure 9: Place metal mandrel with polymer scaffold around it into the desiccator after electrospinning.

APPENDIX D: IMAGE J SOFTWARE ANALYSIS PROTOCOL

Protocol used taken from Yvette Castillo's thesis. Protocol was originally developed by Tiffany Pena and modifications were made by Yvette Castillo.

1. Open program ImageJ. The following screen will appear.

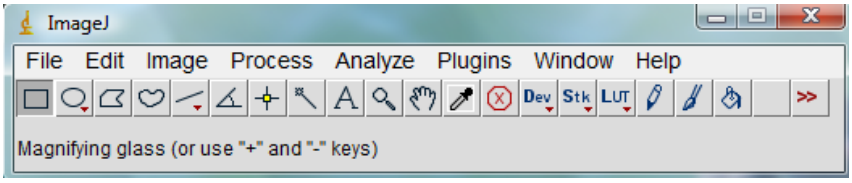

2. Select File > Open. Open a saved SEM image. The image will appear in a separate screen.

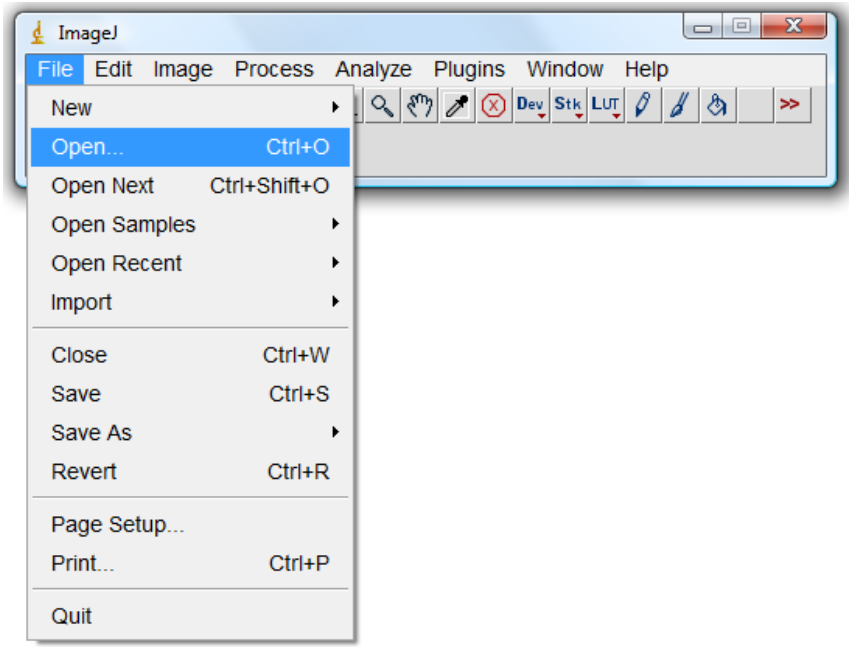

3. Select  and draw a line along the SEM image's scale bar. Visually ensure the line is as close to the length of the scale bar as possible as this will affect the outcome of fiber diameter measurements (See image under Step 4 for further clarification).
4. On the tool bar, select Analyze > Set Scale.

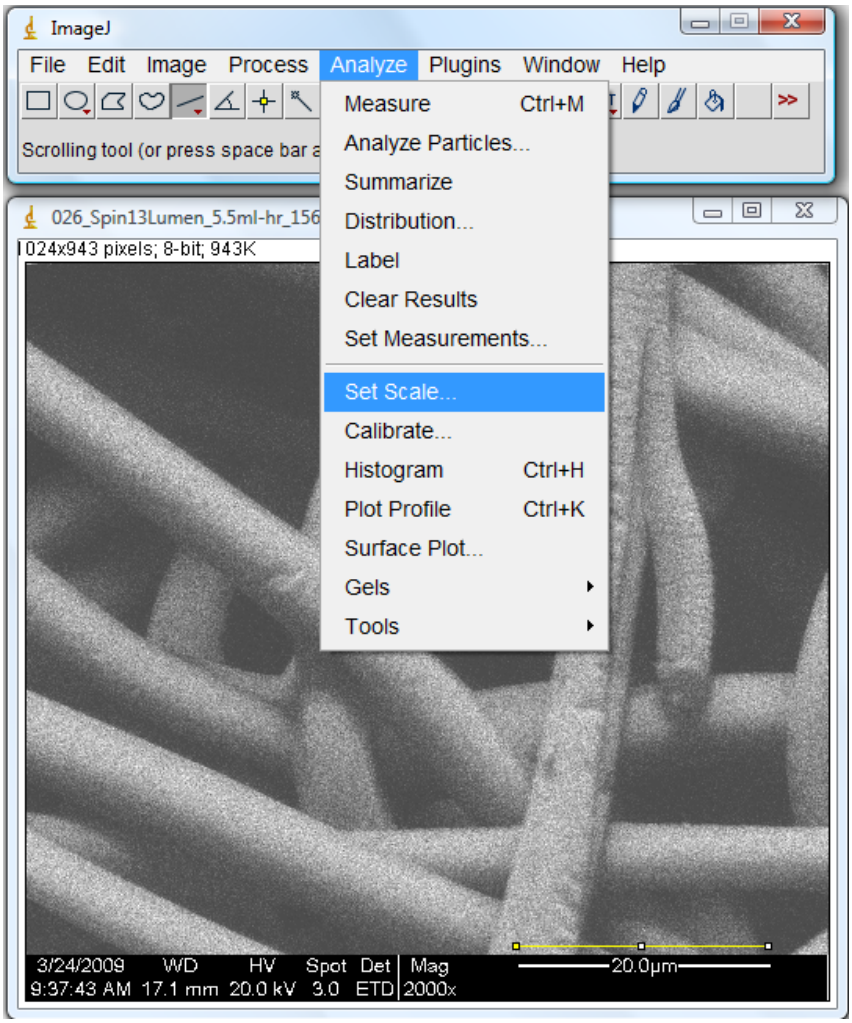

5. Insert known image scale bar distance (ex. 20µm). Set pixel aspect ratio to 1.0 and set appropriate unit length (ex. µm). Select OK. ImageJ is now calibrated to the image,

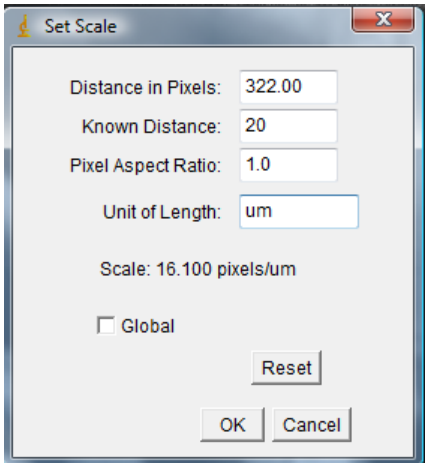

6. From the tool bar, select  . Draw a line across the diameter of a single fiber to be measured.

7. From the toolbar select Analyze > Measure. ImageJ will open a new window reporting Results. Fiber diameter is reported as Length in the Results window in proper units (ex. µm).

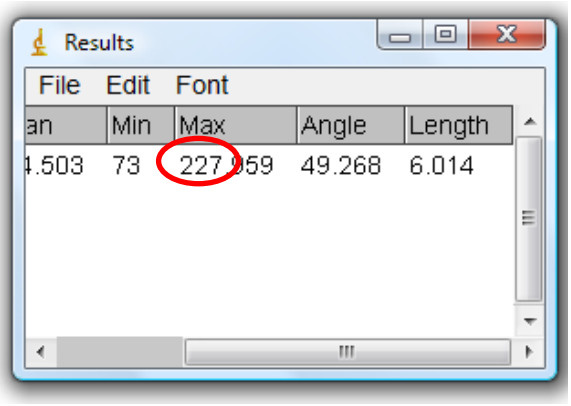

8. Leave the Measure window open and repeat Step 6 for all fiber measurements for the image.
9. Repeat for all images. NOTE: Calibration is only necessary for the first image if all images are being analyzed at the SAME magnification. Re-calibration is necessary for images taken at different magnifications.

APPENDIX E: POROSITY MEASUREMENT PROTOCOL

This fiber diameter measurement protocol was originally developed by Tiffany Pena and was modified to create this porosity measurement protocol.

1. Open program ImageJ. The following screen will appear.

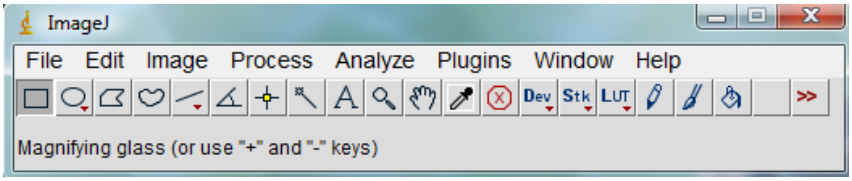

2. Select File > Open. Open a saved SEM image. The image will appear in a separate screen.

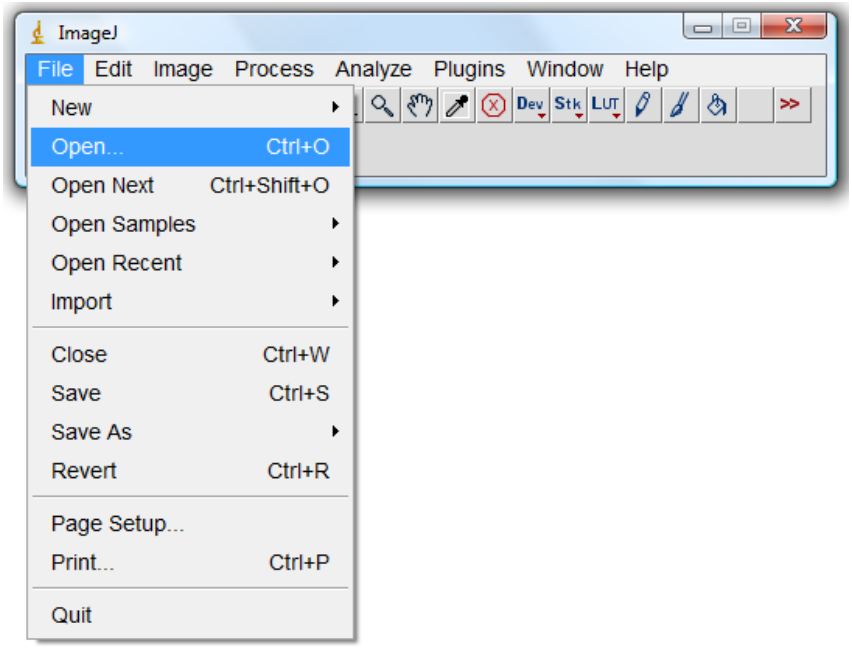

3. Select  and draw a line along the SEM image's scale bar. Visually ensure the line is as close to the length of the scale bar as possible as this will affect the outcome of fiber diameter measurements (See image under Step 4 for further clarification).
4. On the tool bar, select Analyze > Set Scale.

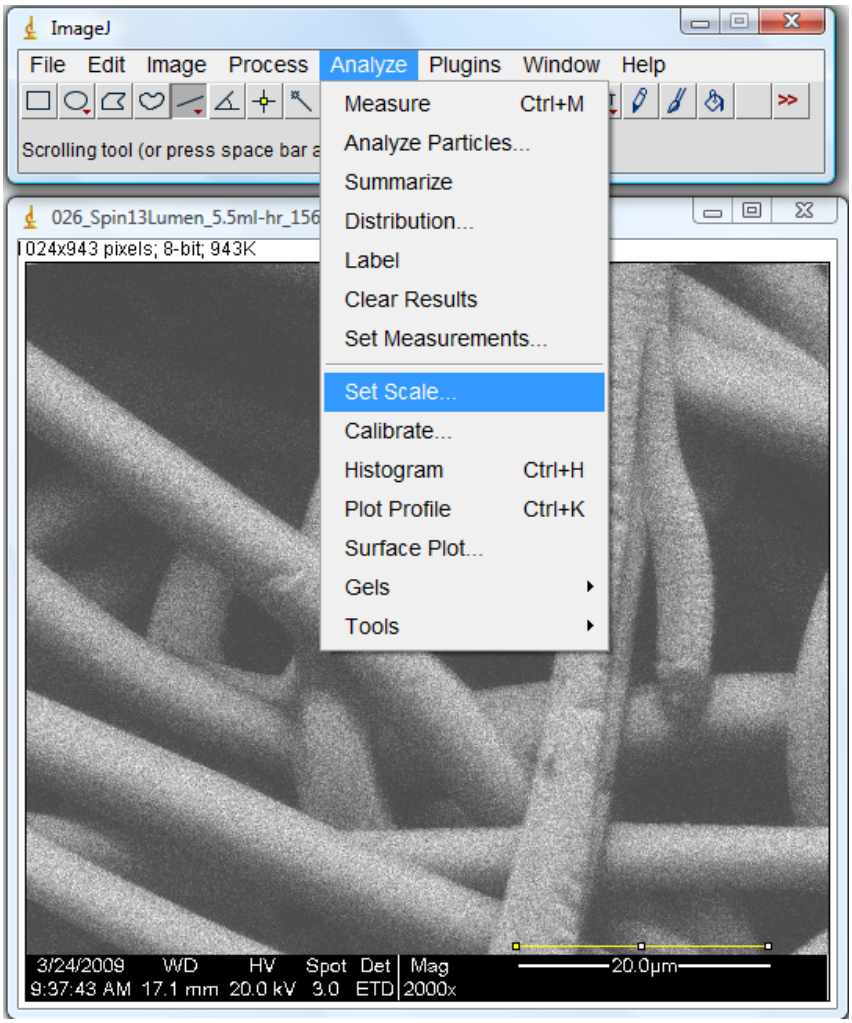

5. Insert known image scale bar distance (ex. 20µm). Set pixel aspect ratio to 1.0 and set appropriate unit length (ex. µm). Select OK. ImageJ is now calibrated to the image.
6. Next on the ImageJ toolbar, select the Process tab and click Enhance Contrast.
7. As seen in the pop up window below, the Saturated Pixels was changed to 10%.

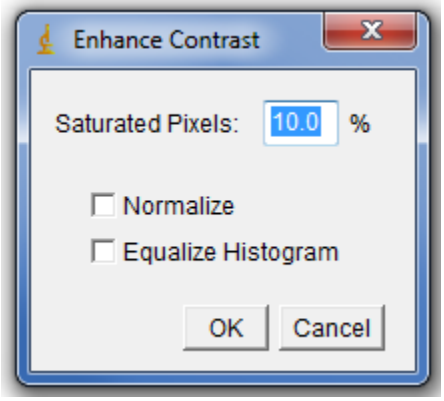

8. Then select the freehand selection tool, and carefully outline (yellow) the desired pore as seen in the screenshot below.

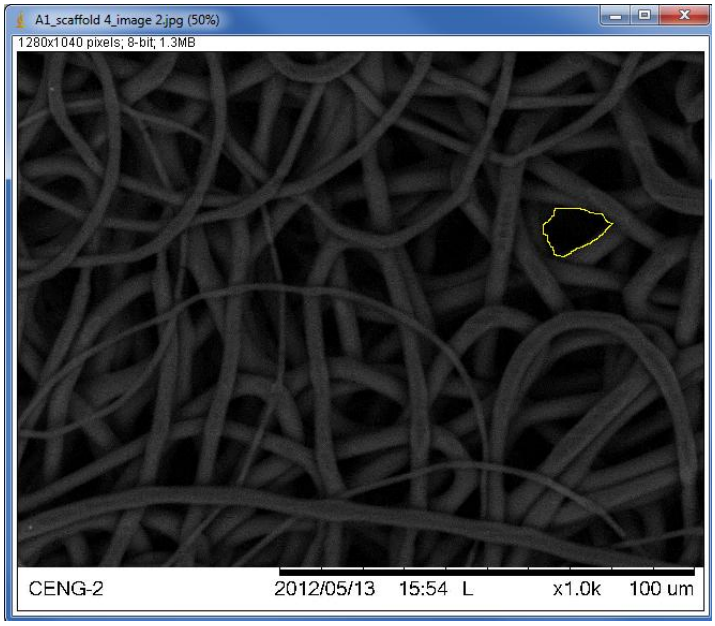

9. From the toolbar select Analyze > Measure. ImageJ will open a new window reporting Results. Porosity is reported as Area in the Results window in proper units (ex. μm^2).

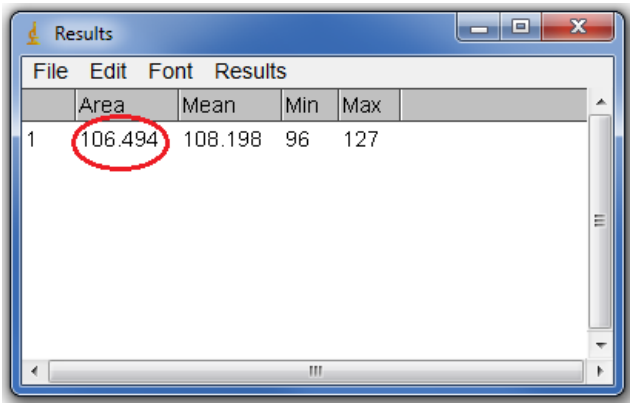

10. Leave the Measure window open and repeat Step 8 for all fiber measurements for the image.
11. Repeat for all images. NOTE: Calibration is only necessary for the first image if all images are being analyzed at the SAME magnification. Re-calibration is necessary for images taken at different magnifications.

APPENDIX F: CHARACTERIZATION AND CONSISTENCY STUDIES SEM IMAGES

Scaffold 1

Section A1

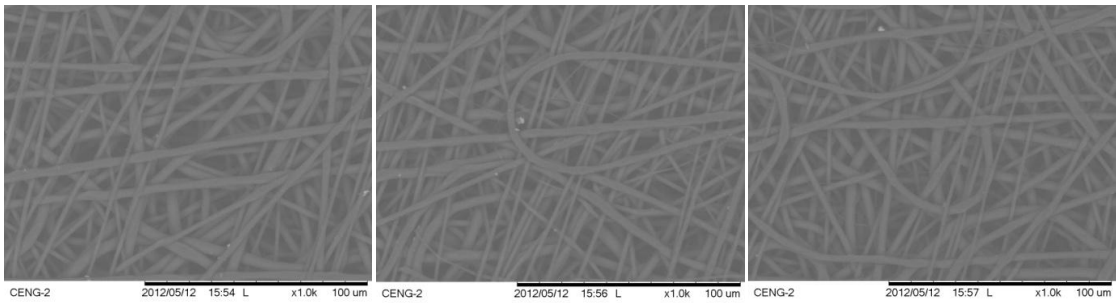

Section A2

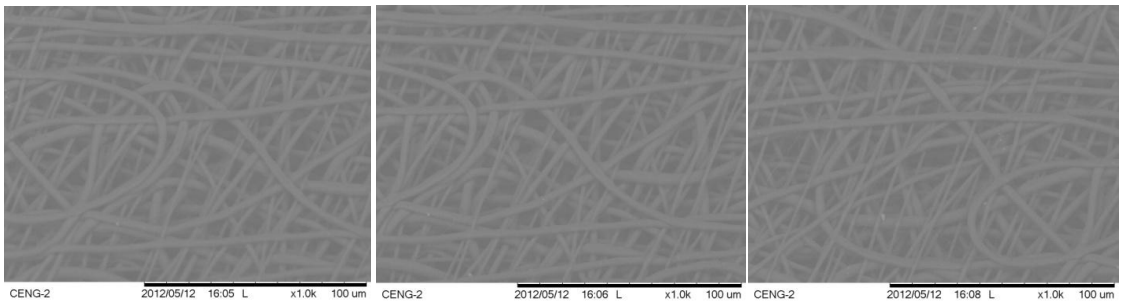

Section A3

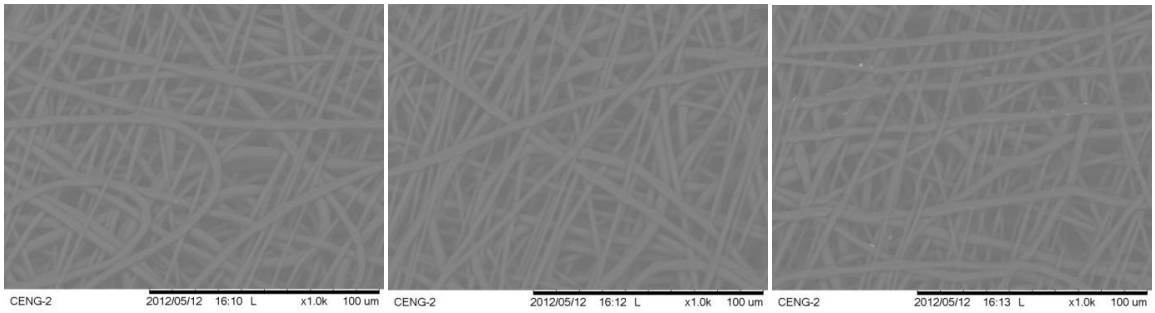

Scaffold 2

Section A1

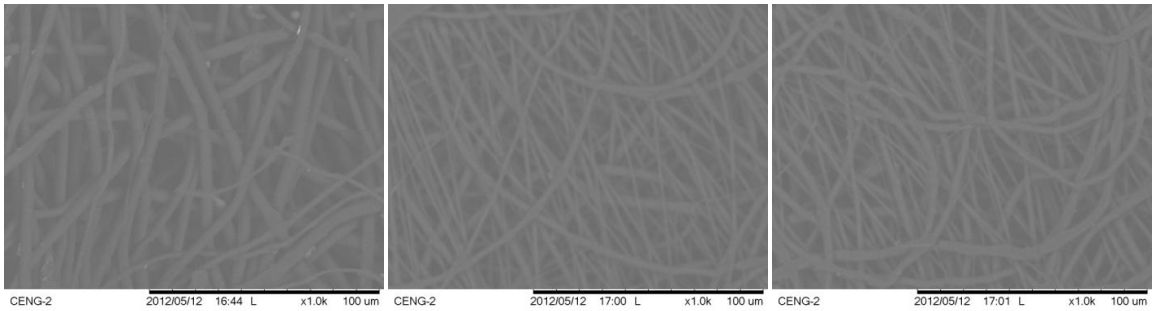

Section A2

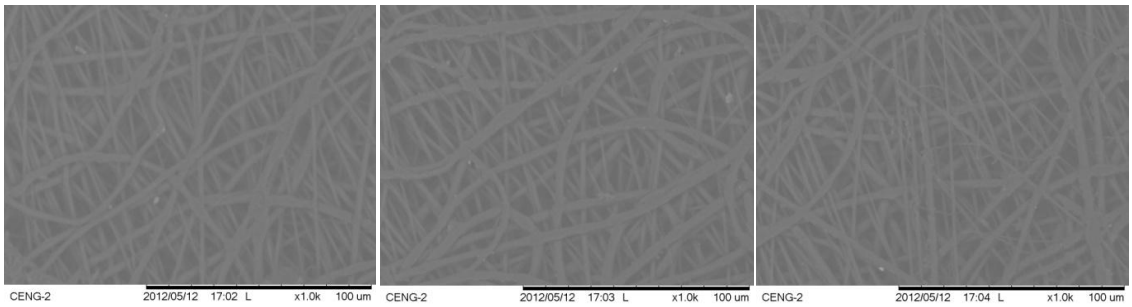

Section A3

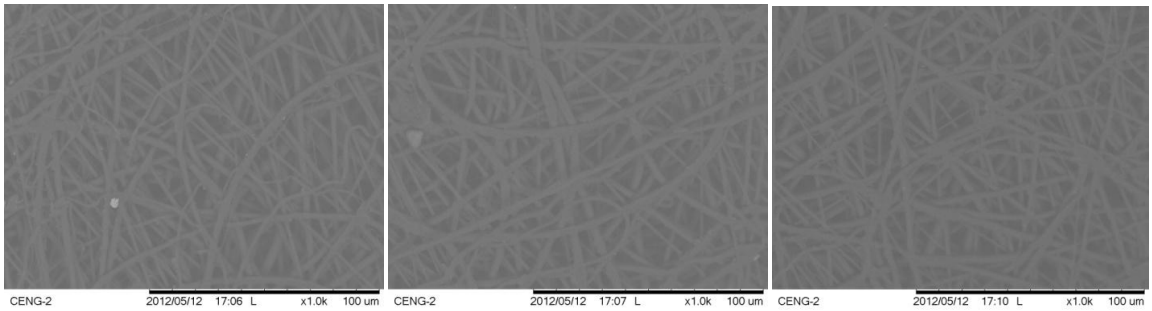

Scaffold 3

Section A1

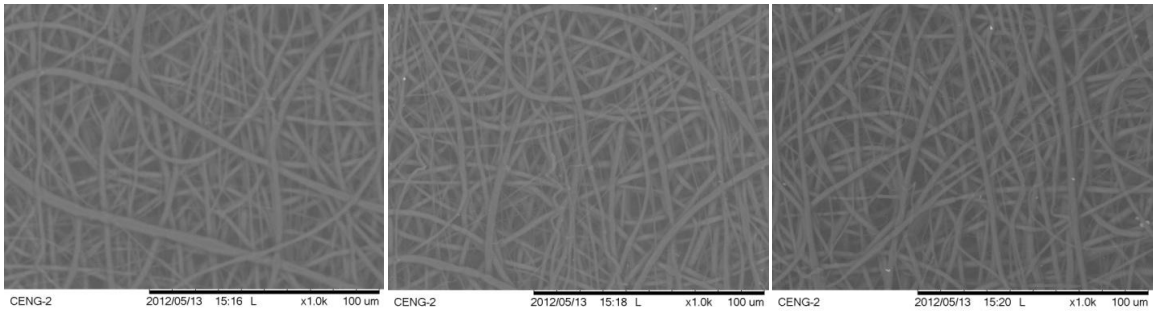

Section A2

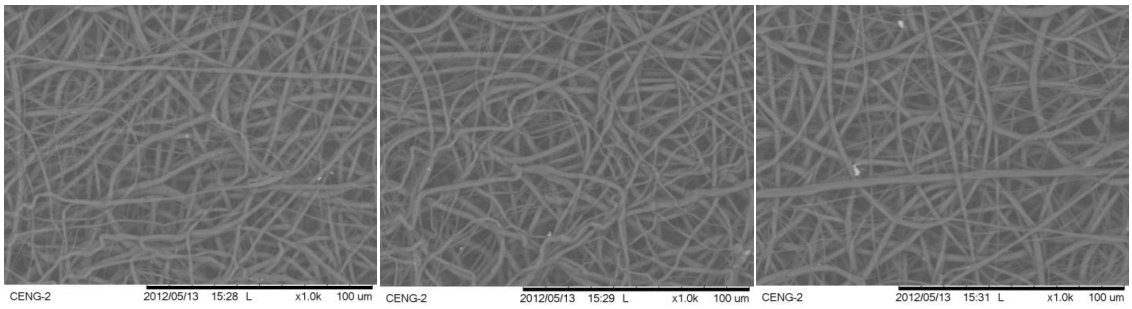

Section A3

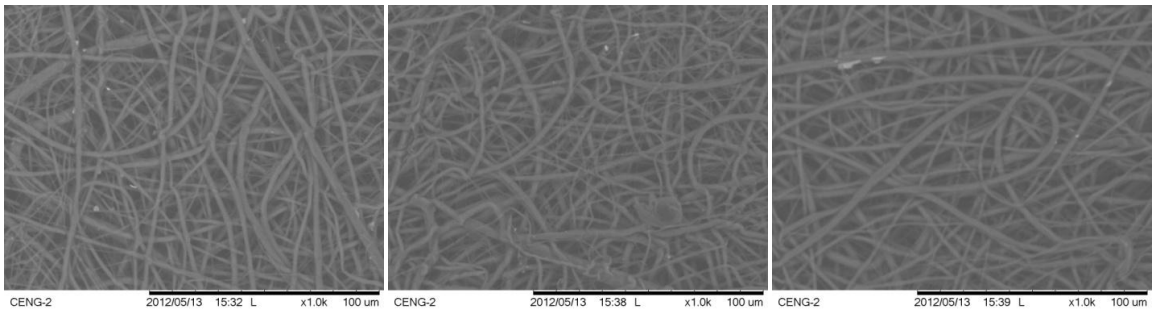

Scaffold 4

Section A1

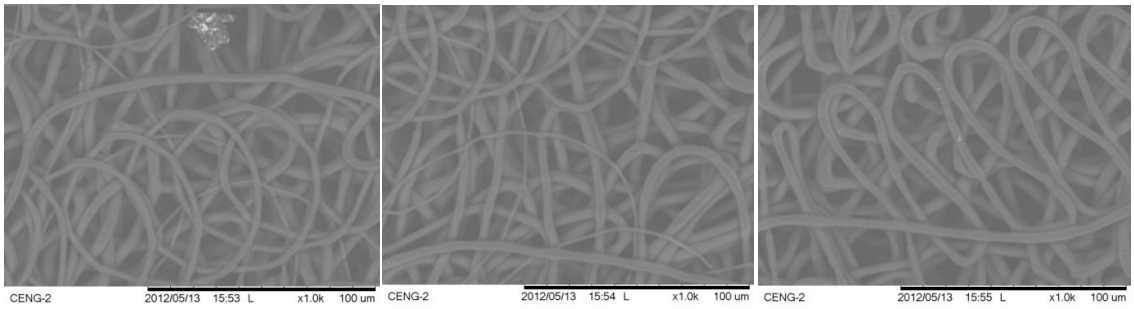

Section A2

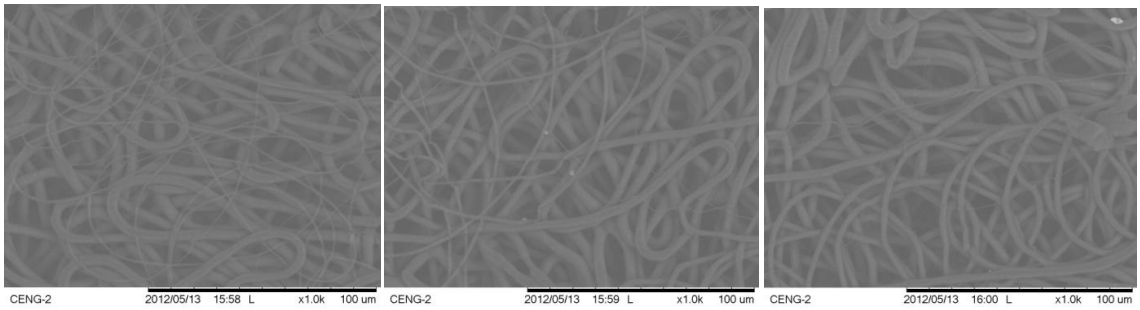

Section A3

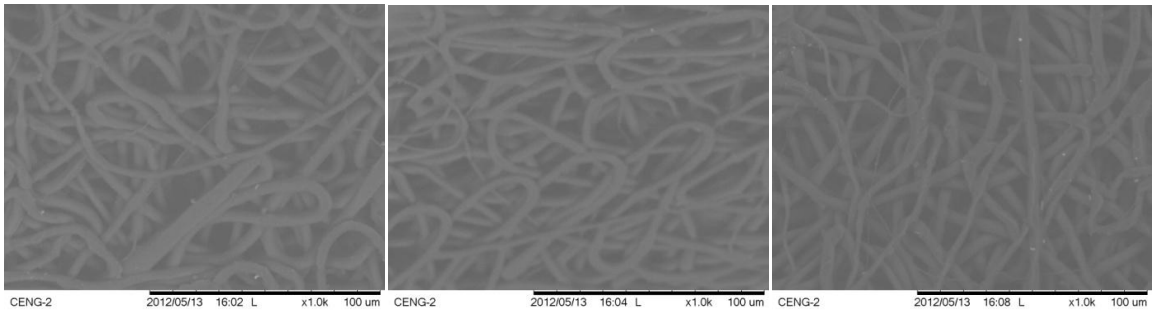

Scaffold 5

Section A1

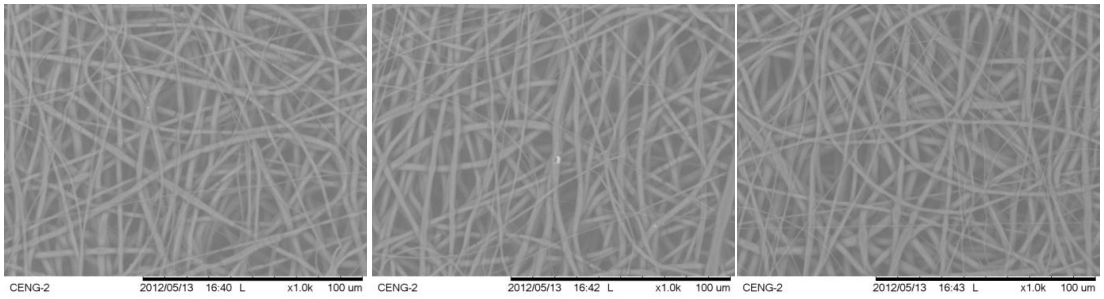

Section A2

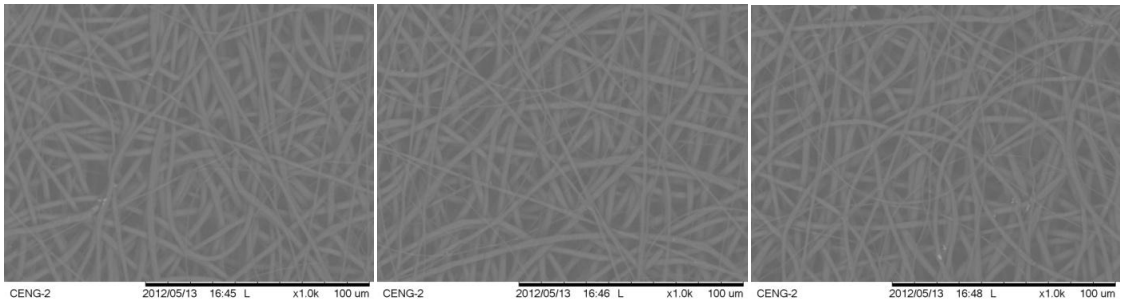

Section A3

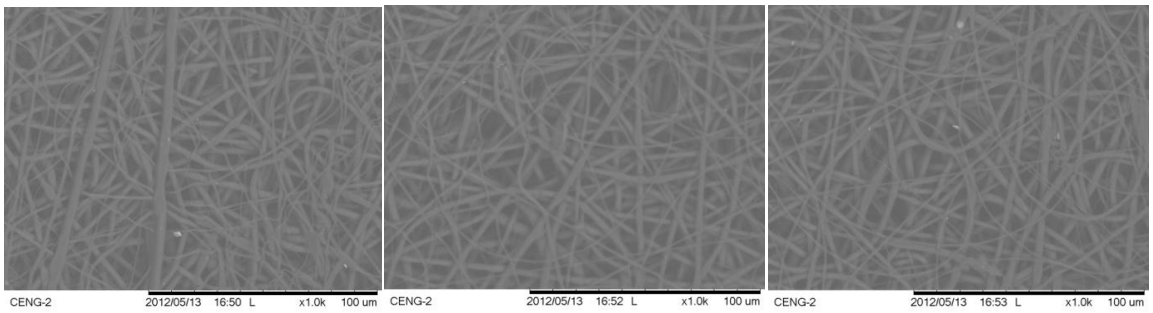

APPENDIX G: TENSILE TESTING FIGURES

Introduction

Tensile testing results for all of the scaffolds electrospun for the Characterization and Consistency study are included in this appendix. An explanation of the procedure used to section and test each scaffold can be seen in Chapter 4. Moreover, the following graphs represent the linear stress behavior, which was extrapolated from the stress versus strain behavior from tensile testing of each section. The slope of the linear section was measured by placing a fitted line, and represents the Young's modulus according to Hooke's Law. Microsoft excel was used to generate all of the figures and equations. The Y-axis represents the stress values, measured in MPa. While the X-axis strain values are dimensionless.

Scaffold 1 - Section C1

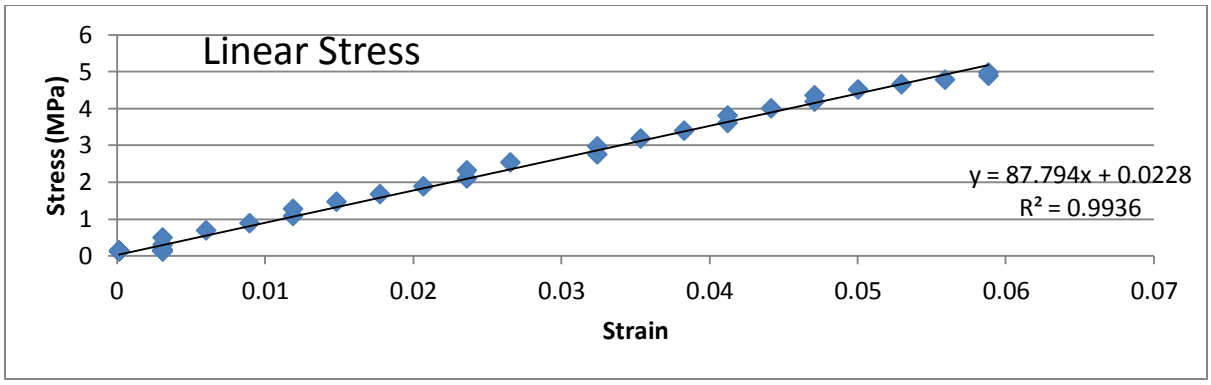

Scaffold 1 - Section C2

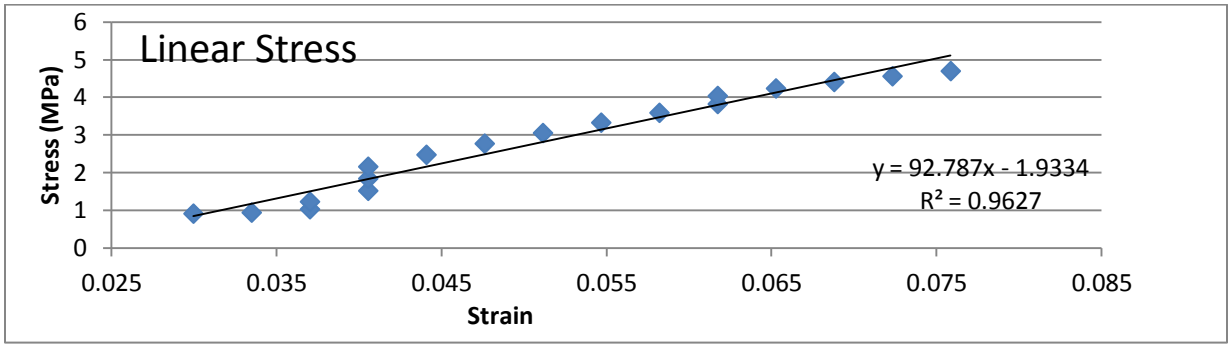

Scaffold 1 - Section C3

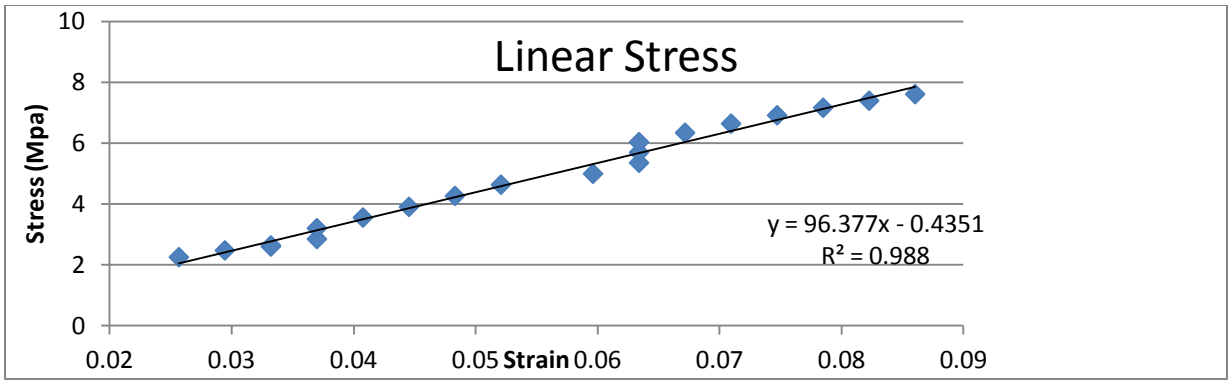

Scaffold 1 - Section C4

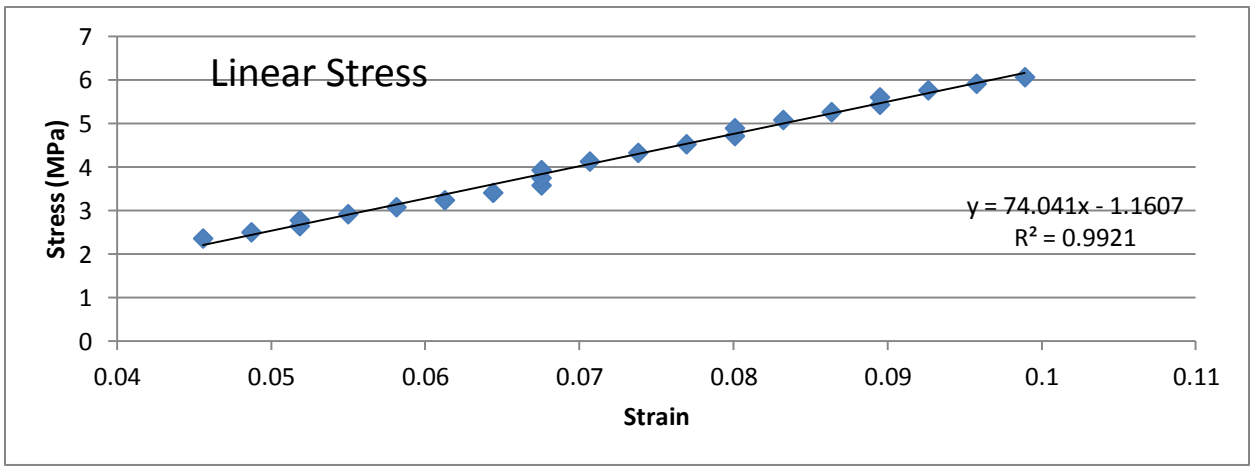

Scaffold 2 - Section C1

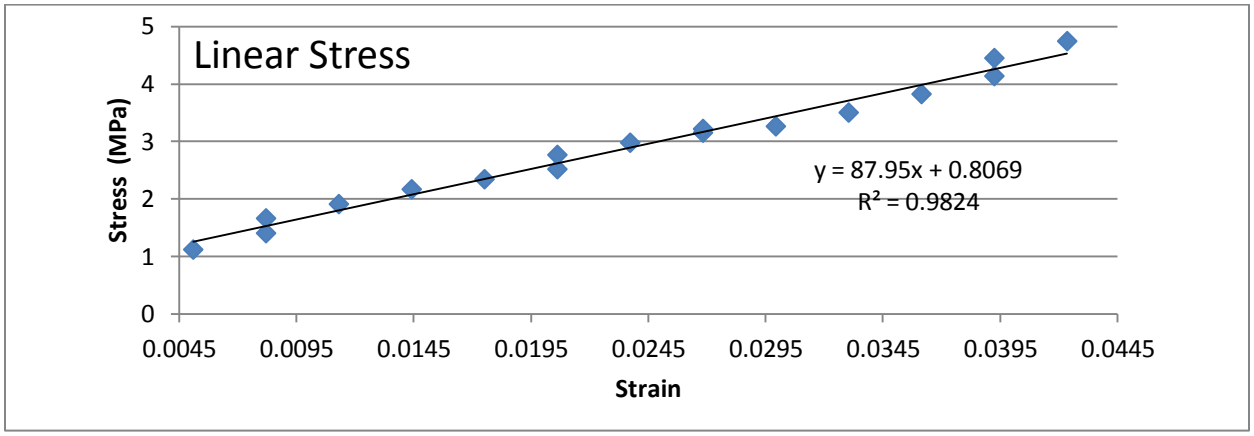

Scaffold 2 - Section C2

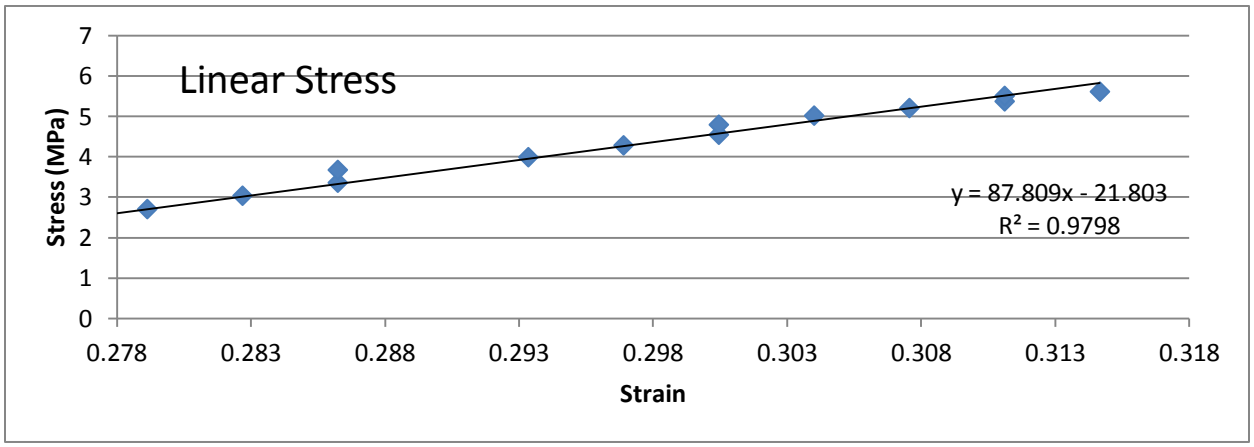

Scaffold 2 - Section C3

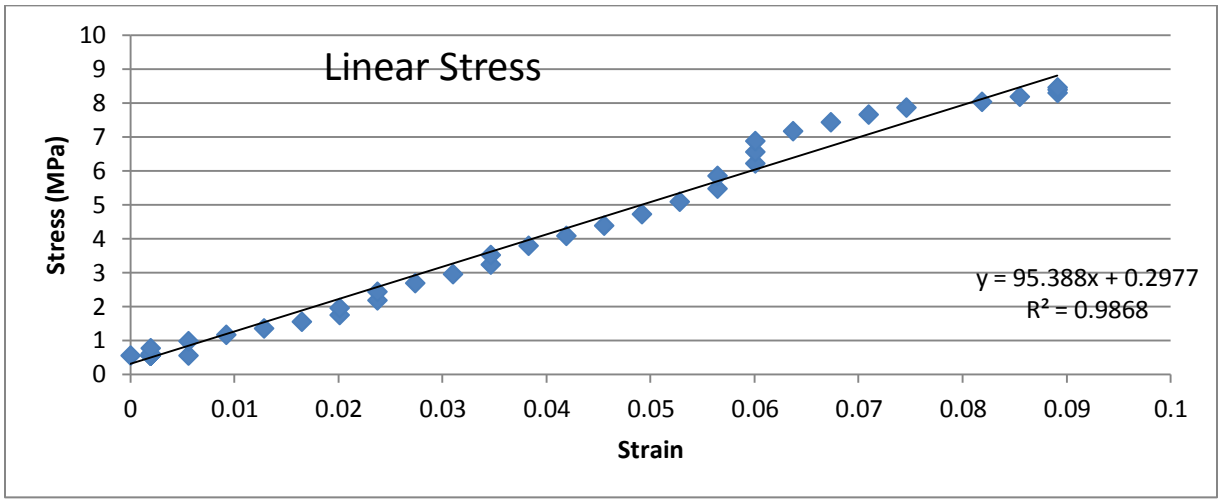

Scaffold 2 - Section C4

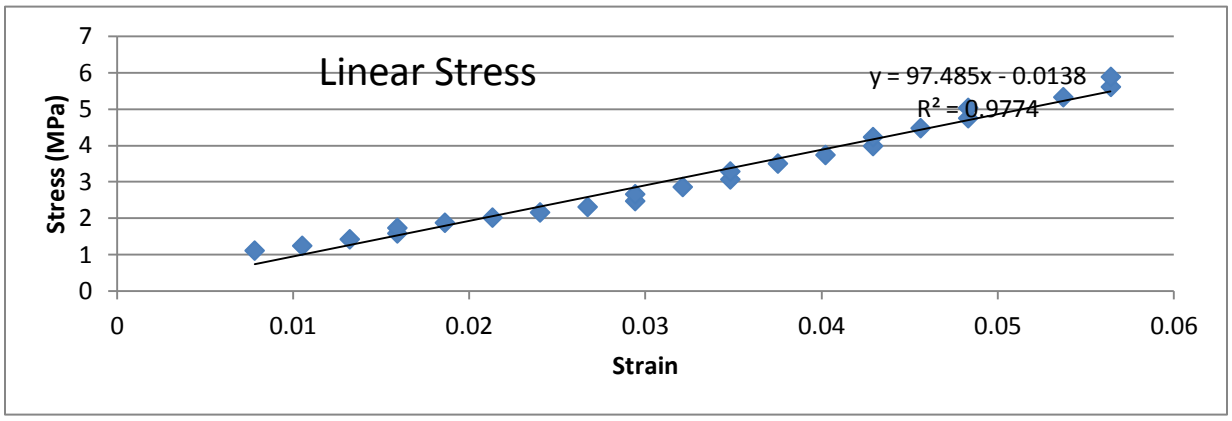

Scaffold 3 - Section C1

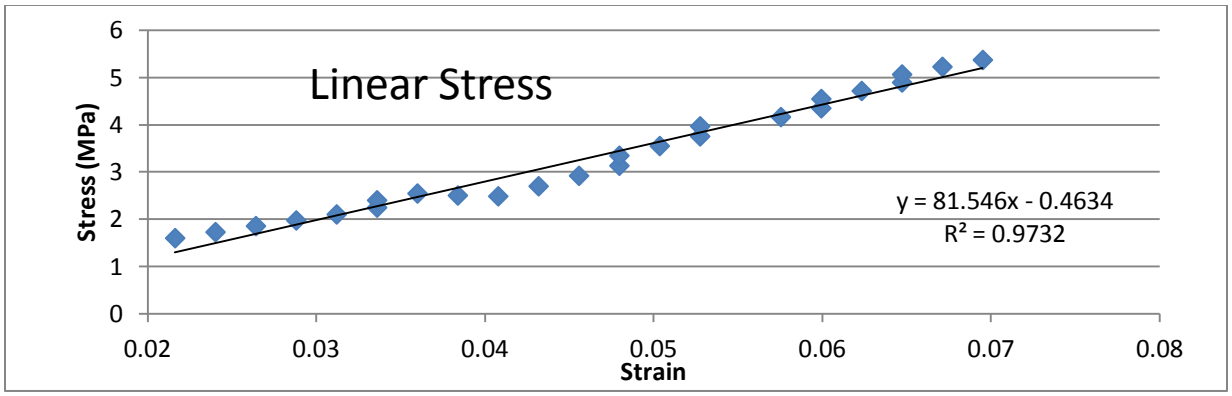

Scaffold 3 - Section C2

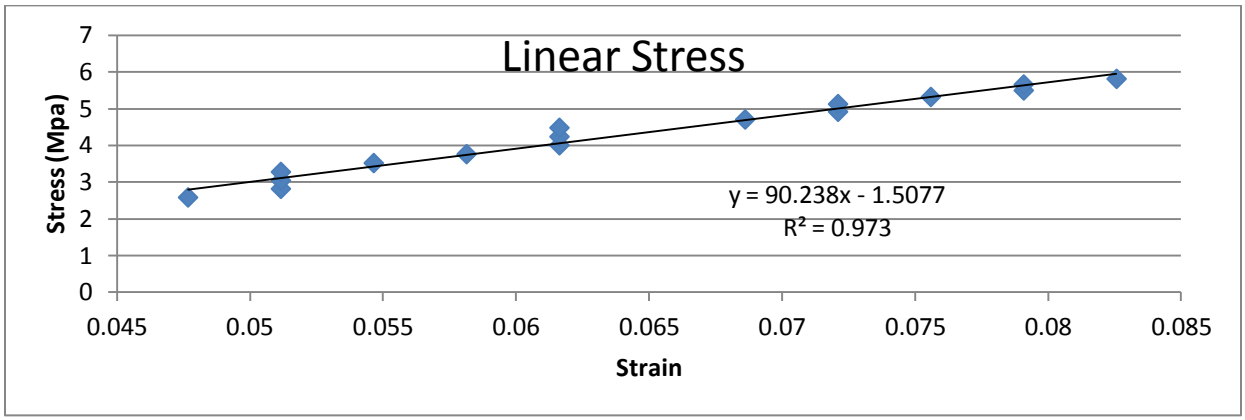

Scaffold 3 - Section C3

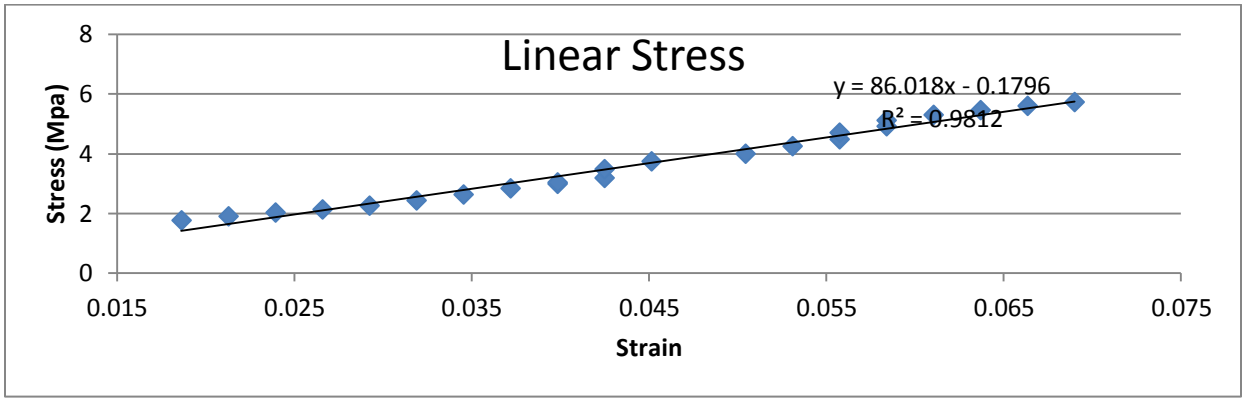

Scaffold 3 - Section C4

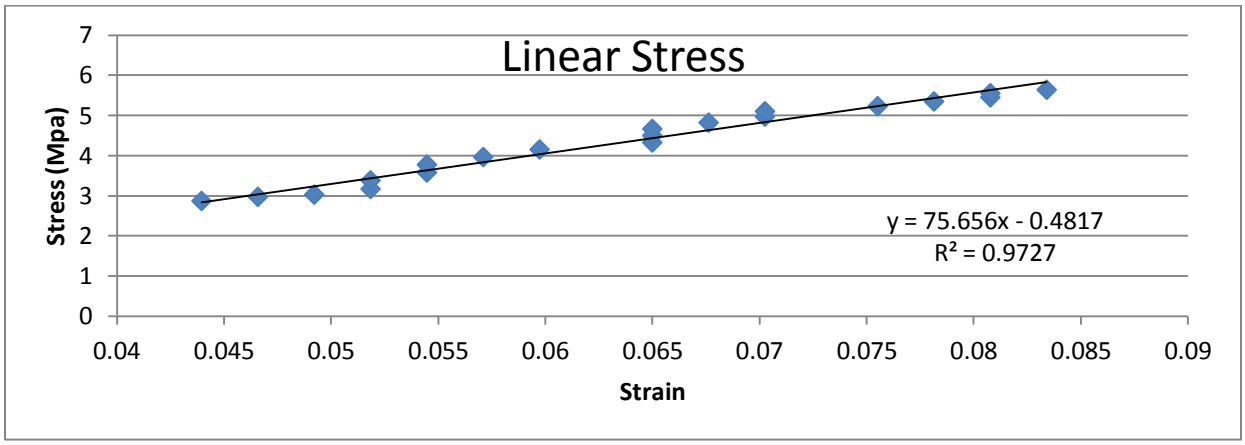

Scaffold 4 - Section C1

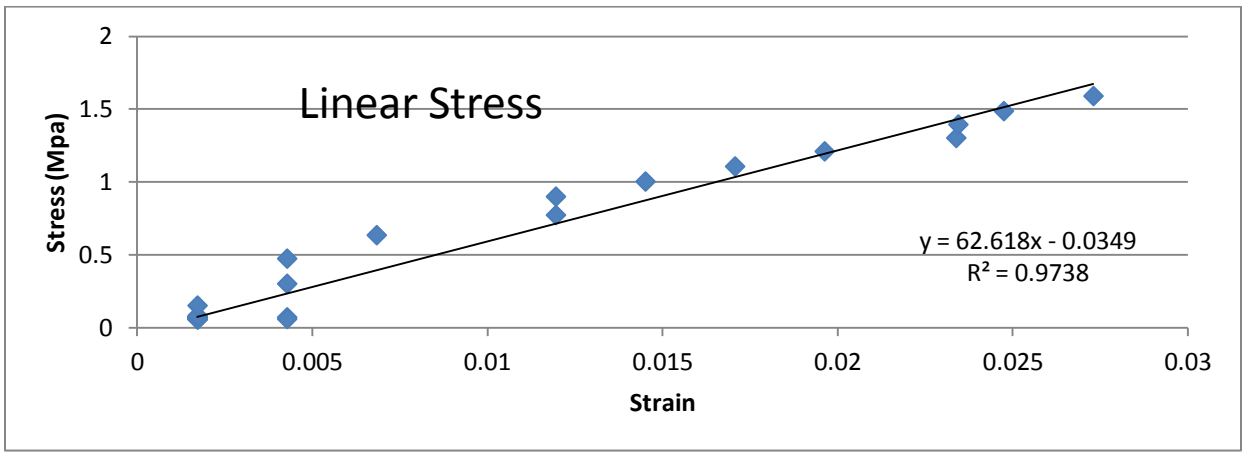

Scaffold 4 - Section C2

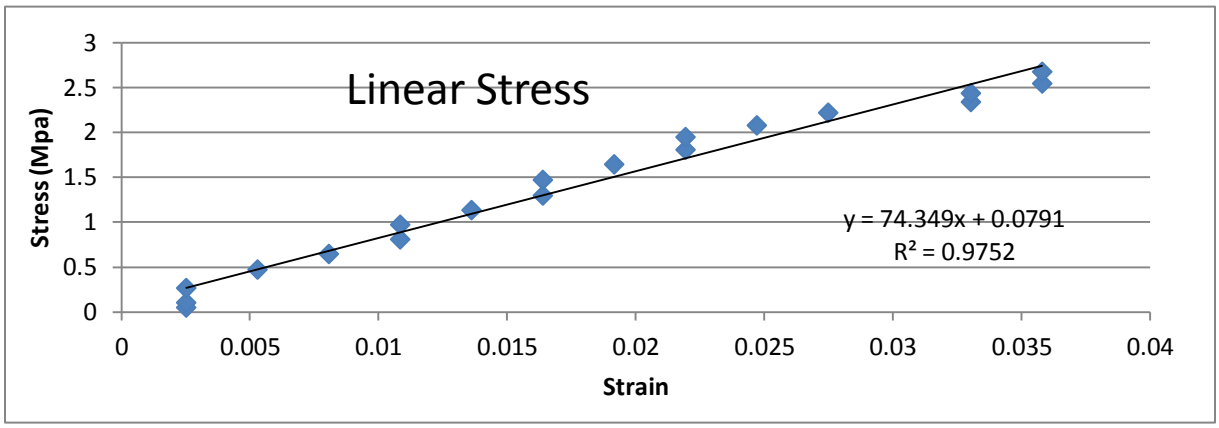

Scaffold 4 - Section C3

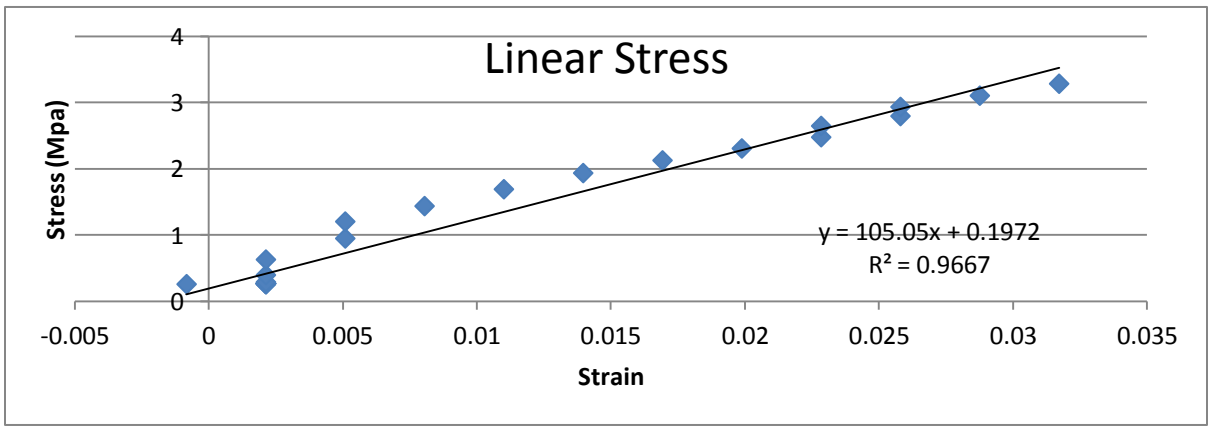

Scaffold 5 - Section C1

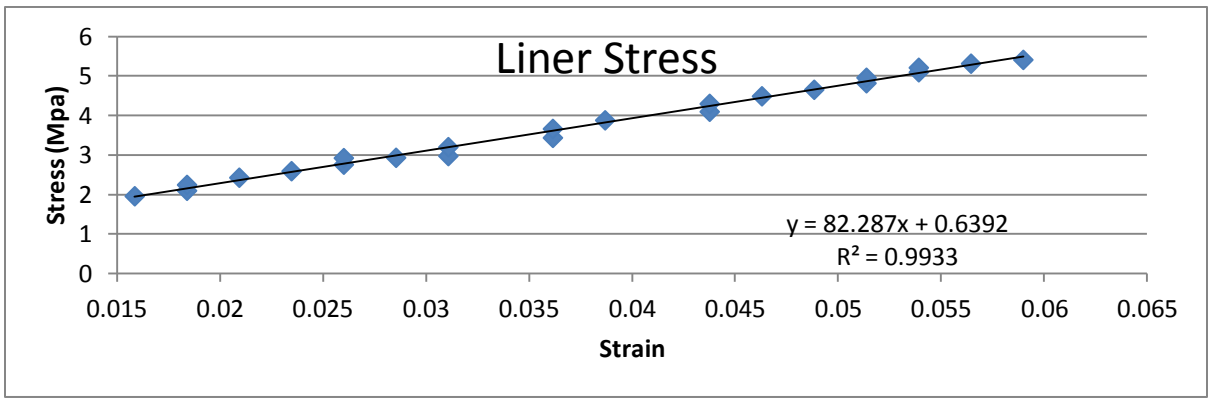

Scaffold 5 - Section C2

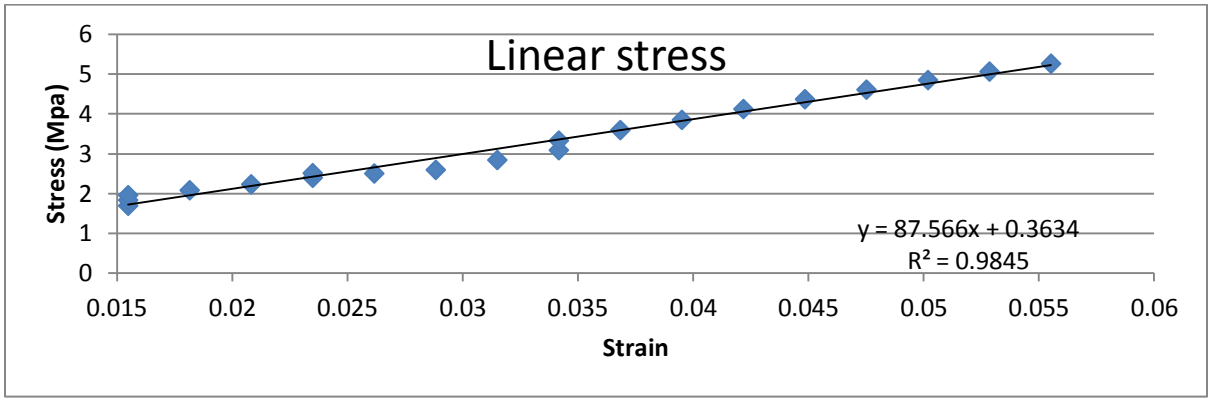

Scaffold 5 - Section C3

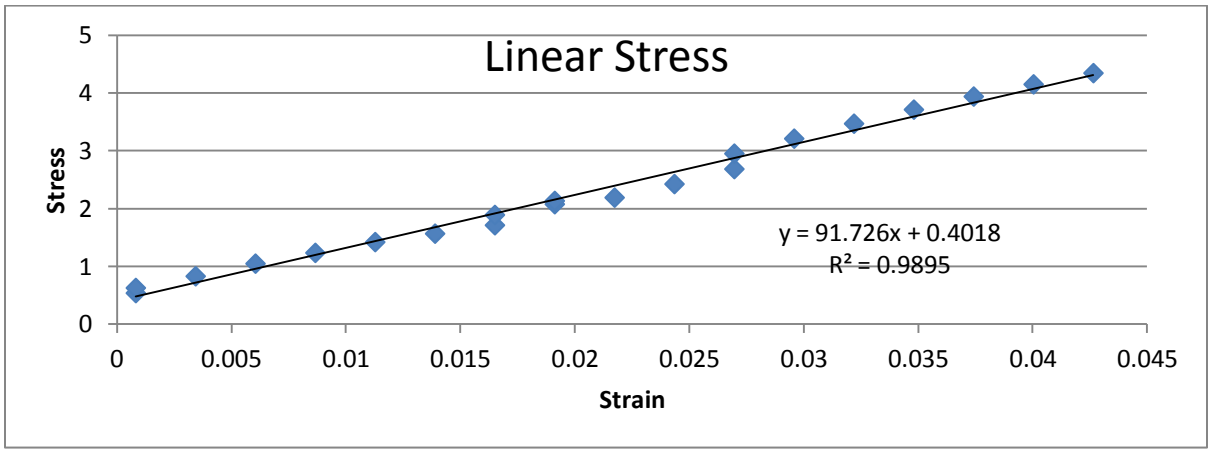

Scaffold 5 - Section C4